NCHRP
REPORT 596

NATIONAL COOPERATIVE HIGHWAY RESEARCH PROGRAM

Rotation Limits for Elastomeric Bearings

TRANSPORTATION RESEARCH BOARD
OF THE NATIONAL ACADEMIES

TRANSPORTATION RESEARCH BOARD 2007 EXECUTIVE COMMITTEE*

OFFICERS

CHAIR: **Linda S. Watson,** *CEO, LYNX–Central Florida Regional Transportation Authority, Orlando*
VICE CHAIR: **Debra L. Miller,** *Secretary, Kansas DOT, Topeka*
EXECUTIVE DIRECTOR: **Robert E. Skinner, Jr.,** *Transportation Research Board*

MEMBERS

J. Barry Barker, *Executive Director, Transit Authority of River City, Louisville, KY*
Michael W. Behrens, *Executive Director, Texas DOT, Austin*
Allen D. Biehler, *Secretary, Pennsylvania DOT, Harrisburg*
John D. Bowe, *President, Americas Region, APL Limited, Oakland, CA*
Larry L. Brown, Sr., *Executive Director, Mississippi DOT, Jackson*
Deborah H. Butler, *Vice President, Customer Service, Norfolk Southern Corporation and Subsidiaries, Atlanta, GA*
Anne P. Canby, *President, Surface Transportation Policy Partnership, Washington, DC*
Nicholas J. Garber, *Henry L. Kinnier Professor, Department of Civil Engineering, University of Virginia, Charlottesville*
Angela Gittens, *Vice President, Airport Business Services, HNTB Corporation, Miami, FL*
Susan Hanson, *Landry University Professor of Geography, Graduate School of Geography, Clark University, Worcester, MA*
Adib K. Kanafani, *Cahill Professor of Civil Engineering, University of California, Berkeley*
Harold E. Linnenkohl, *Commissioner, Georgia DOT, Atlanta*
Michael D. Meyer, *Professor, School of Civil and Environmental Engineering, Georgia Institute of Technology, Atlanta*
Michael R. Morris, *Director of Transportation, North Central Texas Council of Governments, Arlington*
John R. Njord, *Executive Director, Utah DOT, Salt Lake City*
Pete K. Rahn, *Director, Missouri DOT, Jefferson City*
Sandra Rosenbloom, *Professor of Planning, University of Arizona, Tucson*
Tracy L. Rosser, *Vice President, Corporate Traffic, Wal-Mart Stores, Inc., Bentonville, AR*
Rosa Clausell Rountree, *Executive Director, Georgia State Road and Tollway Authority, Atlanta*
Henry G. (Gerry) Schwartz, Jr., *Senior Professor, Washington University, St. Louis, MO*
C. Michael Walton, *Ernest H. Cockrell Centennial Chair in Engineering, University of Texas, Austin*
Steve Williams, *Chairman and CEO, Maverick Transportation, Inc., Little Rock, AR*

EX OFFICIO MEMBERS

Thad Allen (Adm., U.S. Coast Guard), *Commandant, U.S. Coast Guard, Washington, DC*
Thomas J. Barrett (Vice Adm., U.S. Coast Guard, ret.), *Pipeline and Hazardous Materials Safety Administrator, U.S.DOT*
Joseph H. Boardman, *Federal Railroad Administrator, U.S.DOT*
Rebecca M. Brewster, *President and COO, American Transportation Research Institute, Smyrna, GA*
Paul R. Brubaker, *Research and Innovative Technology Administrator, U.S.DOT*
George Bugliarello, *Chancellor, Polytechnic University of New York, Brooklyn, and Foreign Secretary, National Academy of Engineering, Washington, DC*
J. Richard Capka, *Federal Highway Administrator, U.S.DOT*
Sean T. Connaughton, *Maritime Administrator, U.S.DOT*
Edward R. Hamberger, *President and CEO, Association of American Railroads, Washington, DC*
John H. Hill, *Federal Motor Carrier Safety Administrator, U.S.DOT*
John C. Horsley, *Executive Director, American Association of State Highway and Transportation Officials, Washington, DC*
J. Edward Johnson, *Director, Applied Science Directorate, National Aeronautics and Space Administration, John C. Stennis Space Center, MS*
William W. Millar, *President, American Public Transportation Association, Washington, DC*
Nicole R. Nason, *National Highway Traffic Safety Administrator, U.S.DOT*
Jeffrey N. Shane, *Under Secretary for Policy, U.S.DOT*
James S. Simpson, *Federal Transit Administrator, U.S.DOT*
Carl A. Strock (Lt. Gen., U.S. Army), *Chief of Engineers and Commanding General, U.S. Army Corps of Engineers, Washington, DC*
Robert A. Sturgell, *Acting Administrator, Federal Aviation Administration, U.S.DOT*

*Membership as of October 2007.

NATIONAL COOPERATIVE HIGHWAY RESEARCH PROGRAM

NCHRP REPORT 596

Rotation Limits for Elastomeric Bearings

John F. Stanton
Charles W. Roeder
Peter Mackenzie-Helnwein
Christopher White
Colin Kuester
Brianne Craig
Department of Civil and Environmental Engineering
University of Washington
Seattle, WA

Subject Areas
Bridges and Other Structures

Research sponsored by the American Association of State Highway and Transportation Officials
in cooperation with the Federal Highway Administration

TRANSPORTATION RESEARCH BOARD

WASHINGTON, D.C.
2008
www.TRB.org

NATIONAL COOPERATIVE HIGHWAY RESEARCH PROGRAM

Systematic, well-designed research provides the most effective approach to the solution of many problems facing highway administrators and engineers. Often, highway problems are of local interest and can best be studied by highway departments individually or in cooperation with their state universities and others. However, the accelerating growth of highway transportation develops increasingly complex problems of wide interest to highway authorities. These problems are best studied through a coordinated program of cooperative research.

In recognition of these needs, the highway administrators of the American Association of State Highway and Transportation Officials initiated in 1962 an objective national highway research program employing modern scientific techniques. This program is supported on a continuing basis by funds from participating member states of the Association and it receives the full cooperation and support of the Federal Highway Administration, United States Department of Transportation.

The Transportation Research Board of the National Academies was requested by the Association to administer the research program because of the Board's recognized objectivity and understanding of modern research practices. The Board is uniquely suited for this purpose as it maintains an extensive committee structure from which authorities on any highway transportation subject may be drawn; it possesses avenues of communications and cooperation with federal, state and local governmental agencies, universities, and industry; its relationship to the National Research Council is an insurance of objectivity; it maintains a full-time research correlation staff of specialists in highway transportation matters to bring the findings of research directly to those who are in a position to use them.

The program is developed on the basis of research needs identified by chief administrators of the highway and transportation departments and by committees of AASHTO. Each year, specific areas of research needs to be included in the program are proposed to the National Research Council and the Board by the American Association of State Highway and Transportation Officials. Research projects to fulfill these needs are defined by the Board, and qualified research agencies are selected from those that have submitted proposals. Administration and surveillance of research contracts are the responsibilities of the National Research Council and the Transportation Research Board.

The needs for highway research are many, and the National Cooperative Highway Research Program can make significant contributions to the solution of highway transportation problems of mutual concern to many responsible groups. The program, however, is intended to complement rather than to substitute for or duplicate other highway research programs.

NCHRP REPORT 596

Project 12-68
ISSN 0077-5614
ISBN 978-0-309-09918-9
Library of Congress Control Number 2008920212

COPYRIGHT PERMISSION

NOTICE

The project that is the subject of this report was a part of the National Cooperative Highway Research Program conducted by the Transportation Research Board with the approval of the Governing Board of the National Research Council. Such approval reflects the Governing Board's judgment that the program concerned is of national importance and appropriate with respect to both the purposes and resources of the National Research Council.

The members of the technical committee selected to monitor this project and to review this report were chosen for recognized scholarly competence and with due consideration for the balance of disciplines appropriate to the project. The opinions and conclusions expressed or implied are those of the research agency that performed the research, and, while they have been accepted as appropriate by the technical committee, they are not necessarily those of the Transportation Research Board, the National Research Council, the American Association of State Highway and Transportation Officials, or the Federal Highway Administration, U.S. Department of Transportation.

Each report is reviewed and accepted for publication by the technical committee according to procedures established and monitored by the Transportation Research Board Executive Committee and the Governing Board of the National Research Council.

The Transportation Research Board of the National Academies, the National Research Council, the Federal Highway Administration, the American Association of State Highway and Transportation Officials, and the individual states participating in the National Cooperative Highway Research Program do not endorse products or manufacturers. Trade or manufacturers' names appear herein solely because they are considered essential to the object of this report.

Published reports of the

NATIONAL COOPERATIVE HIGHWAY RESEARCH PROGRAM

are available from:

Transportation Research Board
Business Office
500 Fifth Street, NW
Washington, DC 20001

and can be ordered through the Internet at:

http://www.national-academies.org/trb/bookstore

Printed in the United States of America

THE NATIONAL ACADEMIES

Advisers to the Nation on Science, Engineering, and Medicine

The **National Academy of Sciences** is a private, nonprofit, self-perpetuating society of distinguished scholars engaged in scientific and engineering research, dedicated to the furtherance of science and technology and to their use for the general welfare. On the authority of the charter granted to it by the Congress in 1863, the Academy has a mandate that requires it to advise the federal government on scientific and technical matters. Dr. Ralph J. Cicerone is president of the National Academy of Sciences.

The **National Academy of Engineering** was established in 1964, under the charter of the National Academy of Sciences, as a parallel organization of outstanding engineers. It is autonomous in its administration and in the selection of its members, sharing with the National Academy of Sciences the responsibility for advising the federal government. The National Academy of Engineering also sponsors engineering programs aimed at meeting national needs, encourages education and research, and recognizes the superior achievements of engineers. Dr. Charles M. Vest is president of the National Academy of Engineering.

The **Institute of Medicine** was established in 1970 by the National Academy of Sciences to secure the services of eminent members of appropriate professions in the examination of policy matters pertaining to the health of the public. The Institute acts under the responsibility given to the National Academy of Sciences by its congressional charter to be an adviser to the federal government and, on its own initiative, to identify issues of medical care, research, and education. Dr. Harvey V. Fineberg is president of the Institute of Medicine.

The **National Research Council** was organized by the National Academy of Sciences in 1916 to associate the broad community of science and technology with the Academy's purposes of furthering knowledge and advising the federal government. Functioning in accordance with general policies determined by the Academy, the Council has become the principal operating agency of both the National Academy of Sciences and the National Academy of Engineering in providing services to the government, the public, and the scientific and engineering communities. The Council is administered jointly by both the Academies and the Institute of Medicine. Dr. Ralph J. Cicerone and Dr. Charles M. Vest are chair and vice chair, respectively, of the National Research Council.

The **Transportation Research Board** is one of six major divisions of the National Research Council. The mission of the Transportation Research Board is to provide leadership in transportation innovation and progress through research and information exchange, conducted within a setting that is objective, interdisciplinary, and multimodal. The Board's varied activities annually engage about 7,000 engineers, scientists, and other transportation researchers and practitioners from the public and private sectors and academia, all of whom contribute their expertise in the public interest. The program is supported by state transportation departments, federal agencies including the component administrations of the U.S. Department of Transportation, and other organizations and individuals interested in the development of transportation. **www.TRB.org**

www.national-academies.org

CRP STAFF FOR NCHRP REPORT 596

Christopher W. Jenks, *Director, Cooperative Research Programs*
Crawford F. Jencks, *Deputy Director, Cooperative Research Programs*
David B. Beal, *Senior Program Officer*
Eileen P. Delaney, *Director of Publications*
Margaret B. Hagood, *Editor*

NCHRP PROJECT 12-68 PANEL
Field of Design—Area of Bridges

Ralph E. Anderson, *Illinois DOT, Springfield, IL* (Chair)
Thomas K. Koch, *North Carolina DOT, Raleigh, NC*
Brad J. Boehm, *California DOT, El Dorado Hills, CA*
Timothy Bradberry, *Texas DOT, Austin, TX*
Richard A. Bray, *H.W. Lochner, Inc., Rocky Hill, CT*
Robert A. Burnett, *New York State DOT, Albany, NY*
Ralph J. Dornsife, *Washington State DOT, Tumwater, WA*
Neil M. Hawkins, *University of Illinois - Urbana-Champaign, Urbana, IL*
Jose A. Lopez, *New Jersey DOT, Trenton, NJ*
William Henry Pate, *Tennessee DOT, Nashville, TN*
Hamid Ghasemi, *FHWA Liaison*
Stephen F. Maher, *TRB Liaison*

AUTHOR ACKNOWLEDGMENTS

The research reported herein was performed under NCHRP Project 12-68 by the Department of Civil and Environmental Engineering at the University of Washington (UW).

Dr. John Stanton, Professor of Civil Engineering at UW, was the Project Director and co-Principal Investigator. The other authors of this report are Dr. Charles Roeder, Professor of Civil Engineering at UW and co-PI, Dr. Peter Mackenzie-Helnwein, Assistant Professor of Civil Engineering at UW and co-PI, Mr. Christopher White, Mr. Colin Kuester and Ms. Brianne Craig, all Graduate Student Assistants and MSCE recipients at UW. The work was done under the direction of Professors Stanton, Roeder and Mackenzie-Helnwein. The assistance with the laboratory work of Mr. Vince Chaijaroen, Laboratory Manager, Mr. Kevin Soderlund, Instrument Maker, and Mr. Kyle Twitchell, Undergraduate Assistant, is gratefully acknowledged. The specialty test rig that made possible the extensive cyclic testing was based on a concept developed by Mr. Ken Olson and built by Mr. Tim Rodgers, both of whom received their MSCE degrees at UW.

FOREWORD

By David B. Beal
Staff Officer
Transportation Research Board

This report provides elastomeric bearing design procedures suitable for adoption in the AASHTO LRFD Bridge Design Specifications. The report details the experimental and analytical program used to develop the design procedures. The material in this report will be of immediate interest to bridge designers.

Bridges experience translational movements and rotations caused by creep and shrinkage, thermal effects, traffic loading, initial construction tolerances, and other sources. Bridge bearings are designed and built to accommodate these movements and rotations while supporting required gravity loads and providing the necessary restraint to the structure. Elastomeric bearings accommodate movement and rotation by deformation of the elastomer. The bearing must be designed to control the strains and deformations in the elastomer to assure a long service life and good bearing performance.

AASHTO's current elastomeric bearing design limits were developed in NCHRP Project 10-20, but bearing rotation was not considered a high-priority issue for that project. As a result, virtually no experimental research on elastomeric bearing rotation was performed, and design provisions were developed based on conservative interpretation of past theoretical results. For example, the experiments used to validate the tension limits were done nearly 60 years ago and used very small laboratory samples, which are not at all similar to bridge bearings. The limits on lift off, uplift, and shear strain in the elastomer are known to be controlling criteria for elastomeric bearing rotation, but the equations used in the current AASHTO provisions have not been verified experimentally and are believed to be overly conservative. In particular, the load combination of low axial load plus high rotation that may be experienced during construction leads to potential lift-off. Under the 2005 LRFD Specifications, this load combination often unreasonably controlled the bearing design or prevented the use of an elastomeric bearing altogether.

The present conservatism in the rotational design limits results in more expensive bearings and may limit their use. The increased bearing cost is due in part to additional elastomeric material and quality-assurance testing. In some cases, expensive high-load multi-rotational bearings must be used to satisfy the design requirements. For these reasons, it was important to re-evaluate rotational design limits and quality-assurance requirements for elastomeric bearings.

The objective of NCHRP project 12-68 was to develop recommended provisions and commentary for rotational design capacity and quality assurance of elastomeric bearings suitable for inclusion in the AASHTO LRFD specifications. This objective has been accomplished. This research was performed by the University of Washington, Seattle, Washington. The report fully documents the experimental and analytical program used to develop the design procedures.

CONTENTS

SUMMARY

Rotation Limits for Elastomeric Bearings

The response of elastomeric bridge bearings to imposed rotations was studied using testing and analysis. The program concentrated on steel-reinforced elastomeric bearings.

The demand on typical bearings was evaluated by analyzing a range of bridges and evaluating the amplitudes of the axial loads and rotations on the bearings that are likely to occur in practice. During this process, it was found that cyclic axial forces cause larger strains in the elastomer than do the cyclic rotations. However, resource limits in the program precluded cyclic axial testing, and the discovery was anyway made quite late in the program. Thus, in the development of design procedures, the effects of cyclic axial load were taken into account by analysis alone.

The capacity of the bearings to accommodate the loads and rotations without excessive damage was evaluated by a program of testing and analysis of the bearings themselves. The test program included material tests, static and cyclic tests on full bearings, and diagnostic tests on full bearings to evaluate their instantaneous state of damage. In all, 78 bearings were tested. The bearings were purchased from the four largest manufacturers in the country.

Static and low-cycle repeated load tests were conducted under axial load with or without a fixed rotation. Stresses up to 12,000 psi were applied. Bearings with high shape factors (9 and 12) were able to carry the loads with no damage whatsoever, while bearings with lower shape factors suffered various levels of damage. The cyclic rotation tests were conducted in a specially constructed test machine that is capable of applying simultaneously constant axial load, constant shear displacement and cyclic rotation. Peak capacities are 800 kips axial load and +/− 8% rotation. Cyclic loading was found to cause progressive damage, analogous to fatigue in metals. However, the damage was in the form of progressive debonding of the elastomer from the internal steel shims, so failure was never sudden. At the end of every cyclic test, the bearing could still easily carry the axial load, even though other properties had degraded. This finding creates the need for judgment in establishing a level of damage that constitutes failure.

Failure of a component is usually expressed in terms of critical stress or strain, and the same approach was used with the bearings studied here. However, measuring local strains in rubber is difficult, so analysis was necessary to relate the internal stress and strain fields to the external loadings that caused them. Classical, closed-form analytical techniques for laminated incompressible materials were used for the purpose, and nonlinear Finite Element Analysis (NLFEA) was used to verify that the closed-form methods were sufficiently accurate to warrant their use in design procedures. Empirical fatigue models were also generated to predict the progress of damage under cyclic loading.

The results of the tests and analyses were combined to develop design procedures suitable for adoption in the AASHTO LRFD Bridge Design Specifications. Major proposed changes

from the present specifications include the removal of the absolute limit on compressive stress, so that the design of high shape factor bearings for high stresses will be possible, the removal of the previous "no-uplift" provisions, which were causing difficulties for designers, and a change in the testing requirements so that the second-level, more rigorous testing is required for large bearings rather than any bearing deigned by the more comprehensive "Method B."

CHAPTER 1

Introduction and Research Approach

1.1 Bridge Bearings

Elastomeric bearings have been used in bridges since the late 1950s, and have grown in popularity so they are now the most common type of bridge bearing in all regions of the United States. They are capable of resisting typical bridge loads and accommodating deformations without the use of machined or moving parts, which largely eliminates any need for maintenance. This characteristic, together with their economy, has for many years made them an attractive choice. The spread of seismic design requirements throughout the country and the fact that elastomeric bearings typically have better seismic performance than traditional bearing types only adds to their appeal.

Elastomeric bearings are often thought of as having a limited load capacity. When loads exceed a certain threshold, designers tend to use pot, disk, or spherical bearings instead. One reason is practical: the low stresses presently permitted on elastomeric bearings result in a large bearing for carrying a high load, and the space may not be available for it. Molding a large elastomeric bearing also may pose problems. However, there is no inherent reason why they should not be used for high loads. During the course of the research, the team encountered a laminated elastomeric bridge bearing designed for 16,000 kips service load. However, such large bearings are likely to have limited rotation capacity, and that may ultimately prove more of a limit than the load capacity.

1.2 Bearing Mechanics

Elastomeric bridge bearings come in four principal types:

- Plain elastomeric pads, used primarily in low-load situations,
- Cotton duck pads, made from very closely spaced layers of elastomer and woven cotton. Relatively rigid, they often are equipped with a slider to accommodate horizontal displacements.
- Fiberglass-reinforced pads, like cotton duck pads, have the advantage that they can be cut from a large sheet and do not need to be molded individually, but are seldom used today,
- Steel-reinforced elastomeric bearings, used for the highest loads.

The main focus of this research is on rectangular steel-reinforced elastomeric bearings, as shown in Figure 1.1. Steel plates are bonded with rubber, either natural or polychloroprene, in alternating layers to form a sandwich. The finished product contains rubber cover on the top and bottom and around the edges, creating a sealed system in which the plates are protected against corrosion.

The rubber and steel layers are bonded together by an adhesive that is activated when the rubber is cured. Curing, or vulcanization, is the process of subjecting the raw rubber compound to high temperature and pressure, which both change its chemical structure and cause it to take the shape of the mold.

The concepts underlying behavior of laminated elastomeric bearings are quite different from those of conventional structural components made from concrete, metal, or timber. They depend on the fact that elastomers can undergo reversible, elastic deformations that are enormous compared with those of conventional materials, but that fact also brings with it the need for special design procedures.

The simplest concept for accommodating expansion or contraction of the girders is to do so through the elastic shear deformations of a plain rubber block. As the bridge expands, the block changes shape from a rectangle to a parallelogram as shown in Figure 1.2.

To accommodate the necessary deformations the block would have to be thick, and so it would be unacceptably flexible in axial compression; trucks would experience steps in the roadway as they passed from the end of one girder to another. The challenge is thus to stiffen the bearing in compression

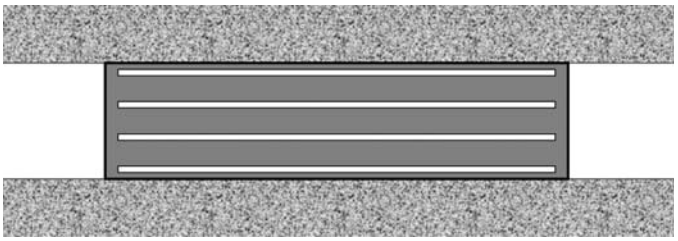

Figure 1.1. Cross-section of a steel-reinforced elastomeric bridge bearing.

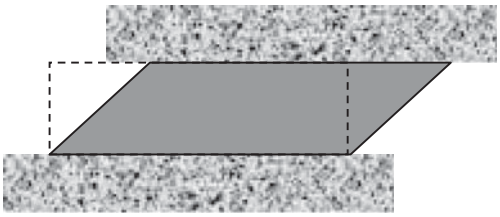

Figure 1.2. Elastomeric plain pad shearing to accommodate girder expansion.

without losing its shear flexibility. This is achieved by adding internal horizontal reinforcing plates known as shims in the bearing. Behavior under compressive load is illustrated in Figure 1.3.

A plain elastomeric pad responds to vertical load by expanding laterally and slipping against the supporting surface as shown in Figure 1.3a. The rubber at the top and bottom surfaces of the pad is partially restrained against outward movement by friction against the support, but the rubber at mid-thickness is not. This results in some bulging at the edges. The lateral expansion leads to significant vertical deflections. By contrast, the rubber in the laminated pad is largely prevented from such expansion by its bond to the steel plates, and the layers only form small bulges, as shown in Figure 1.3b.

Rubber is almost incompressible, so the volume of rubber remains almost constant under load, and the small lateral expansion leads to only a small vertical deflection. The laminated bearing is much stiffer and stronger in compression than a plain pad. However, the steel plates do not inhibit the shear deformations of the rubber, so the bearing is still able to undergo the same shear deformations as the plain pad for the purpose of accommodating changes in length of the girders.

1.3 Failure Modes, Analysis, and Design Criteria

The elastomer in a bearing experiences large shear strains. These occur for axial load, rotation and shear, and are illustrated in Figure 1.4. The shear strains can be envisaged by considering regions or elements of the rubber that are rectangular when unstressed, but are forced to become parallelograms when the bearing is under load.

The shear strains caused by axial load and rotation reach their maxima at the same place, namely the very edge of the layer where the rubber is bonded to the plate. Imposed shear deformations cause shear strains that are relatively constant over the whole layer, including the critical end of the plate.

If the steel reinforcing plates have square edges and if no cover exists, the shear stress at the corner of the rubber layer is theoretically singular. (The shear stress must be zero on the vertical free surface of the rubber, but most methods of analysis predict non-zero shear stress along the horizontal interface between steel and rubber. Yet, for equilibrium, the vertical and horizontal shear stresses must be equal.) In practice, these plates have slightly rounded edges because they are deburred, and rubber cover exists, so the stress is concentrated there rather than being truly singular. Under severe loading, this stress leads to local detachment of the elastomer from the steel. This starts with tensile debonding of the cover from the ends of the plates as shown in Figure 1.5 then propagates inwards along the surface as shear delamination. In this report, the terms debonding and delamination are used to indicate these two different behaviors.

Debonding is easy to see on the surface because two bulges merge into one larger bulge, as shown in Figure 1.5. However, distinguishing between local tensile debonding of the cover and shear delamination of the internal layers is difficult. This is unfortunate, because the former has little immediate effect on the bearing's performance, whereas the latter has significant adverse consequences. The shear delamina-

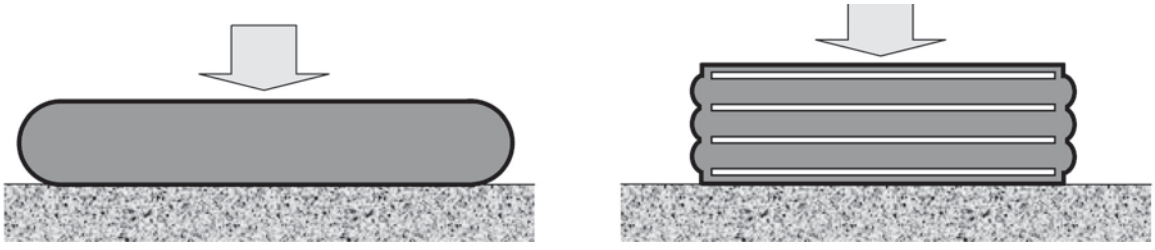

(a) (b)

Figure 1.3. Bulges without (a) and with (b) steel plates.

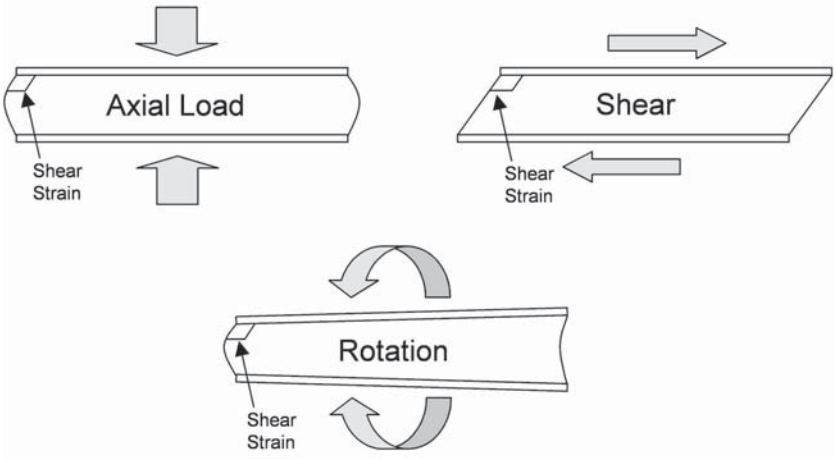

Figure 1.4. Deformations of a laminated elastomeric bearing layer.

tion always is preceded by the tensile debonding, so the one acts as a precursor of the other.

The lateral expansion of the rubber layers causes tension in the steel plates. At extreme loads, the plates may fracture, typically splitting along the longitudinal axis of the bearing, as shown in Figure 1.6. With plates of the thickness used in practice, this behavior does not occur until the load has reached five to 10 times its design value, so shim fracture seldom controls design. Theoretically the plates could be made thinner and they still would be strong enough in tension, but they would be more flexible in bending. Keeping them plane during molding would then become problematic.

Shear delamination is the most important potential mode of failure. If it were to occur in practice, the elastomer would start to extrude from the bearing, which would in turn cause significant vertical deflection, horizontal forces of unpredictable magnitude, and possible hard contact between the girder and the support. While none of these necessarily creates collapse conditions in the bridge itself, any one of them will seriously degrade the serviceability and reduce the performance of the bridge.

It is necessary to relate the delamination to a local strain measure, so its onset can be predicted. Prediction of any local deformations is difficult, because elastomeric bearings have three characteristics that make conventional stress analysis invalid:

- Rubber is almost incompressible (Poisson's ratio ≈0.50),
- Parts of the bearing undergo very large displacements, so the geometry of the system changes significantly during the loading, and
- Rubber obeys a nonlinear stress-strain law.

Further difficulties are caused by stress-strain behavior that is often somewhat rate-dependent (for example, visco-elastic) and it changes with cycling as the internal crystal structure changes with loading. The only viable way of predicting internal deformations throughout the entire rubber mass is by using FEA, but even that tool has its own additional challenges,

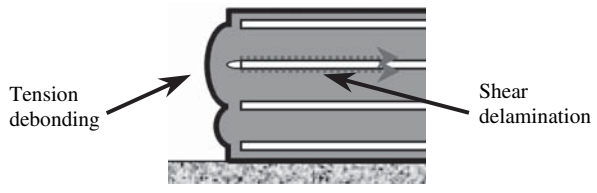

Figure 1.5. Tension debonding at the shim end and shear delamination at the shim surface.

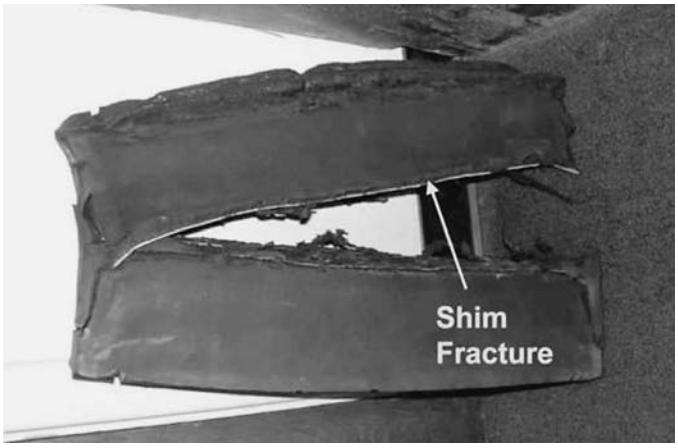

Figure 1.6. Fractured steel plates in bearing.

such as element instability and difficulties with convergence of the iterative calculations. Furthermore, FEA is not an appropriate design tool for a component that may cost as little as $100.

Gent and Lindley (1959a) pioneered a simplified analysis of laminated bearings that uses small-deflection theory and depends on an assumed displacement field. It provides a remarkably accurate estimate of the strains in the rubber layers up to a point near the edge. It breaks down in the region at the very edge of the shims where the local shear stresses become singular, and it does not address the cover rubber at all, but its relative simplicity does provide the basis for estimating the shear strains near the critical region and the fact that it provides closed-form analytical solutions is beneficial. It has formed the basis for the computations in nearly every specification to date, and was used extensively in this research.

The method was originally developed for a completely incompressible material, for which conventional analysis fails. It treats the lateral deformation of the rubber layers as distributed parabolically through the layer thickness, and depends on calculating the shear stresses in the material from that assumed displacement field. It is discussed briefly in Appendix F, and in detail in Gent and Lindley (1959a), Conversy (1967), Gent and Meinecke (1970), and Stanton and Lund (2006). The latter paper provides numerical values for all the coefficients needed to evaluate stiffnesses and strains, for rectangular bearings of all aspect ratios.

The behavior can be characterized in terms of the shape factor of the layer, defined by

S = shape factor of the elastomer layer

$$= \frac{\text{loaded area}}{\text{perimeter area free to bulge}} \tag{1-1}$$

For a rectangular bearing,

$$S = \frac{LW}{2t(L+W)} \tag{1-2}$$

where

L = length of the bearing, parallel to the span of the bridge

W = width of the bearing, measured perpendicular to the length.

The definition of shape factor given in Equation (1-1) is expressed in terms of the gross bearing dimensions. As described in Section 2.2.4.1, a definition based on effective dimensions was found to correlate better with computed strains, and is used in the design procedures.

The shape factor defines the thinness of the layer compared with its lateral dimensions. For an infinitely wide strip bearing, W is infinite and $S = L/2t$. For a square, $S = L/4t$, and for other rectangular shapes, S lies between those two bounds. Common bearings have S in the range $3 < S < 8$. The shape factor also provides a useful basis for normalizing the compressive stress, since the shear strain caused by compression is, according to small displacement theory, directly proportional to σ/GS. Increasing S therefore increases the axial stiffness and strength, but it reduces the ability of the bearing to accommodate rotation.

These opposite tendencies may cause a dilemma in design. A larger bearing with a higher shape factor would carry the axial load better, but it would reduce the bearing's ability to accommodate rotations. It is worth noting that such design involves the use of a mixture of force and displacement loadings and this combination presents challenges. The axial load is a force yet the rotation is a displacement. Designing for both simultaneously requires that the bearing be stiff in compression yet flexible in rotation. That may be difficult, because the features (size, shape factor) that make it stiff in compression also tend to make it stiff in rotation.

Rubber is not completely incompressible, and for high shape factor bearings the slight compressibility affects the stiffness in response to both axial load and rotation. It has the greater effect on axial stiffness. The effect can be captured in the small-displacement, linear theory by means of the compressibility index, λ, developed in Stanton and Lund (2006). It characterizes the extent to which the slight compressibility of the material affects the stiffnesses, and appears naturally in the closed form equations for them. It is defined by

$$\lambda = S\sqrt{\frac{3G}{K}} \tag{1-3}$$

where

K = bulk modulus of the rubber, and

G = shear modulus of the rubber.

Gent's linear, small-deflection theory has another major attraction. The assumption of linear behavior implies that the Principle of Superposition is valid, which allows strains from different load cases to be added directly. This vastly simplifies the calculations.

Many bearings, such as those in Figure 1.1, support the girder by direct bearing and do nothing to prevent it from lifting off should upward load occur. Such separation of the girder from the bearing is referred to in this report as lift-off. This configuration is common in concrete bridges, for which elastomeric bearings have been used for many years. It may be due to the difficulty of making a tension connection between the concrete and the rubber. Other bearings are fabricated with bonded external plates that permit bolting or welding to the support or girder. These are commonly used in steel bridges, in which the bearings have traditionally been made of steel and for which a tension attachment has been obligatory. With such bearings the girder cannot lose partial contact with

the bearing. If large rotations occur, one side of the sole plate experiences net upward movement, the bearing necessarily follows and the elastomer experiences direct tension. That is referred to here as uplift. The two configurations give rise to two distinct behaviors.

When no tension connection exists between the bearing and girder, the pattern of deformations in the rubber changes after lift-off starts. Prior to lift-off, the system is approximately linear. After lift-off, it becomes a contact problem in which the boundary conditions at the loaded surface change as the loading progresses. The problem is thus inherently nonlinear. From an analysis viewpoint, this creates complications that require the use of approximations if reasonably simple design equations are to be developed.

In a bearing with externally bonded steel plates, the bearing is forced to follow the rotation angle dictated by the girder or sole plate, even if it results in local tension stress and strain in the rubber on the tension side. The local tension stress may result in hydrostatic tension, which in extreme cases can cause the rubber to suffer sudden, brittle, internal rupture (Gent and Lindley, 1959b). The process is somewhat analogous to the brittle fracture of a weld if the surrounding metal provides 3-dimensional restraint. Such rupture is likely only under axial uplift loading or when the loading consists of a light compressive load and a large rotation. Axial uplift is rare, occurring primarily in continuous bridges or in some skew or curved bridges. Light axial load plus large rotation is more common and may occur when the girder is first set and the full camber is still present. That problem is most likely to be encountered in steel bridges, for which the girder self-weight is a relatively small fraction of the final load, and for which a bearing with external bonded plates is more likely to be specified.

Prevention of internal rupture should be a design consideration. In the existing AASHTO Design Specifications internal rupture is prevented by the provisions that completely disallow uplift or lift-off, so no explicit calculation of the hydrostatic tension stress is required.

One more potential failure mode exists. The bearing may become thick enough that instability affects their performance. By the standards of steel columns, bearings are very short and squat, and the possibility of buckling appears remote. However, as with other aspects of their behavior, the layered construction and the very low shear modulus of the rubber combine to render conventional thinking invalid. Stability *is* a potential problem, although only for relatively thick bearings. Analysis is complicated by the shear-flexibility of the layered system, which dramatically reduces the buckling load below the conventional Euler Load value, and because the bearing becomes thinner so the length of the column reduces as the load increases. The early analysis for shear-flexible systems was performed by Haryngx (1948), was considered by Timoshenko and Gere (1961) for helical springs, specialized for linear analysis of laminated bearings by Gent (1964), and modified for nonlinear behavior in bearings by Stanton et al. (1990).

Stability criteria come into play if design rotations are large. Then the bearing needs to be thick in order to reduce the rotation per layer and the corresponding shear strain due to rotation. However a bearing that is too thick will become unstable. It also is relevant to the selection of a minimum length for the bearing. Quite often the bearing is made as wide as possible (transverse to the bridge axis) to prevent lateral-torsional buckling of the girder during construction (for example, Mast 1989). Then only a short length is needed to provide sufficient bearing area for supporting the axial load. However, too short a length would again risk instability. In such bearings, the axial stress may therefore be significantly lower than the limit because of the indirect influence of stability requirements.

1.4 Current Design Specifications

The AASHTO LRFD Bridge Design Specifications, 4th Edition, Section 14 pertains to bridge joints and bearings and contains two design methods for elastomeric bridge bearings: Method A and Method B. Method A is very simple and has tighter limits on stresses, while Method B requires a more detailed design but allows for greater loads. It also is associated with more stringent testing procedures.

1.4.1 Method A

Method A specifies that shear modulus of the elastomer should be between 0.080 ksi and 0.250 ksi, and nominal hardness should be between 50 and 70 on the Shore A scale, and all other physical properties should conform to ASTM D 4014.

The service level axial stress is limited by

$$\sigma_a \le 1.0GS \tag{1-4}$$

and

$$\sigma_a \le 1.0 \text{ ksi} \tag{1-5}$$

where

σ_a = the average axial stress, and
G = the shear modulus of the elastomer.

(The terminology used here is intended to be consistent within the report, and in some cases differs slightly from that used in AASHTO.) This stress can be increased by 10% if the bearing is fixed against shear displacement. The shear deflection is governed by

$$\Delta_s \le \frac{h_{rt}}{2} \tag{1-6}$$

where h_{rt} is the total thickness of elastomer. To ensure that lift-off is prevented, the rotation and axial stress must satisfy

$$\sigma_a \geq 0.5GS\left(\frac{L}{h_{ri}}\right)^2 \frac{\theta_x}{n} \quad (1\text{-}7)$$

where

θ_x = the rotation applied to the bearing about the x-axis,
h_{ri} = the thickness of one rubber layer, and
n = number of internal rubber layers

Lastly, the length and width of the bearing must each be greater than three times the total thickness to prevent instability.

1.4.2 Method B

Method B specifies that shear modulus of the elastomer should be between 0.080 ksi and 0.175 ksi, and nominal hardness should be between 50 and 60 on the Shore A scale. All other physical properties should conform to ASTM D 4014.

For bearings subject to shear deformations, total axial stress is governed by

$$\sigma_a \leq 1.66GS \quad (1\text{-}8)$$

and

$$\sigma_a \leq 1.60 \text{ ksi} \quad (1\text{-}9)$$

The live load stress also is required to be less than 0.66GS. Total load stress limits are increased to 2.0 *GS* and 1.75 ksi if shear displacement is prevented. The limit for shear displacement, Δ_s, is identical to that in Method A.

Combinations of axial load and rotation are governed by the need to prevent lift-off and to avoid excessive shear strain on the compressive side of the bearing. The requirement for prevention of lift-off is based on previous studies. Caldwell et al. (1940) studied fatigue of small rubber coupons, and the results suggest that the rubber fatigues much more readily if the strain changes direction during cycles of load. Roeder et al. (1987) conducted fatigue tests on bearings loaded (separately) in shear and compression, and the present AASHTO Design Specifications are based on those results, at least partly. However, prior to this study, no extensive investigation had been made of the effects of cyclic rotation on elastomeric bearings.

The governing equation for prevention of lift-off is

$$\sigma_a \geq 1.0GS\left(\frac{L}{h_{ri}}\right)^2 \frac{\theta_x}{n} \quad (1\text{-}10)$$

and for preventing excessive shear strain on the compressive side

$$\sigma_a \leq 1.875GS\left[1 - 0.2\left(\frac{L}{h_{ri}}\right)^2 \frac{\theta_x}{n}\right] \quad (1\text{-}11)$$

These two equations bound the axial stress. Any stress/rotation pair lying between them will neither lift off nor cause excessive local compression.

These two equations do not distinguish explicitly between bearings with and without external plates. They do not need to, because the no-uplift condition mandated by Equation (1-10) ensures not only that the stresses on the compressive side can be computed without the need to consider the geometric nonlinearity caused by lift-off, but also that hydrostatic tension will never occur in a bearing with external plates. This is a simple and effective solution to avoiding those problems, but it proves to be unduly restrictive in some cases, in which it prevents the engineer from finding a design that meets all the requirements simultaneously. The only options are then to turn a blind eye to some code provisions or to use a different type of bearing.

Method B also includes detailed requirements for stability of the bearing.

1.5 Motivation for this Study

The present bearing design rules were introduced in the 1st edition of the AASHTO LRFD Specifications, in 1994. They have been modified slightly in the intervening years, but never subjected to wholesale review. During that time, several drawbacks have come to light:

- The equations governing combined loading in Method B prove to be unrealistically restrictive. In particular, the no uplift requirement of Equation (1-10) introduces difficulties for construction conditions. In a steel bridge, girder self-weight plus a large camber might result in an axial compressive stress of only 100 psi, plus a rotation of 0.04 radians. To prevent lift-off under these circumstances, the bearing has to be very thick, but it may then violate the stability requirements. Many engineers believe that temporary lift-off under these circumstances is unlikely to damage the bearing, and that a bearing with no external plates would in reality provide a good solution, even though it would be disallowed by the present specifications.
- In some cases the requirements of Method A allow a bearing that would not satisfy the Method B requirements.
- In some cases, a design that has been used by a state for many years does not satisfy the AASHTO specification requirements, yet it has given good service without problems.
- The absolute stress limit of 1.6 ksi and 1.75 ksi and the combined stress equations in Method B impose restrictions that are perceived as unnecessarily severe for design of unusual or high-load bearings.

The existing design rules for combined loadings were developed without the benefit of a rotation testing program, for which resources were unavailable at the time. Investigating the effects of fatigue, and the need to avoid lift-off or uplift in bearings, was not possible, so the conservatism in the rules is understandable and appropriate. Because of the cost-effectiveness of elastomeric bearings, and their good service over many

years, AASHTO determined that rotation of those bearings warranted further study, with the intent of proposing updated design provisions that would address the problems outlined above.

1.6 Previous Studies

Elastomeric bearings were developed for commercial use in the 1950s, although references exist to earlier developments, and a good summary of general research and practice up to 1980 is provided in NCHRP Report 248. Further work, on low temperature and experimental studies of fatigue loading under compression, was reported in NCHRP 298 and 325. More recently, studies were conducted on low-temperature behavior and on the effects of various materials tests, and were reported in NCHRP 449.

Many experimental studies have reported on elastomeric bearing behavior and design. The great majority have addressed compression with or without shear (for example, for seismic isolation applications), but very few have been devoted to rotation. The main reason is believed to be that designing, developing, and building a suitable test apparatus is difficult and expensive. (The researchers know of one only other machine, in Germany, but it automatically imposes a shear displacement simultaneously with the rotation.) One of the few investigations devoted to rotation was conducted by Lund (2003), who conducted analytical and experimental studies on the rotation stiffness of bearings for the purpose of determining its effect on the lateral stability of long bridge girders during transportation and erection. However, cyclic loading, damage, and fatigue in the bearings were not studied.

Considerable effort has been devoted to developing FEA approaches that can address the many difficulties posed by analysis of rubber. The Ogden family of constitutive models (Ogden 1984) provides a versatile basis for modeling rubber, and many authors have conducted analyses of bearings, particularly under compressive loading (for example, Simo and Kelly, 1986; Seki and Fukahori, 1989; Bradley, Taylor, and Chang, 1997; Imbimbo and De Luca, 1998, and so forth). Herrmann and his research team also developed some composite models that average the stiffness of the rubber and steel reinforcement over the whole domain in order to permit more economical analyses (for example, Herrmann et al., 1988).

1.7 Survey of Practice

At the start of this research study, a telephone survey of states and manufacturers was conducted. It is reported in detail in Appendix B and is summarized here. Follow-up visits were conducted to states or manufacturers that had provided responses that were unusual or particularly enlightening. The questions focused on:

- How often elastomeric bearings were used,
- What design methods were used,
- What type of rubber was used (neoprene or natural rubber),
- The manufacturer(s) from which bearings were usually purchased,
- Any field issues that have occurred, and
- Any design problems caused by rotation requirements.

Responses were eventually received from 46 states. They revealed that elastomeric bearings are the bearings of choice in the overwhelming majority of applications and states. Engineers appreciate their economy, but also like the bearings and regard them as forgiving. The majority of states use Method A for design. One common reason is that many bearings are located in freeway overpasses, for which prestressed concrete girders are widely used. The bearing is made (nearly) the same width as the bottom flange of the girder to promote lateral stability of the girder during erection. This criterion essentially decides the dimensions of the bearing, which prove to be large enough to keep the stress relatively low. Method B is unnecessary for such bearings.

The most common design problem reported by the states was with rotation, and particularly with load combinations that include light axial load and large rotation. Some agencies also reported field problems with bearings slipping out of place.

Four manufacturers dominate the U.S. market for laminated bearings: DS Brown (Ohio), Dynamic Rubber/Cosmec (Texas), Scougal Rubber (Washington), and Seismic Energy Products (Texas). Considerable geographic diversity was found in their sales patterns. Some states did not know which manufacturer provided most of their bearings because the supplier is chosen by the main bridge contractor.

1.8 Goals, Scope, and Organization of Report

The primary goal of this research was to propose improved design provisions for rotation to be considered for use in the AASHTO LRFD Specifications. To reach this goal, it was necessary to conduct physical tests and numerical simulations of bearings, from which a better understanding of their behavior could be obtained. Secondary goals included a review of quality assurance/quality control (QA/QC) procedures for manufacturing and installing elastomeric bearings.

The details are in Appendices A-G. The main chapters of the report provide summaries of the work described in the appendices. Chapter 2 contains the primary findings of the report, the interpretation of them is in Chapter 3, and the conclusions are found in Chapter 4.

CHAPTER 2

Findings

2.1 Physical Testing

A comprehensive test program was conducted to evaluate the performance of elastomeric bearings under static and dynamic rotation. Seventy-eight bearings were tested in seven major test series. Table 2.1 summarizes the major test series, and the complete test matrix is presented in Table 2.2.

Table 2.1 provides a brief overview of the seven test series included in the study. Most test bearings were 9 in. × 22 in. steel-reinforced elastomeric bearings, approximately 2 in. thick overall, with a shape factor of approximately 6. The bearings were made of Neoprene with a Shore A durometer hardness of approximately 50. The use of a standard bearing permitted:

- Consistent evaluation of theories and design models,
- Comparisons of bearings produced by different manufacturers and manufacturing methods, and
- comparisons of the effects of different loads and deformations.

Discussion with elastomeric manufacturers showed that this 22 in. × 9 in. bearing is the most commonly manufactured size in the United States. It is the standard bearing for the state of Texas, which uses many thousand of these bearings each year, and is commonly produced by all major manufacturers. The size is suitable for medium-span bridges with moderate movements and rotations, so it provided a good basis for the research study. However, additional bearings of different shapes, sizes, shape factors, and material properties were tested to provide a broad basis for the experimental investigation.

Each bearing was carefully inspected before testing. An individual test required a minimum of several hours and a maximum of several weeks to complete. Electronic instruments were used to monitor the bearing throughout each test, but each bearing also was inspected visually and manually at intervals throughout each test. PMI series tests were usually completed in one day, but all other tests included cyclic rotation and lasted longer. The longest test (CYC15) lasted more than 2 weeks.

The bearings in this test program were subjected to rotations much larger than currently permitted in design or expected under normal bridge service conditions in order to accelerate the onset of damage. This procedure was adopted to shorten each individual test and to permit a larger number of different tests to be conducted. Had the researchers applied realistic rotation levels to the bearings, each test would have required many millions of cycles, and the test program would have lasted many, many years.

The cyclic rotation rate was selected to be as fast as possible without introducing spurious effects on the bearing response. A pilot test program was first carried out to investigate the rate of heat build-up. The data gathered was used to construct a thermal analytical model that related temperature rise to bearing geometry, rotation amplitude, and frequency. The model was used to determine suitable rotation frequencies that would permit the main testing to be conducted as rapidly as possible while limiting the temperature rise of the bearing.

A complete, detailed description of each test cannot be provided here because of the large volume of test data. However, Appendix A and Appendix D provide significant detail on each test and more detailed interpretation of the test results. Appendix A provides summary information on the properties and characteristics of each individual test. Plots of force-deflection, moment-rotation, bearing deformation, progression of damage, and deterioration of resistance and stiffness are provided for each specimen. Specific data values at key points of the tests are tabulated. Appendix D contains more detailed comparisons, analyses, and evaluations of the test data and identifies trends in behavior. It contains initial conclusions regarding test results, and these conclusions are combined with the analytical studies to develop final design recommendations. Appendix C provides details of the test apparatus and procedures.

A full battery of material property and quality control tests was required of the manufacturer for each bearing purchase.

Table 2.1. Summary of the test series.

Series	Type of test	No. of specs.	Primary goals of tests
PMI	Monotonic or cyclic compression. Some with static rotation.	24	To develop an interaction diagram for failure under monotonic axial force and moment. ("P-M Interaction").
CYC	Tests with constant axial load and cyclic rotation.	29	Establish relationship among static axial load, cyclic rotation, number of cycles and damage level.
MAT	As CYC tests, but different materials.	3	Determine effect of material properties on resistance to combined axial load plus cyclic rotation.
SHR	As CYC tests, but with constant shear deformation added.	6	Determine effect of shear displacements on resistance to combined axial load plus cyclic rotation.
SHF	As CYC tests, but with different S.	6	Determine effect of shape factor on resistance to combined axial load plus cyclic rotation.
ASR	As CYC tests, but different aspect ratio.	4	Determine effect of bearing geometry on resistance to combined axial load plus cyclic rotation.
PLT	As CYC tests, but shims have various edge profiles.	6	Determine effect of shim plate edge treatment on resistance to combined axial load plus cyclic rotation.

Additional tests were performed at the University of Washington on some bearings to evaluate material properties and estimate the deterioration in performance at various times during the tests. They are summarized in Appendix D.

The progression of tensile debonding, followed by shear delamination failure, is illustrated in Figure 2.1 through Figure 2.4. (The initial debonding is quite difficult to see in Figure 2.2, but occurs in the foreground, where two discrete bulges have coalesced into one.) Those figures illustrate the difficulty in distinguishing from outside the bearing between tensile debonding and shear delamination.

The tests showed that limited debonding does not have a significant or immediate impact on bearing performance, but delamination develops in the presence of large or repeated shear strains. If delamination becomes severe, as illustrated in Figure 2.3, it adversely affects the service performance of the bearing to the extent that the bearing may be considered to have failed. Thus, while limited debonding is tolerable, extensive delamination requires replacement of the bridge bearing. The extent of both debonding and delamination increases with increasing numbers of rotation cycles, and their rates of propagation are higher, with larger cyclic rotations or larger compressive loads. The growth is illustrated in Figure 2.4.

The tests showed that large shear strains associated with rotation, compressive load, and shear deformation combine to cause delamination of the bearing. Repeated cycles of shear strain also were found to be significantly more damaging than constant shear strains of the same magnitude. The number of cycles required to achieve a given damage level decreases with an increase in the cyclic strain level. However, considerable scatter was evident in the results, especially among the different manufacturers. For example, Figures F-24 and F-25 in Appendix F show that the bearing from Manufacturer B performed the best in test CYC09 but not in test CYC11. However, despite this scatter, the effects of the amplitude and number of the cyclic strain cycles remain the dominant influence on the accumulation of debonding damage.

These parameters characterize the loading aspect of the equation. The resistance side is characterized by the material properties, shape factor, and plan geometry of the bearing. A higher shape factor is predicted to improve axial load capacity by reducing the shear strain for a given load. This prediction was borne out in the tests. The improvement in performance with shape factor was even better than predicted, but the number of high shape factor tests was too small to permit development of a better theory to explain this result.

The manufacturing process, and particularly the treatment of the edges of the shims, also is important. This was first observed when testing in rotation bearings that had been specially ordered for testing in the torsion box rig described in Section C.4 of Appendix C. That rig was intended for diagnostic tests, to determine the level of debonding damage at various intervals throughout the main rotation tests. The bearings required nonrectangular shims, which were produced by machining, and that process left their edges sharp and square. Under cyclic rotation, the sharp edges caused debonding to occur faster than in the other bearings.

Table 2.2. Bearing test matrix.

Name	No.	Manufacturer/ Batch	Plan Dimensions	Aspect Ratio	Shape Factor	Material	Axial Stress	Static Rotation	Cyclic Rotation	Shear Disp.
PMI	1a	A1,A2,B1,C1,D1	9 x 22	2.44	6	CR50	step load			
PMI	1b	A1,A2,B1,C1,D1	9 x 22	2.44	6	CR50	cyclic to 8000psi			
PMI	1c	A2,B1	9 x 22	2.44	6	CR50	vary to fail	4%		
PMI	1d	A2,B1	9 x 22	2.44	6	CR50	cyclic to 8000psi	4%		
PMI	2	A1	9 x 22	2.44	6	CR50	2.5 GS	vary to 8%		
PMI	3	A1	9 x 22	2.44	6	CR50	3.5 GS	vary to 8%		
PMI	4	A1,A2,B1	9 x 22	2.44	6	CR50	3.0 GS	vary to 8%		
PMI	5	A1,A2,B1,C1,D1	9 x 22	2.44	6	CR50	4.0 GS	vary to 8%		
CYC	5	A1,A2,B1,C1,D1	9 x 22	2.44	6	CR50	5/8 P_0		6/8 θ_0	
CYC	7	A1,A2,B1,C1,D1	9 x 22	2.44	6	CR50	5/8 P_0		4/8 θ_0	
CYC	8	A1	9 x 22	2.44	6	CR50	5/8 P_0		2/8 θ_0	
CYC	9	A1,A2,B1,C1,D1	9 x 22	2.44	6	CR50	7/8 P_0		6/8 θ_0	
CYC	11	A1,A2,B1,C1,D1	9 x 22	2.44	6	CR50	7/8 P_0		4/8 θ_0	
CYC	12	A1,A2,B1,C1,D1	9 x 22	2.44	6	CR50	7/8 P_0		2/8 θ_0	
CYC	13	A1	9 x 22	2.44	6	CR50	5/8 P_0	2 ± 0.5%		
CYC	14	A1	9 x 22	2.44	6	CR50	5/8 P_0	2 ± 1.75%		
CYC	15	C1	9 x 22	2.44	6	CR50	7/8 P_0		0.005 rad	
SHR	1	B1	9 x 22	2.44	6	CR50	4.0 GS	vary to 8%		50%
SHR	2	B1	9 x 22	2.44	6	CR50	7/8 P_0		4/8 θ_0	70%
SHR	3	B1	9 x 22	2.44	6	CR50	7/8 P_0		4/8 θ_0	30%
SHR	4	B1	9 x 22	2.44	6	CR50	5/8 P_0		6/8 θ_0	30%
SHR	5	B1	9 x 22	2.44	6	CR50	7/8 P_0		6/8 θ_0	30%
SHR	6	A2	9 x 22	2.44	6	CR50	7/8 P_0		2/8 θ_0	30%
MAT	1	C2	9 x 22	2.44	6	CR60	5/8 P_0		6/8 θ_0	
MAT	2	C2	9 x 22	2.44	6	CR60	7/8 P_0		6/8 θ_0	
MAT	3	C2	9 x 22	2.44	6	CR60	7/8 P_0		4/8 θ_0	
SHF	1	C2	9 x 22	2.44	9	CR60	cyclic to 8000psi			
SHF	2	C2	9 x 22	2.44	12	CR60	cyclic to 8000psi			
SHF	3	C2	9 x 22	2.44	9	CR60	5/8 P_0		6/8 θ_0	
SHF	4	C2	9 x 22	2.44	9	CR60	7/8 P_0		6/8 θ_0	
SHF	5	C2	9 x 22	2.44	9	CR60	7/8 P_0		4/8 θ_0	
SHF	6	C2	9 x 22	2.44	12	CR60	5/8 P_0		6/8 θ_0	
ASR	1	C2	9 x 9	1	6	CR60	cyclic to 8000psi			
ASR	2	C2	9 x 9	1	6	CR60	5/8 P_0		6/8 θ_0	
ASR	3	C2	9 x 9	1	6	CR60	7/8 P_0		6/8 θ_0	
ASR	4	C2	9 x 9	1	6	CR60	7/8 P_0		4/8 θ_0	
PLT	1	A3 - sharp shim	9 x 22	2.44	6	CR50	5/8 P_0		6/8 θ_0	
PLT	2	A3 - sharp shim	9 x 22	2.44	6	CR50	7/8 P_0		6/8 θ_0	
PLT	3	A3 - deburred	9 x 22	2.44	6	CR50	5/8 P_0		6/8 θ_0	
PLT	4	A3 - deburred	9 x 22	2.44	6	CR50	7/8 P_0		6/8 θ_0	
PLT	5	A3 - rounded	9 x 22	2.44	6	CR50	5/8 P_0		6/8 θ_0	
PLT	6	A3 - rounded	9 x 22	2.44	6	CR50	7/8 P_0		6/8 θ_0	

Figure 2.1. Undamaged bearing under load.

Figure 2.2. Initial debonding of bearing.

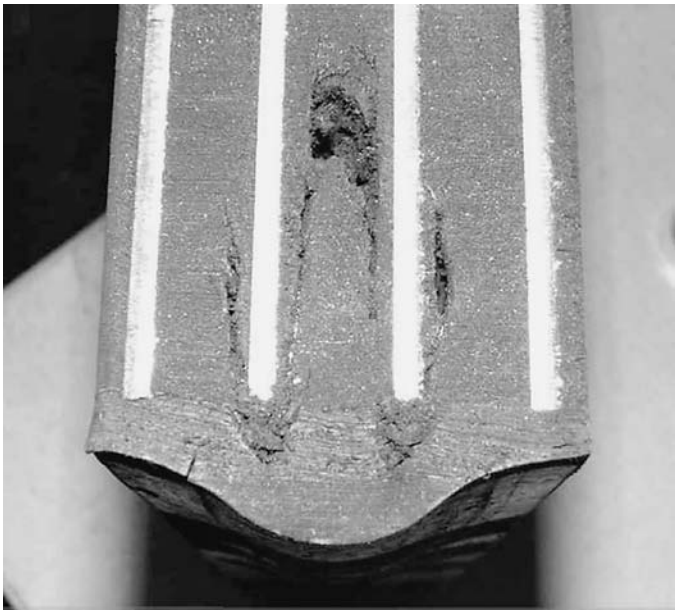

Figure 2.3. Internal damage caused by severe cyclic loading.

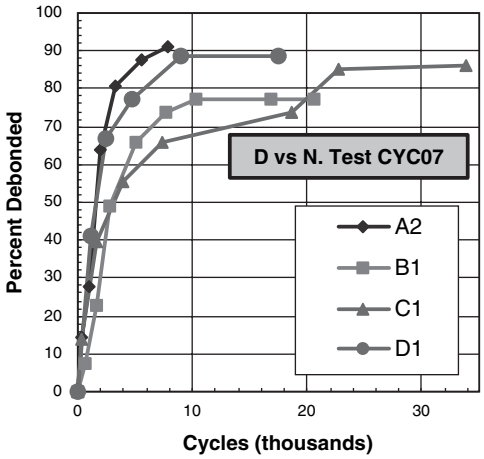

Figure 2.4. Progression of debonding with increased load cycles.

In order to isolate the effect of the shim edge shape from the effect of the nonstandard plan geometry of the shim, more bearings were ordered with standard rectangular shims, and edges prepared in three different ways: sharp and square-cut (as-sheared), deburred (using a belt-sander) or perfectly rounded (with the edge machined to a radius equal to half the shim thickness). These test results are in Figure 2.5. Deburring of the as-sheared, sharp edges leads to a significant increase in the bearing life expectancy up to about 75% debonding, but machine-rounding of the edges does not provide much additional benefit. In the figure, the relative ranking of the curves representing the different processes is important, but the absolute number of cycles is not, because the amplitude of the rotation was 0.0375 radians. That value is 10 to 30 times larger than the cyclic rotation expected in practice.

Bridge bearings experience shear strains due to rotation, compression, and shear displacements. The strains caused by shear deformations differ from those caused by rotation and compression in two respects. First, in most cases, the shear displacements are caused by expansion and contraction of the bridge deck, so the number of cycles is small compared with those induced by traffic. (In some bridges, the superstructure may be configured in such a way that truck passage causes shear as well as rotation and compression in the bearing. In that case the shear strains due to shear displacement are clearly more numerous and should be treated as cyclic loading. Theoretically, this is true in all bridges, since bending of the girders implies elongation of the bottom flange. However, in most cases the corresponding horizontal move-

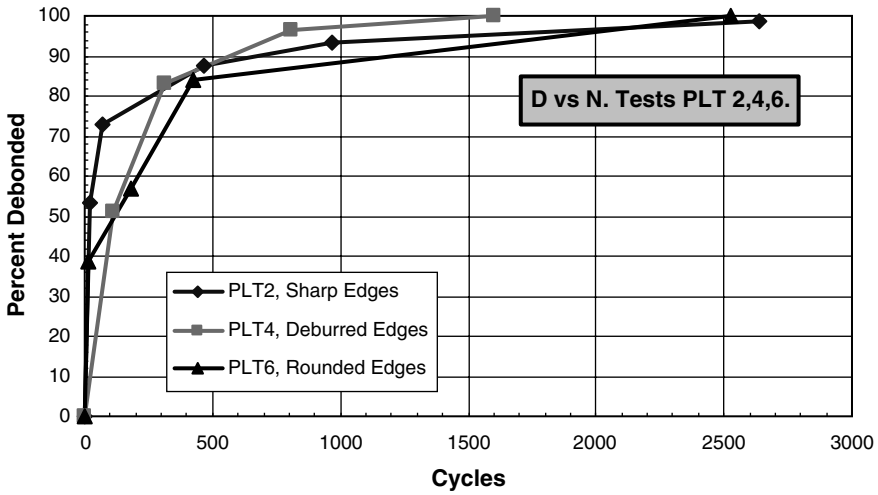

Figure 2.5. Debonding for PLT test series.

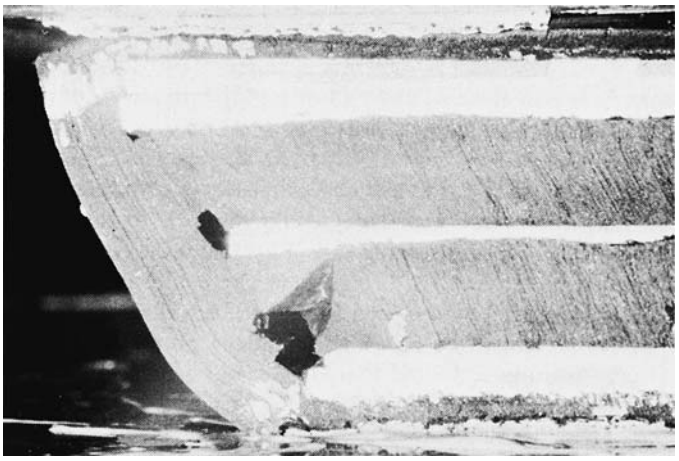

Figure 2.6. Damage due to cyclic shear displacements (from NCHRP Report No. 298).

ment causes shear deformations in the elastomer that are too small to be of much consequence.)

Second, if the shear displacements of the bearing are large, they may involve some roll-over at the end of the layer, which leads to a complex state of stress there, consisting of combined shear and vertical tension. That combination appears to promote cracking at the end of the shim, as shown in Figure 2.6, taken from NCHRP Report 298 (Roeder, Stanton, and Taylor 1987). Thus, one feature of shear displacements leads to their being less important than traffic effects, and one suggests that they are more important. However, tests conducted in this research suggest that shear displacements play only a small role and that the cyclic rotations under traffic loads are expected to be a more critical aspect of bearing design.

2.2 Finite Element Analysis

2.2.1 Objectives

The project focused mainly on the experimental investigation of the rotational behavior of elastomeric bearings and the development of suitable design procedures. This requires the identification of characteristic engineering design parameters which (1) can be measured in the experiment (directly or indirectly), and (2) lead to a simple design methodology.

FEA provides a tool to simulate structural behavior and evaluate states of deformation and stress. It is particularly valuable when internal quantities, such as stress or strain, cannot be measured. Then external quantities such as load and displacement can be measured experimentally, and FEA can be used to correlate them with local, internal quantities that are sought. However, this is possible only for a well-defined structure made of materials whose properties are homogeneous and known. The level of accuracy of the end result depends on the type of material and the quality of the available material properties. For rubber, the constitutive laws are nonlinear and complicated, and depend on many characteristic constants, some of which are not readily available. Despite this limitation, FEA was used to identify the relationship between external loads or applied displacements and rotations, and the engineering design parameters, such as shear strain, used in a design procedure. These relationships were then used to evaluate and justify simplified design equations.

The structural testing and evaluation of the experimental data identified the local shear strain γ_{zx} in the elastomer at (or near) the ends of the reinforcing steel shims as a suitable engineering design parameter. (The coordinate system is that x is parallel to the bridge axis, y is transverse, and z is vertical.) Gent and Lindley (1959a) presented a simplified linear analysis for incompressible elastomeric bearings. Stanton and Lund (2006) extended this theory for slightly compressible elastomers and rectangular shapes of all aspect ratios. Both formulations provide simple relations between axial force and average axial strain, as well as between moment and rotation. The shape of the bearings enters these relations solely through the shape factor S of its layers. The formulations also provide a convenient correlation between those global deformation measures and the local shear strain $\gamma_{zx,max}$ inside the bearing. Their linearity provides a convenient basis for a design procedure. That approach, however, utilizes superposition of responses to different loadings, and the validity of doing so has to be proven.

Appendix E presents a series of numerical simulations by which the following hypotheses will be proven to hold for common bearings:

- *Superposition* of axial and rotational effects provides a reasonably accurate representation of the response predicted by nonlinear FEA at small strain levels.
- The *stiffness coefficients* predicted by the linear theory of bearings by Stanton and Lund are in good agreement with a nonlinear FEA at small strain levels.
- The *local shear strain* predicted by the linear theory of bearings by Stanton and Lund are in good agreement with a nonlinear FEA at small strain levels.
- *Internal rupture* due to excessive tensile hydrostatic stress can only occur in bearings with bonded external plates and very low axial loads.

Proving these four hypotheses is necessary if use of the simple linear analysis approach of Stanton and Lund (2006) is to be justified in design.

A further problem arises in the effort to validate the linear model. The simplicity of that model is achieved partly by treating the bearing as uniform across the cross-section. This implies the absence of edge cover, which is present in field bearings and in the FE model. In the linear model, the critical strains occur at the outer edge. In the FE model, that location

is occupied by the cover, in which the displacement field is drastically different from that in the body of the bearing layer. It is necessary in the FE model to extrapolate the strain field from a point just inside the edge of the shim to the outer edge of the bearing, if strains in corresponding locations are to be compared. When the strain field is linear, such extrapolation is simple. When it is nonlinear, as is the case under combined compression and rotation, the exact procedure to be used for extrapolation becomes less clearly defined, and correlation of the linear and nonlinear FE models becomes more difficult.

2.2.2 Modeling Techniques

The model may be discussed in terms of three main characteristics: geometry of the model and the boundary conditions, constitutive models for the materials, and loading.

All nonlinear analyses presented in this chapter were performed using the multipurpose FEA program MSC.Marc 2003r2 by MSC software (MSC.Marc, 2003). All analyses were performed in 2-D, using a large deformation plane strain analysis in a Lagrange setting. The 2-D analysis implies an infinite strip bearing, with an aspect ratio of zero. Three-dimensional analyses could not be performed at the necessary level of refinement due to numerical instabilities of the nearly incompressible element formulation at high hydrostatic stress. The computational demands of 3-D analyses, in terms of run time and file size, are also much heavier than those of comparable 2-D analyses, and acted as a further disincentive for 3-D analysis.

Simulations of physical tests revealed that the commonly known problems of large deformation simulations of elastomers, that is, extensive mesh distortion and the potential loss of element stability, impose a serious limitation on the numerical analysis. (Element instability is illustrated by the hourglass modes visible in the right hand side of the mesh in Figure E-14 in Appendix E.) This problem is intrinsic to the element formulation for nearly incompressible materials and varies little between different software packages.

Local mesh distortions always were observed near the end of the reinforcing steel shims. When they reached a critical value, an element inverted and the analysis stopped. This limited the analysis to average stresses of $\sigma = 2$ to 3 GS and rotations of 0.008 to 0.020 rad./layer. However, these values include essentially the full range relevant to practice.

When the loading caused hydrostatic tension stresses, hourglass modes occurred (for example, Figure E-14 in Appendix E) and eventually caused the analysis to become unstable. However, reliable results were available for hydrostatic tensile stresses (that is, positive values of mean normal stress) up to $\sigma = E \approx 3G$, where G is the shear modulus and E is Young's modulus. This is approximately the magnitude described by Gent and Lindley (1959b) for the onset of internal rupture. Hence, the FEA model can be used to evaluate hydrostatic tension stress up to the level corresponding to rupture in real bearings.

2.2.2.1 Geometry and Boundary Conditions

Figure 2.7 shows the geometry and the typical FEA mesh for a 3-layer bearing with $S = 9$. (Symmetry allows only the top half of the bearing to be modeled. The figure is also not to scale.) Reference Point A is the point at which shear strains are evaluated for comparison with those predicted by the linear theory. Due to the applied rotation, the model possesses only one symmetry plane. More detail on the meshes used is available in Section E.2 of Appendix E.

Bearings with rigid top and bottom plates were modeled using the same mesh and loading, but the interface properties were changed from frictional contact to glue. This permanently attached the bearing surface to the rigid loading surface and allowed identical load histories to be applied to bearings with and without rigid end-plates.

2.2.2.2 Materials

The elastomer was modeled as a nonlinear, elastic, nearly incompressible material. Bearing manufacturers typically report Shore A hardness, elongation at break, and nominal stress at failure, but these properties alone do not uniquely define the material. This presents a challenge because it allows some variability on the manufacturer's side, and leads to a problem for the analyst of nonuniqueness of material

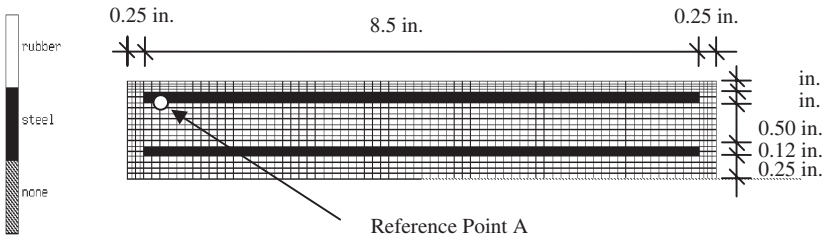

Figure 2.7. Geometry and FEA mesh for a strip bearing with S = 9.

parameters. Following a suggestion by the project Advisory Group, the simplifying assumptions by Yeoh (1993) were adopted. The shear modulus G was estimated from the hardness. It was later confirmed by shear tests performed on elastomer samples extracted from the bearings tested in the laboratory. The bulk modulus K was estimated from Holownia (1980) and was later verified through a similar process.

Parameters for Yeoh's model were calibrated to match these values and an appropriately scaled representative stress-strain curve for rubber taken from Yeoh (1993). Yeoh's model can be represented as a subset of the generalized Mooney model (Ogden 1984) which is available in MSC.Marc2003r2.

2.2.2.3 Loading

One major consideration of creating the model was how to portray the loading conditions realistically. In all the physical tests the bearing was placed between two metal plates to ensure uniform loading. To simulate the experimental conditions the loading plates were represented using rigid surfaces and frictional contact between these surfaces and the bearings. The coefficient of friction used was 1.0.

The motion of the rigid loading surface can be controlled in the simulation by defining the position (or velocity) of a reference point on the surface and an angle (or angular velocity) to identify its orientation. This requires the loading to be displacement-controlled rather than load-controlled. The loading of the bearing was composed of slow axial compression to various levels of average axial strain, ε_a, followed by rigid body rotation of the loading surface. Forces and moments on the loading surface, as well as local strain and stress measures, were recorded for each load history.

2.2.3 Analyses Conducted

Bearings of various shape factors were considered in the numerical analysis. The most representative bearings were those with a cross section similar to the 9 in. × 22 in. bearings with S = 6 that were tested in the experimental program. Analyses were conducted on plane strain, 2-D models, which correspond to infinite strips, so either the shape factor or the layer dimensions could be kept the same, but not both. Most of the analyses were made with t = 0.75 in. which gives S = 6, but some also were conducted using layer thicknesses of 0.50 in. and 0.375 in., which correspond to S = 9 and S = 12.

The load histories were characterized by the normalized load intensity σ / GS and the imposed rotation per, θ_L. All combinations of shape factors (6, 9, and 12) and load histories were carried out until excessive mesh distortion near the ends of the shims or the presence of hourglass mode patterns caused the analysis to fail. For most bearings, reliable analyses were possible within the range of $0 < \sigma / GS < 2$ and $0 < \theta_y < 0.006$ rad./layer. Depending on axial load intensity and applied rotations, some analyses could be performed beyond that domain. These were used to verify conclusions drawn based on the reduced data set. However, these extended analyses did not support an extended parameter domain but rather represent subdomains with tighter restrictions on achievable rotations outside the confidence domain.

Several analyses were performed to help understand effects of imperfect seating or non-parallel bearing surfaces on the observed test data. These simulations are not documented in Appendix E since they do not contribute independent knowledge. However, they were very helpful for the identification and interpretation of initial loading effects.

All bearings were analyzed separately as (1) bearings with the potential for lift-off and (2) bearings with bonded external plates. From the analysis perspective, the first set of analyses allowed the rigid loading surface to separate from the bearing, using the friction interface property. Postprocessing was performed to identify the amount of lift-off, its effect on the local strain distribution, and maxima of local shear strain. The second set of analyses treated the bearings as permanently attached to the loading surface. These analyses were used to investigate the hydrostatic tensile stresses identified by Gent and Lindley (1959b) as responsible for internal rupture.

2.2.4 Results

2.2.4.1 Evaluation and Validation of Stiffness Coefficients

Gent and Meinecke (1970) demonstrated that axial stiffness and rotational stiffness of bearings can be expressed in terms of shear modulus G and shape factor S. Introducing four coefficients A_a, B_a, A_r, and B_r yields the following relations for the equivalent Young's modulus for axial stiffness (in the z-direction)

$$E_a A = 3G\left(A_a + B_a S^2\right)A \tag{2-1}$$

and the effective Young's modulus for bending stiffness about the y-axis

$$E_r I = 3G\left(A_r + B_r S^2\right)I \tag{2-2}$$

Stanton and Lund extended the formulation for slightly compressible material and proved that by properly adjusting the stiffness coefficients, the general form of Equations (2-1) and (2-2) remains valid. They also adopted Gent and Meinecke's assumption that $A_{az} = A_{ry} = \frac{4}{3}$ for all strip bearings. In their analyses, they included the effects of the slight compressibility of the elastomer by defining the Compressibility Index, λ,

$$\lambda = S\sqrt{\frac{3G}{K}} \tag{2-3}$$

and making the coefficients such as B_a functions of λ. In Equation (2-3), G is the shear modulus, K is the bulk modulus of the elastomer, and S is the shape factor.

Figure 2.8 shows the coefficients that relate the characteristic mechanical quantities. The left side of the figure shows the variables used for axial analysis, and the right side addresses rotation, or bending. The first circle contains the global force loading (σ/GS or M), the second shows the corresponding global displacement, and the third defines the peak internal local strain ($\gamma_{zx,max}$, with superscript ε or θ to indicate the loading that causes it). These local shear strains from the two loadings are superimposed in the linear theory, and it is the validity of that process that is evaluated here using FEA. The symbols next to the arrows indicate the dimensionless coefficients defined in the linear theory that relates the quantities in the circles. The typical design input is the average load intensity, σ / GS, and the total rotation θ_y (or rotation per layer θ_L). The average axial strain ε_a or the applied moment M also may be used as input values, but their use is uncommon in practice.

The aim of this section is to back-calculate these coefficients based on numerical results from nonlinear FEA. This provides insight into both the potential model error of the linear theory by Stanton and Lund (2004) and the significance of nonlinearity over the common load range for elastomeric bearings. Details of the analysis are provided in Section E.3 of Appendix E.

2.2.4.1.1 Summary for the axial stiffness coefficient B_a. The stiffness coefficient B_a was evaluated for bearings with $S = 6$, 9, and 12. These shape factors are nominal values computed using the total length of the bearing (9.0 in.). The analytical equations by Stanton and Lund (2006), however, are based on bearings without edge cover. To evaluate the significance of the cover layer for the computation of the axial stiffness of a bearing, B_a was back-calculated from the FEA results using Equation (2-1) and three different ways of defining the shape factor:

- Using the total length of the bearing, that is, including the cover layer ($L = 9.0$ in),
- Using the length of the shim ($L = 8.5$ in), and
- Using the average of shim length and total length of the bearing ($L = 8.75$ in).

These three different definitions of S lead to three different back-calculated values for B_a. Figure 2.9 compares the three B_a values obtained from the FEA (see Figures E-11 through E-13 in Appendix E) with one taken from linear theory (see Figure F-3 in Appendix F) for λ. The value of B_a computed from the FEA changes with the mesh size used in the FEA, the way that L is defined, and the compressive stress. The mesh size effect is essentially an error in FEA, so the mesh used was the finest practical, and was the same for all three definitions, so it is expected to make little difference in the comparison. The load level has an effect on the comparison because the load-deflection curve is nonlinear, so the value of the secant stiffness depends on the stress applied. Thus, in Figure 2.9 the relative error is presented both at zero load and at $\sigma = 1.0$ GS, and six curves are shown (three nominal shape factors and two different load levels).

If the objective of the comparison is to determine whether the linear theory is correct, the comparison should be made at zero load, which represents as closely as possible the assumption of infinitesimally small displacements that underlies the theory. If the objective is to find a value of B_a that provides the best match for design purposes, the comparison should be made at the design load level. And that varies from bearing to bearing. The approach adopted here was to address separately the errors due to geometric modeling (that is, can the linear model without cover model the real bearing with cover, under linear conditions?) from the errors associated with constitutive laws (linear versus nonlinear stress–strain relationships). Thus the best match was selected using zero load, and was found to occur when the length of the

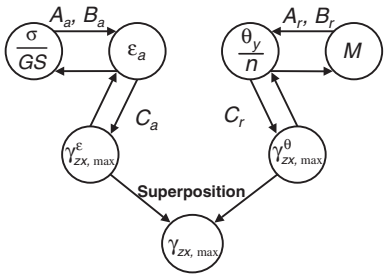

Figure 2.8. Relation between engineering quantities and coefficients for the linear analysis by Stanton and Lund (2006).

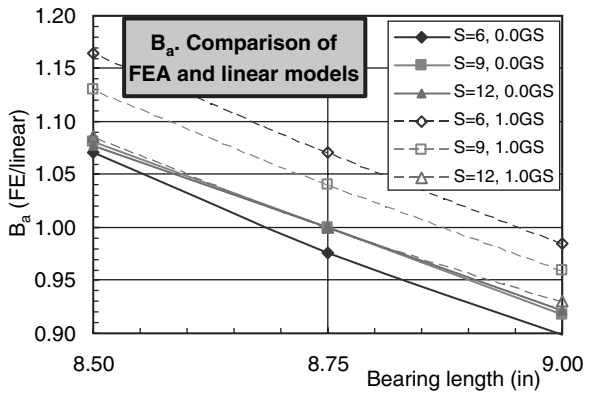

Figure 2.9. Stiffness coefficient B_a for various S, based on various definitions of L.

bearing was taken as the average of the gross length and the shim length.

Nonlinear effects also were found to become less important as the shape factor increased. No significant nonlinear effect was observed for SF 12. This behavior is attributed to the fact that the displacement field is different in the core of the bearing, where it is nearly parabolic, and near the edge where it is highly nonuniform. The nonuniform, outer displacement field penetrates about one half a layer thickness back from the edge of the shim. This distance can be expressed as (0.5/S) of the half-width of the bearing, which implies that the influence of that region decreases for larger *S,* as was observed in the FEA.

2.2.4.1.2 Summary for rotational stiffness coefficient B_r. The rotational stiffness coefficient B_r was analyzed for four different combinations of axial compression and simultaneous rotation. Back-calculation was performed for the same three definitions of the shape factor that were used for axial loading. The question of the conditions under which the comparison should be made is similar to that faced with the axial loading, except that an additional complication is present. The analyses were conducted by applying an axial displacement first, which then was held constant while the rotation was applied. Different axial loads were used in the four analyses, thereby presenting a larger variety of conditions under which the comparison could be made. For the same reasons used in the B_a comparison, the analyses were compared at zero axial load and low rotation (Figures E-15 through E-17 in Appendix E). Again, the best match was found when L was defined as the average of the gross and shim dimensions, and S was computed from it. Furthermore that match was essentially perfect. This finding is convenient for development of a design method, because it allows a single definition of L to be used for all loadings. That definition was used in the subsequent development of design procedures (Appendix F), and in the proposed specifications (Appendix G).

2.2.4.1.3 Shear strain coefficient C_a for axial loading. In linear theory, the shear strain due to axial force is obtained using the coefficient C_a defined in Equation (F-21) of Appendix F. Stanton and Lund (2006) used linear theory to compute values of C_a for different bearing geometries and compressibility indices, and their values are presented in Figure F-4. Comparable FEA values were obtained by taking the local shear strain predicted by the FEA and solving Equation (F-21) for C_a, knowing the average axial strain, ε_a, and the shape factor, S. The difference between the values obtained by FEA and linear theory was found to be less than 7.5% in all cases. The difference is attributed to the error introduced by the simplifying assumption of an isotropic stress state in the linear analyses versus a general stress state under plane strain conditions in the FEA.

The relatively small model error justifies the use of theoretical relations for the definition of design strains.

2.2.4.1.4 Shear strain coefficient C_r for rotation loading. Due to extreme but local mesh distortion, the numerical analysis could not provide the local shear strain at the very end of the shim. (See Appendix E for a detailed discussion of the issue.) Instead, the shear strain at a distance of ¼ in. in from the end of the shim was recorded from the FEA and extrapolated to the end of the shim. This location corresponds to a distance of a half layer thickness in from the shim end for the bearing with $S = 9$. The distribution of shear strain along the shim is parabolic rather than linear, which makes the extrapolation difficult and subject to error. The extrapolation can be based on the location of zero shear strain along the shim, but for load combinations other than pure rotation, that point moves as the imposed rotation changes, introducing significant uncertainty and hence error to the procedure.

Due to the unreliable nature of the extrapolation procedure outlined in Section E.4.4 of Appendix E, analyses for bearings with different shape factors were not conducted. Instead, an alternative procedure was developed to verify the basic hypothesis that use of superposition results in an acceptably small error. This procedure and the results obtained are discussed in detail in Section E.5 of Appendix E.

2.2.4.1.5 Effect of lift-off on local shear strain. If lift-off occurs, it affects the relationship between local shear strain and applied rotation. The behavior was studied by analyzing load combinations for which an axial load is applied first, and then is held constant while the rotation is applied. Force, moment, local strain, and length of lift-off were recorded.

In the unloaded region of the bearing, that is, the region where the lift-off occurs, the shear strain remains small and approximately constant after the start of lift-off. By contrast, the loaded region experiences a significant increase in shear strain. Because the dimensions of the loaded area change with the applied rotation, by definition the behavior is geometrically nonlinear.

In the FEA, both the axial and rotation components of the loading were displacement-controlled. This approach reduces the amount of iteration that would otherwise be necessary in the analyses and reduces the run times. However, the use of applied displacements in a geometrically nonlinear problem leads to nonconstant axial loads. This caused the FEA to underestimate the amount of lift-off compared with what would be seen under conditions of constant load, which are the ones likely in practice. Despite this difference between test and analysis, the FEA provided an understanding of the mechanism of lift-off and aided the development of the simplified semilinear formulation for design of bearings with lift-off, as described in Appendix F.

2.2.4.1.6 Local effects at the ends of the steel shims. Various levels of mesh refinement were applied to study local effects near the end of the steel shims. The shim itself remained elastic and almost rigid throughout the analysis. Very large strains were observed in the elastomer locally near the edge of the shim. If linear analysis were to be conducted, the sharp edge of the shim would introduce a singularity. The numerical simulation would predict a finite rather than infinite value of stress there, but its magnitude would increase as the mesh size was reduced. The shape of real edges of shims varies between manufacturers from sharp cuts (as-sheared) to slightly rounded (with a deburring tool or belt-sander). Both numerical limitations and variability of the real product require some special consideration when analyzing and comparing numerical data and results from a linear analysis. This subsection contains a brief discussion of special phenomena observed at the ends of the steel shims.

At high axial strains or applied rotations, the effect of outward expansion of the elastomer becomes the dominant mechanism in the vicinity of the end of a shim. This mechanism forces the elastomer of the cover layer to expand outward and, due to the nearly incompressible nature of the material, to experience vertical contraction (that is, perpendicular to the direction of maximum principal strain) of approximately 50%. Figure 2.10 illustrates the situation. At zero load, the top and bottom boundaries of all the elements were straight and horizontal. The extreme local deformations visible in the figure cause tension in both the horizontal and vertical directions. They create locally high hydrostatic tension stress, despite the fact that the average vertical stress on the bearing is compressive.

The figure shows that over most of the domain the hydrostatic stress is compressive. It is shown grey, corresponding to the very bottom block of the scale. (The stress in the figure is given in Pa.) However, at the edge of the shim and at the outer surface of the cover, it is tensile and locally quite large. The results are shown for an average maximum stress on the bearing of $\sigma_a = 1.02GS$. The high hydrostatic tension at the edge of the shim leads to local debonding there. The tension at the surface occurs at the mid-height of the layer and can cause a split under extreme loading. Such splits have been seen in practice, especially in bearings with thick layers.

At the shim edge, the volume of material subjected to hydrostatic tension is larger at low load levels and shrinks as loading progresses. However, the intensity of the hydrostatic tension stress, σ_{hyd}, increases as the applied load increases. At $\sigma_a \approx 1.02\ GS$, the localized hydrostatic tension at the end of the shim reaches the magnitude of $\sigma_{hyd} \approx E \approx 3G$. This has to be viewed in relation to observations by Gent and Lindley (1959b), that showed internal rupture of rubber starts at $\sigma_{hyd} \approx 0.9E$ (with $E = 300\ psi \approx 2.0\ MPa$).

This observation has far-reaching consequences since it indicates that separation of the cover layer can be initiated by internal rupture of the elastomer rather than failure of the adhesive bond between the elastomer and steel. During visual inspection, the failure mechanism could be incorrectly attributed to debonding since the highest hydrostatic tension occurs close to the interface.

The intensity of the local hydrostatic tension and the local extreme shear strains cannot be predicted by the linear theory, which ignores the cover. However, they are directly related to

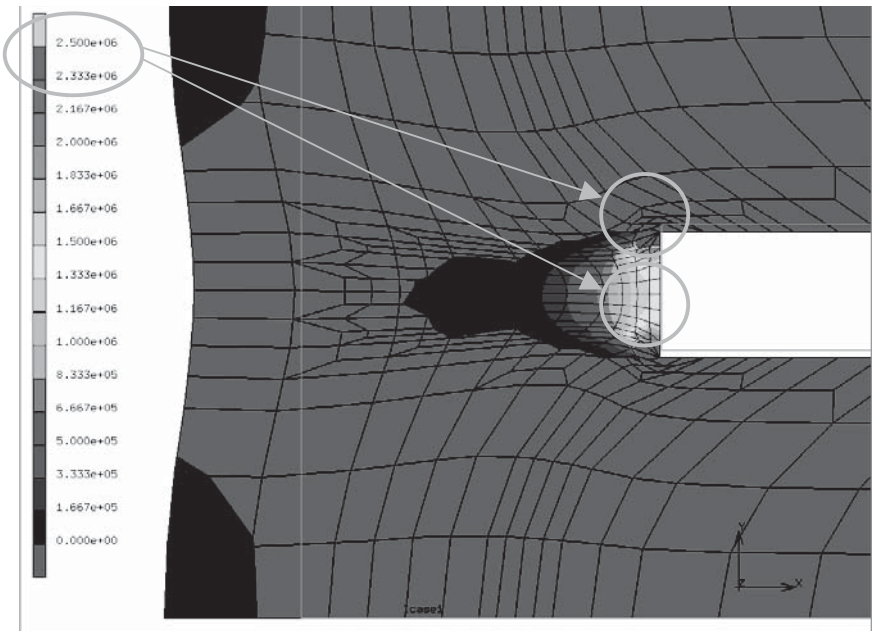

Figure 2.10. Computed hydrostatic stress, σ_{hyd}, (in Pa) at average stress on bearing of $\sigma_a = 1.02GS$.

the shear strain at the elastomer–steel interface close to the edge of the shim and are predicted by the linear theory. This permits the shear strain obtained from the linear theory to be used as a proxy for the local hydrostatic tension.

2.2.4.2 Bearings with Rigid External Plates—Uplift

Bearings with rigid end-plates are used where lift-off cannot be permitted, or where low axial forces provide insufficient friction to hold the bearing in place against applied shear forces. These bearings do not experience the nonlinear geometric effects observed in bearings with lift-off. A problem that can arise in bearings with rigid end-plates is the presence of hydrostatic tension in the interior of the layer. (This is distinct from the hydrostatic tension at the end faces of steel shims discussed in Section 2.2.4.1.6.) Internal hydrostatic tension becomes most significant under combinations of light axial load and large rotation, at which conventional elastomeric bearings experience lift-off.

FEAs were conducted on such bearings to investigate the phenomenon. In most of the FE analyses conducted for this research, the load or rotation was limited by inversion of the elements near the end of the shims when the local compression strain becomes too large. However, for these analyses of uplift, the local compression strain there was modest, and the analyses were limited by "hour-glassing" of the elements in the hydrostatic tension region. The elements should remain approximately rectangular, but when hydrostatic tension becomes too large they become unstable and assume the waisted shape of an hour glass. Results obtained after the onset of this phenomenon are unreliable. However, in all cases the analyses were able to progress until the hydrostatic stress reached approximately E, the value at which Gent and Lindley (1959b) found internal rupture in their experiments. That physical and analytical instabilities occur at the same load is purely coincidental, but they allowed the analyses to cover the critical range.

Hydrostatic tension is addressed in Section F.1.1.5 of Appendix F. Peak hydrostatic stress can be predicted using the linear theory using only the variables α, a function of the load combination, and λ, a function of the bearing properties. Furthermore, the influence of λ is small.

FEAs were conducted on strip bearings with $S = 6$ and $S = 9$. The results were converted to the form of Figure F-14, which shows the dependence of the peak hydrostatic stress on α and λ. The comparison of FEA and linear model analysis is shown in Figure 2.11.

Results were obtained using linear theory for both incompressible and compressible cases. (G and K were taken as 100 psi and 450,000 psi, so the Compressibility Index was only 0.18 and 0.27 for S = 6 and 9 respectively. The effect of compressibility was therefore small.) FEAs were conducted by applying an axial load, holding constant the compressive displacement at the middle of the bearing, and then rotating the top surface. Results are shown for a bearing with $S = 6$ and various axial loads, expressed in terms of the average axial stress, normalized with respect to GS. As can be seen, the agreement is very good and substantiates use of the linear theory for design. The slight flattening out at the top of the FEA curves is due to the onset of hour-glass instability in the elements, which caused the analysis to become invalid before reaching the higher rotations that would lead to higher hydrostatic tension stresses.

The linear theory assumes that the hydrostatic tension is uniform through the thickness of the layer, and equal to the vertical direct stress. The FEA showed that neither statement is

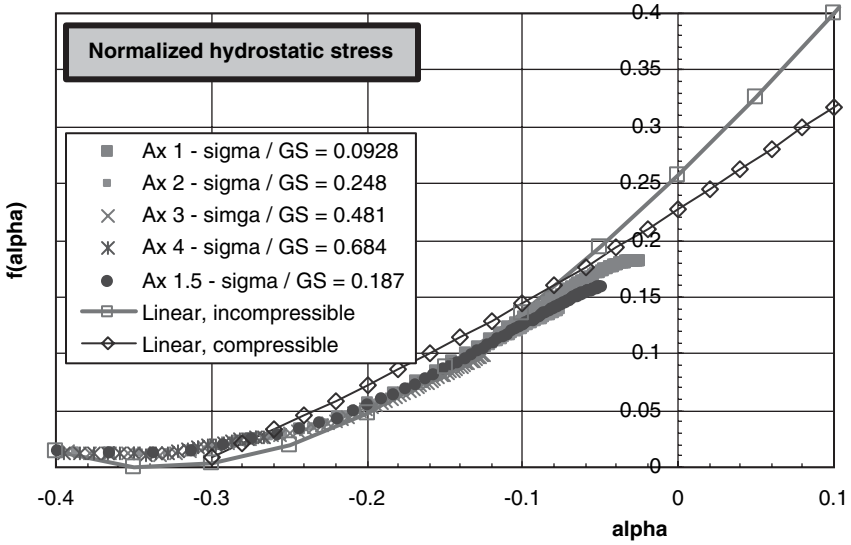

Figure 2.11. Hydrostatic stress: comparison between linear theory and FEA results.

precisely true, but especially at low loads, they both prove to be excellent approximations. They are particularly true for thin rubber layers, which correspond to high shape factors, which in turn are the conditions under which hydrostatic tension is likely to be critical. The hydrostatic tension is largest at the interface between the shim and the rubber. There the lateral constraint provided by the bond to the steel increases the mean tension stress for a given vertical stress. The behavior is analogous to the hydrostatic compression found when a short concrete cylinder is tested between platens with high friction.

2.2.4.3 Significance of Nonlinear Effects—Superposition Error

One key research question behind the numerical analysis concerns the validity of the superposition principle based on the design relations by Stanton and Lund (2006). Strictly speaking, after considering the nonlinear elastic nature of elastomers and the locally large strains as observed near the ends of the steel shims, superposition is not valid for the given problem. However, nonlinear analysis provides the means to quantify the error introduced by the use of a linear theory and by application of the superposition principle. The following analysis proves that the error introduced by these assumptions remains within acceptable bounds for all reasonable combinations of axial loads and imposed rotations.

This proof is performed as follows:

1. Verify that the obtained results from nonlinear FEA and those obtained from the linear theory by Stanton and Lund are closely related. This was performed in Section 2.2.4.1.
2. Represent a characteristic numerical result, for example, the local shear strain at the end of a shim, as a smooth function of average axial stress and the applied rotation.
3. Extract the linear portion of the function. This represents all possible combinations as characterized by superposition of linear models for axial and rotational behavior.
4. Analyze the difference between both functions, that is, the error introduced by linearization and superposition. This provides an error map over the entire range of average axial stress and applied rotation.
5. Verify that the model error does not exceed an acceptable value.

Evaluating the significance of nonlinear behavior requires analysis of numerical data over the given load history for a large number of different load combinations. For elastomeric bearings, the numerical information of primary interest is the maximum local shear strain at the end of each steel shim. Each loading consists of a different sequence of axial loads and rotations. Thus each nonlinear simulation represents a single curve on a force-rotation plot.

Processing data curves for information such as load combinations that cause equivalent $\gamma_{zx,max}$, or the significance of nonlinear effects, is difficult. The simulation data were analyzed by fitting an approximating surface to the data points in axial-force-rotation space. That surface then could be used to represent the data for comparing it with other models such as the linear one. In the present case, the simulation data was fitted, using a least squares criterion, by a function of the following type:

$$\gamma_{zx,\max} = \sum_{i=0}^{m}\sum_{j=0}^{m} a_{ij}\left(\frac{\sigma}{GS}\right)^{i}(\theta_L)^{j} \tag{2-4}$$

where i and j were restricted to $i + j \le m$. Using the full series given in Equation (2-4) did not improve the fit obtained.

This fitting analysis was performed for four series of simulations:

- Strip bearings with S = 6 and bonded external plates. This series creates uplift at larger rotations.
- Strip bearings with S = 9 and bonded external plates. This series creates uplift at larger rotations.
- Strip bearings with S = 6 without bonded external plates. This series allows for lift-off with increasing rotation at low axial forces.
- Strip bearings with S = 9 without bonded external plates. This series allows for lift-off with increasing rotation at low axial forces.

For both S = 6 and S = 9 an almost linear relation between σ / GS, θ_L, and the local shear strain γ_{zx} was observed over most of the range of practical loads and rotations. However, the relation became nonlinear at small axial loads. This reflects the effect of lift-off.

The smooth fitted function defined by Equation (2-4) provided further insight into the overall behavior and allowed further interpretation of the analysis. Use of the linear terms in (2-4) that is,

$$\gamma_{zx,\max} = a_{00} + \sum_{i=1,j=1}^{1} a_{ij}\left(\frac{\sigma}{GS}\right)^{i}(\theta_L)^{j} = a_{00} + a_{10}\left(\frac{\sigma}{GS}\right) + a_{01}(\theta_L) \tag{2-5}$$

provides the ideal approximation of the nonlinear behavior by means of a linear theory of bearing deformation. It is used to identify the difference between using a geometrically and physically nonlinear theory and a much simpler (and thus more usable) linear theory. This difference is measured in terms of a relative error of a linear solution defined as

$$\text{Error}_{\text{model}} = \frac{(\gamma_{zx,\max})_{\text{nonlinear}} - (\gamma_{zx,\max})_{\text{linear}}}{(\gamma_{zx,\max})_{\text{linear}}} \tag{2-6}$$

Equation (2-6) defines the error caused by analyzing a nonlinear mechanism with a linear model. Figure 2.12 shows an iso-error plot for bearings with bonded external plates for SF 9 up to normalized load levels of $\sigma / GS \approx 2.5$ and rotations per

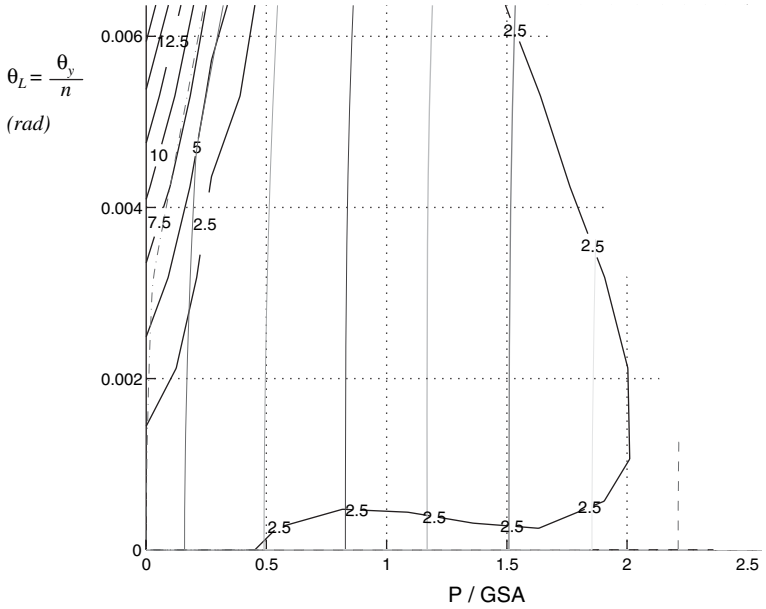

Figure 2.12. Iso-error plot (in %) for shear strain, γ_{zx}. Bearing with S = 9 and bonded external plates, based on a fourth-order fit. (Constructed for Shear Strain at ¼ in. Distance from the Critical Edge of the Shim).

layer of $\theta_L = 0.006$ rad./layer. An iso-error plot shows contours of constant error, or difference, between linear and nonlinear results. Figure 2.13 shows the equivalent results for similar bearings without bonded external plates.

Bearings that have bonded external plates and are subjected to rotations typically show a model error less than 5%, reaching maxima around 10%. (Higher error values on the left side of Figure 2.12 lie outside the domain in which the elements remained stable.) The largest model error is observed along the rotation axis ($\sigma / GS = 0$).

Bearings without bonded external plates experience lift-off at low load levels. This is reflected in the iso-error plots shown

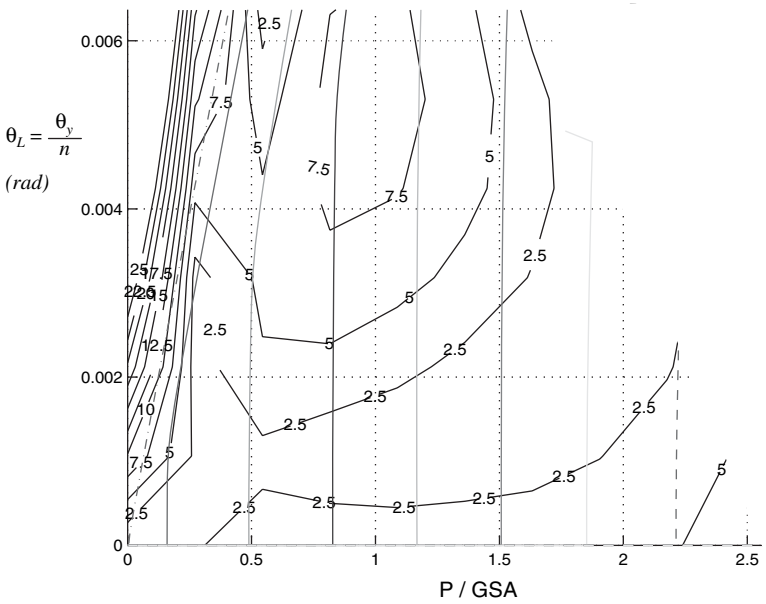

Figure 2.13. Iso-error plot (in %) for shear strain, γ_{zx}. Bearing with S = 9 and no external plates, based on a fourth-order fit. (Constructed for Shear Strain at ¼ in. Distance from the Critical Edge of the Shim).

in Figure 2.13. The typical model error lies below 5%. The exception is the region at the left of the plot, where lift-off occurs, behavior becomes nonlinear and the error increases. At high axial loads, higher error values are observed outside the supported domain and represent extrapolation errors introduced by the fit functions. At low axial force, the higher error value may be affected by extrapolation errors, but also due to the geometric nonlinearity due to lift-off. This latter contribution has to be addressed in a semi-linear analysis by introducing the amount of lift-off into the analysis. This issue of implementing the effect of lift-off into a semi-linear analysis model is addressed in Appendix F.

2.2.5 Discussion

Section 2.2 has presented key results from the numerical simulations. The extracted information provided proof of the key hypotheses needed for an effective, simple design procedure. These findings support the following statements.

- *Superposition* of axial and rotational effects provides a reasonably accurate representation of nonlinear FEA. The error analyses proved that model errors combined with errors due to superposition are typically below 7.5%. Only load combinations that cause significant lift-off were found to reach model errors in shear strain of up to 20%.
- The *stiffness coefficients* predicted by the linear theory of bearings by Stanton and Lund are in good agreement with a nonlinear FEA and thus provide a simple way to predict axial and rotational stiffness of elastomeric bearings. Typical model errors are below 5% for load combinations expected in practice.
- The *local shear strain* predicted by the linear theory of bearings by Stanton and Lund is in good agreement with a nonlinear FEA. Typical model errors are in the range of 5%.
- The predicted *tensile hydrostatic stress* agreed closely with the predictions of the linear theory.

The relatively small overall error identified in this section justifies the general use in design of the linear analysis by Stanton and Lund (2006).

The worst model error of approximately 20% occurs in bearings where lift-off is permitted. Most standard bearings can be designed safely within this error range. For special bearings in which extensive lift-off is expected to occur, the additional accuracy obtainable by using a custom nonlinear FE analysis may be warranted.

2.3 Development of Design Procedures

Design of structural components for service loads usually includes calculation of stresses caused by different load cases. The stresses then can be added and compared with an allowable value. Because elastomeric bearings are composite structures, and one of the materials is very nearly incompressible, it is not the peak direct stresses that should be added, but rather the peak shear strains. Compression, rotation and shear loadings all cause shear strains in the elastomer, as shown in Figure 2.14, and the values within the layer are all maximal at the same location, namely at the edge of the steel shim.

The shear strains eventually lead to delamination of the elastomer from the steel. This process may occur under a monotonic load of sufficient intensity, but is more commonly caused by cyclic loading. That process is one of fatigue. Deriving a precise limit that the total strain must satisfy then is more difficult than it would be if failure were controlled by a single application of monotonic load.

Regardless of whether the loading is cyclic or monotonic, a method for computing the shear strains is needed. This, too, is complicated by the fact that elastomers can and do undergo strains that are very large compared with those that occur in conventional structural materials. The elastomer also is materially nonlinear. For these reasons accurate analysis for loads other than very small ones can only be achieved using FEA, as discussed in Section 2.2 and Appendix E. However, such analyses are not appropriate for the design office, so a simpler alternative is needed. An approximate, linearized theory is discussed in Section 2.3.1.

2.3.1 Computation of Shear Strains using the Linearized Theory

Gent and his coworkers (for example, Gent and Lindley, 1959a, Gent and Meinecke, 1970, and Lindley and Teo, 1978) pioneered the analysis of laminated bearings and developed a linearized analysis procedure. Conversy (1967) extended it to allow for finite values of bulk modulus, and Stanton and Lund (2006) provided numerical values of all necessary coefficients for different bulk modulus values. That approach forms the

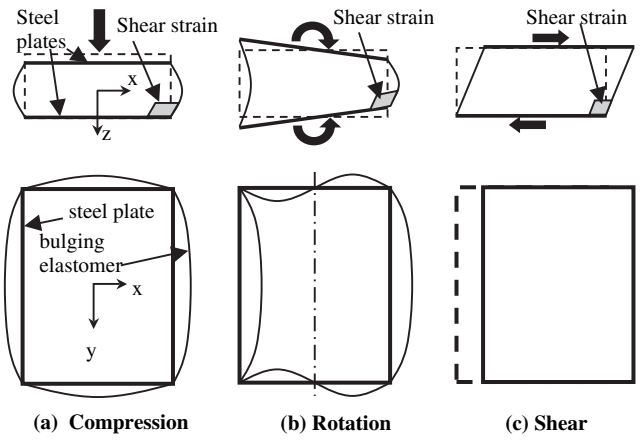

Figure 2.14. Shear strains in the elastomer due to different loadings.

basis of the procedure used for the design method used in this research, and is summarized here. It is approximate because it assumes a parabolic distribution of displacement through the thickness of the elastomer within a layer, but, as the FEA shows, that approximation proves to be remarkably good, and, for the geometries and stresses used in practical bearings, the errors are small compared with those arising from other sources, such as characterization of material properties. Its simplicity compared with any other alternative makes it an attractive choice.

In a bearing that does not lift off, either because the rotation is too small or external bonded plates prevent it, the girder always remains in contact with the bearing. The boundary conditions then remain constant during the loading. The linearized theory can then be used to relate three fundamental quantities shown in Figure 2.8. For compression they are: external load (average stress or force), external displacement (average strain or deflection), and maximum local internal deformation (defined here by shear strain γ_a). Similar parameters exist for rotation (bending). The parameters that relate these quantities define functional relationships that are analogous to those used in conventional beam theory (for example, $M = EI *$ curvature, stress $= My/I$).

As shown in Appendix E and Section 2.2, the full nonlinear model of a bearing reduces to Gent's linear theory if the strains are small enough. This finding satisfies a basic requirement for using the linear theory for design. The strain levels expected in practice are not infinitesimally small, so the problem strictly is no longer linear, superposition no longer strictly holds, and strains from different load cases strictly cannot be added directly. However it was shown in Appendix E that in practice errors involved in doing so are acceptably small compared with other uncertainties in the problem.

Details of the linear theory are given in Appendix F. However, for the no lift-off case, two results are important. First, for a bearing subjected to combined compression and rotation, the peak shear strain on the compressive side must be computed. That can be done by computing the shear strain caused by each loading separately and adding the results. Second, if the load is light and the rotation is large, and the bearing has external plates, the interior of the elastomer may experience hydrostatic tension stress on the tension side. Gent and Lindley (1959b) showed that such stress can lead to brittle rupture of the elastomer at a relatively low stress (in the range $0.9E$ to $1.0E$, or $2.7G$ to $3.0G$). Equations for computing the hydrostatic stress also were developed using the linearized theory, and values were verified against the FEA. The validation process is complicated slightly because the location of the peak hydrostatic stress varies with the ratio of axial deformation to rotation. This causes a need to search for the element with the highest stress in the FEA, rather than simply monitoring a single element.

For the case where lift-off is possible, a closed-form analysis is more difficult, because even under small strains and using the linear theory the dimensions of the contact region between the sole plate and bearing change throughout the loading. The problem then becomes inherently geometrically nonlinear. Hydrostatic tension is essentially eliminated, so the important issue concerns computation of the peak shear strain on the compressive side. A geometrically nonlinear, approximate variant of the linear theory was developed in closed form by assuming that the bearing can be divided into two parts, one that lies under the loaded region and the other remains unstressed, as shown in Figure 2.15. It is described in detail in Appendix F.

This semi-linear model ignores any horizontal stresses applied by the elastomer on one side of the interface to material on the other. The response that it predicts was compared with the nonlinear FEA, and reasonable agreement was found. (Shear strains differed by 20% in the worst case.) As explained in Section 2.2, precise comparisons were difficult because they required extrapolation in the FE model. However, the semilinear model showed that total shear strain (due to rotation plus compression) always was smaller than that computed using the truly linear no-lift-off model, with a peak error of approximately 20%. This result provides support for the use of the semilinear model. Appendix F described not only the mathematical development, but also offers a physical explanation of why the strains in the semilinear model should be an upper bound to the true peak strain on the compressive side. This result is valuable because it allows the linear no-lift-off model to be used safely for prediction of the critical shear strains. Doing so simplifies the calculations because it allows one model to be used for all load cases.

2.3.2 Shear Strain Capacity

The procedures outlined in Section 2.3.1 are sufficiently simple for use in design and can be used to compute the critical shear strains. However design involves the computation

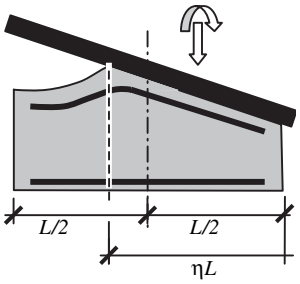

Figure 2.15. Lift-off: bearing behavior assumed in "semi-linear" model.

of both shear strain demand and capacity. This section addresses capacity.

The shear strain capacity of the elastomer was indirectly established by test, using test procedures detailed in Appendix C and results given in Appendices A and D.

The test results were modeled for monotonic and cyclic loads. The cyclic modeling in particular was done in some detail, so as to provide the best possible basis for a design procedure. Several difficulties were encountered. The primary ones were:

- The shear strains in the elastomer cannot be measured during the test because the deformations are too large for conventional instrumentation and because the presence of sensors would alter the strain field where the measurements are needed. Indirect methods for establishing the strains were necessary. One approach was to measure the heights of bulges of the rubber layers with a micrometer gage. However, the rubber cover smoothed out the serious shear distortions in the underlying material so the bulge height measurements, though accurate, ultimately proved unusable.
- The shear strains were computed from the axial strains using the constants C_a and so forth, developed using linear theory. Even the average axial strains could not be measured during the rotation tests, because the instrumentation could be installed only after the bearing was secured in place by the clamping action of the plates of the test rig, and by that time the axial strain had been imposed. Thus the average axial stress versus average axial strain relationship for each bearing was obtained from the axial test series (PMI 1b) on that bearing batch. Separate calibrations were needed for each batch because of the slight differences in material properties. For example, for batch A2 bearings, the axial stress-strain curve was obtained from Test PMI 1b-A2 and was used in obtaining the axial strain from the measured axial stress in tests CYC05-A2 through CYC012-A2. Use of the linear theory to link axial and shear strains, through constants C_a and so forth, was justified because the same constants would be used in both the design procedure and the analysis of the test data.
- The axial response of the bearing was not linear, even at low loads. At higher loads, the nonlinearity became significant. This behavior has been observed by many researchers.
- The material was not elastic, so cyclic loading caused a response that was both hysteretic (because of slight viscoelasticity) and, at least during the first few cycles, nonrepeatable because of the gradual breakdown of crystallization.

Despite these difficulties, the shear strain capacity of the bearings was characterized at various levels of damage. Both debonding and delamination damage were observed. Both caused bulge patterns that appeared similar from outside the bearing, and they could be distinguished only by cutting open the bearing, which precluded further testing. That procedure was used sparingly. As discussed in Sections 1.3 and 2.2.4.1.6, debonding always started by separation of the rubber cover from the vertical edge of the shim. As loading progressed, and only if it was severe, the internal cracks caused by the tension debonding then propagated as shear delamination into the interior of the rubber layers. An example is shown in Figure 2.16.

The crack typically propagated through the rubber and not along the steel-rubber interface. That indicates good bond. The tension debonding has essentially no adverse effect on the performance of the bearing, but the shear delamination renders it less stiff and less able to resist load.

The monotonic tests consisted of different combinations of axial and rotation loading. All monotonic specimens that debonded started doing so at approximately the same computed shear strain of approximately 6.7. Details are given in Table F-1. This provided a value for the static shear strain capacity. All of the pure axial tests were taken up to the test machine capacity of 2400 kips (a stress of 12 ksi, or approximately 10 times the present AASHTO limit for that bearing). In some cases the shims fractured, but only at the very end of the loading, some bearings suffered some debonding, while in others there was no damage at all.

The cyclic loading test produced a large amount of data, and developing a model to represent the results was difficult. Two approaches were used. In the first, the Nonlinear Model, the axial strains were obtained from the axial stresses using an empirical, nonlinear model, because the measured axial load-deflection curves in the PMI series were clearly nonlinear. The shear strains then were derived from the axial strains using Gent's linear theory. The shear strains due to rotation were derived directly from the rotations using Gent's linear

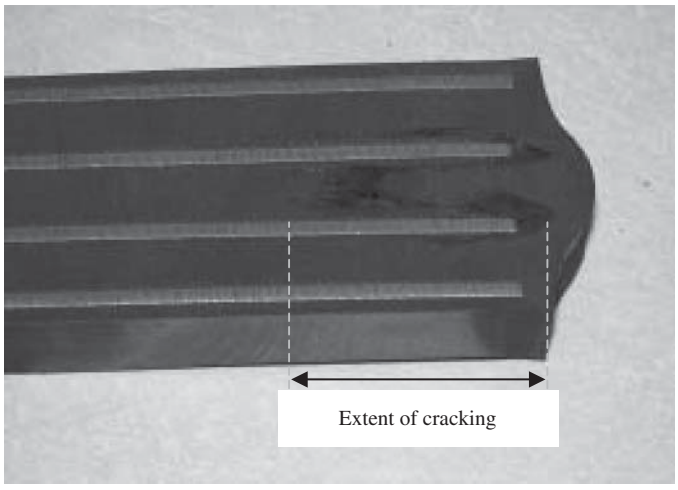

Figure 2.16. Shear crack propagation into elastomer layer.

theory. In the second approach, the Linear Model, all strains were obtained from stresses using Gent's linear model.

The next step required that the shear strains applied in the tests be related to a capacity. Because capacity is not a fixed number but depends on the extent of debonding that is tolerable, an attempt was made to reflect that fact in the equations. In addition, the shear strain demand depends on the number of cycles applied, evident from the fact that the damage increases as more cycles are applied. Therefore the cyclic component of the shear strain demand, which in the tests consisted only of the rotation component, was multiplied by an amplification factor that was a function of the number of cycles. The final form of the Nonlinear Model is described by Equation (2-7).

$$\left(\gamma_{a,st} + \gamma_{r,st} + \gamma_{s,st}\right) + c_N\left(\gamma_{a,cy} + \gamma_{r,cy} + \gamma_{s,cy}\right) \le \gamma_{cap} \qquad (2\text{-}7)$$

Details of the capacity equation were developed first for the Nonlinear Model. The load amplification factor c_N was treated as a function of the number of cycles of loading, and the capacity γ_{cap} was treated as function of the level of debonding, D. The model fitted the data well, and reflected appropriate asymptotic behavior as the relevant variables approached their limits (for example, as N, the number of cycles, reached 1 or infinity). However, when the model was applied to a typical bearing for a freeway overpass, it predicted extensive damage after only a million cycles. Such damage has not been reported from the field, so the constants were recalibrated. However, no set of constants could be found that matched the test data well and gave plausible results for common field bearings. The calibration and evaluation of the Nonlinear Model is described in detail in Appendix F.

These difficulties appeared to raise insurmountable obstacles to the generation of workable design provisions. Therefore the Nonlinear Model was not developed to the stage of design provisions. However, it is described in detail in Appendix F so that it could be developed to form design provisions if the necessary cyclic axial load data were to become available in the future.

A second model, the Linear Model, was created. Its general form again is given by Equation (2-7). It is similar to the Nonlinear Model, but differs in three major respects:

- The shear strains are all derived from stresses using Gent's linear theory,
- The cyclic amplification factor is a constant and not a function of the number of cycles, and
- The shear strain capacity, represented here by the term γ_{cap}, is a constant and not an explicit function of the level of debonding deemed acceptable.

These simplifications make the model easier to use. However, because the amplification factor is not a function of the number of cycles, it is not possible to relate the progressive damage continuously to the cycle count. Instead, the total shear strain was correlated with the cycle count for two discrete levels of debonding. The plot for 25% debonding is shown in Figure 2.17. It includes all the test data that reached 25% debonding, that is, all the tests except SHF-05. That was a high shape factor bearing that hardly debonded at all and had not reached 25% debonding when the test was abandoned to allow other specimens to be tested. Specimen SHF-06, with $S = 12$, also performed much better than the average. In Figure 2.17, it is the point highest and furthest to the right on the graph, with a total strain of 10.5 at $\log(N) = 4.2$.

The cycle count is plotted on a log scale, to reflect the distribution of the data. The best fit line through the data then can be used to predict the number of cycles needed to reach 25% debonding for a given effective strain demand. The effective strain is the quantity on the left hand side of Equation (2-7), and consists of the total static strain plus the amplified cyclic strain. A similar plot, but for 50% debonding, is shown in Figure F-20 in Appendix F. Rather than the initiation of debonding, 25% debonding was used because of the scatter in the latter.

In the Linear Model, the only two parameters to calibrate are c_N and γ_{cap}. To establish c_N, different values were tried and the scatter of the data, as represented by the correlation coefficient R^2, was plotted against c_N, as shown in Figure 2.18. The best correlation was found with $c_N = 2.0$, so that value was accepted for design. To establish γ_{cap}, the best fit line was extended to a cycle count of 50 million, on the basis that that represents the number of passages of fully laden trucks over the lifetime of a heavily used freeway lane. The corresponding effective strain was 4.7 at 25% debonding. It is argued (see Appendix F) that the number would be higher if the plot had included the bearings that did not debond at all. (That is by definition impossible in a plot to 25% debonding.) For that

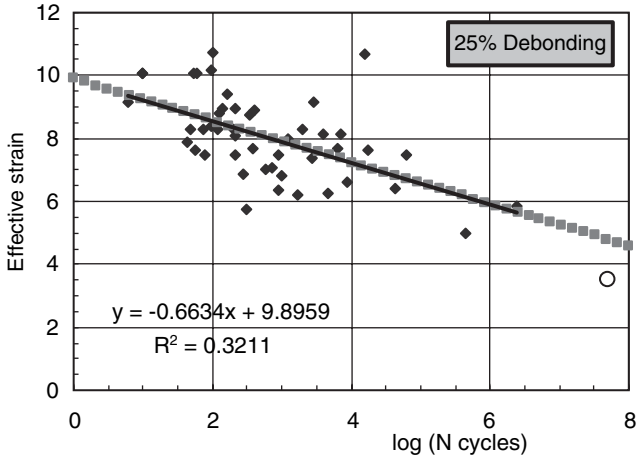

Figure 2.17. Effective strain vs. number of cycles: 25% debonding.

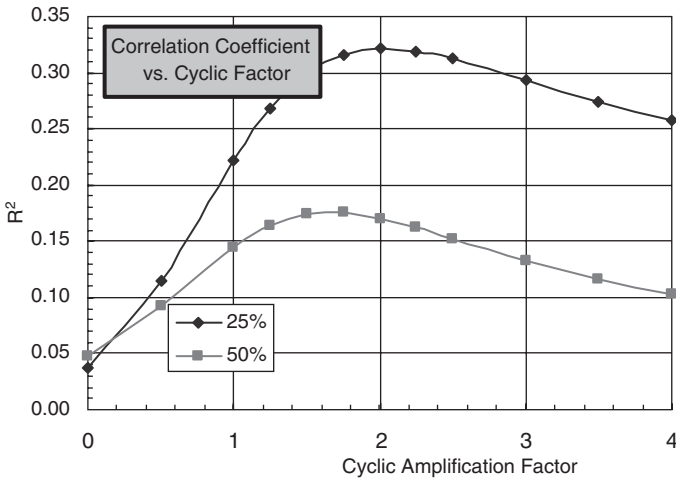

Figure 2.18. Correlation coefficient vs. cyclic factor.

reason, the strain capacity was rounded up to 5.0. This value is still significantly less than the 6.7 corresponding with the start of debonding in the PMI series of monotonic tests. That static data was not included in the calibration of the Linear Model because of minor questions over its accuracy; observing the start of debonding was in some cases not easy, because the lateral shift of the steel plates under large rotations pulled the critical region of the elastomer inwards so that seeing it was difficult.

Checks of the Linear Model against the performance of typical field bearings suggested that its predictions were satisfactory, in that it predicted very low levels of damage in a typical freeway overpass bearing after 50 million cycles. (A typical 22 in. × 9 in. freeway overpass bearing is shown as an open circle at 50 million cycles in Figure 2.17, and lies well below the design line.) The Linear Model was accepted as the basis for the proposed design procedure. Its advantages over the Nonlinear Model are that it is simpler to use, it fits the test data in an average sense at discrete levels of debonding, and it gave plausible values for typical bearings in practice. The disadvantages are it does not reflect the nonlinearity in the observed axial force–displacement curves from the PMI test series, and it does not provide a way of tracking the progression of damage with increasing cycles.

2.3.3 Analysis of Rotation and Axial Force Demand

The primary demands on the bearing consist of axial compression and rotation. Sample bridges were analyzed to determine the combinations of load and rotation that are imposed by truck traffic crossing the bridge. Details are in Appendix F.

The analyses demonstrated two important findings. The first was the truck imposes a cyclic axial force, which causes shear strains due to compression γ_a that are much larger than the shear strains due to the corresponding rotation γ_r. Both are cyclic. If cyclic shear strains are the appropriate measure for determining the propagation of debonding damage, the shear strains caused by axial loading will dominate the calculation. This finding came to light after the bearing testing was complete, so the time and resources were not available to conduct cyclic axial compression tests. Cyclic axial fatigue tests have been conducted in the past (Roeder et al., 1987), but the specimens had no cover and the debonding was measured in a different way than was done here. Those tests were considered in Appendix F in an attempt to account for the axial fatigue experienced by a bearing. The findings from them were consistent with the expected trends, but the differences in test conditions prevented use of numerical values from them.

The second finding is the cyclic rotation due to truck loading almost always will be less than ±0.003 radians and may be as low as ±0.001 radians if the bridge satisfies the AASHTO requirement that the midspan deflection under live load be less than $l/800$. A simple check of typical prestressed concrete girders showed that their stiffnesses were significantly greater than the minimum needed to meet this criterion. Steel bridges are typically more flexible than their prestressed concrete counterparts, especially if high-strength steel is used, so their midspan deflections are likely to be closer to the limit. The value of the cyclic rotation that is relevant may be further reduced by the fact that the peak shear strain of interest is the one caused by the combination of axial and rotation effects. For bridges less than 200 ft. long (which constitute the great majority), the peak combined shear strain in the bearing occurs as the truck is just entering the bridge. Then, the axial load component is at its individual maximum, but the rotation typically is not. Therefore, the use of the sum of the shear strains due to the individual peak compression and peak rotation is inherently conservative.

Last, an evaluation was conducted to determine the contribution of thermal camber to girder end rotation. The AASHTO temperature gradients were used, and bridges from 80 to 180 ft. span were considered. Only concrete girder bridges were evaluated, because the specified thermal gradient is higher for them. Details of the analyses are given in Appendix F.

Figure 2.19 shows the results for a high and a low temperature zone (AASHTO Zones 1 and 3 respectively). As can be seen, the rotations vary from about 0.0010 to 0.0016 radians. This value is the same order of magnitude as the rotation caused by truck loading. However, because it occurs much less frequently, its damaging effects are likely to be much less and may reasonably be regarded as a static rotation. It can be concluded that thermal rotations play only a minor role. Furthermore, thermal effects typically cause upward camber, whereas the live load causes downward deflection, so the two are usually not additive.

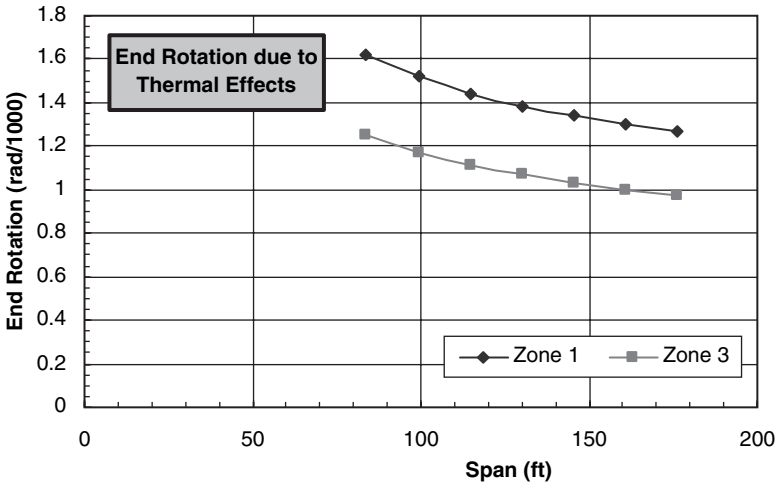

Figure 2.19. Rotation due to thermal gradient on girder.

2.3.4 Evaluation of the Design Model

The Linear Model for design was evaluated in the light of the findings described in Sections 2.3.1 to 2.3.3. It brought to light several issues summarized here and discussed in detail in Appendix F.

First, the analysis of demand showed that the cyclic axial load caused shear strains that were 5 to 10 times larger than those caused by cyclic rotations. (See Appendix F, Section F.3.3.2, and the illustration in Figure F-36). If damage attributable to debonding is to be the basis for failure, it is appropriate that the shear strains due to axial load should form a substantial part of the design specification. However, no test data were available to evaluate the relationship between cyclic axial load and debonding. For want of a better alternative, it was assumed that all cyclic shear strains of the same magnitude, regardless of their source, would contribute equally to the fatigue damage. This assumption allowed the test data on cyclic rotation to be used to evaluate shear strains due to cyclic compression.

The design procedure was developed using the Linear Model and uses a cyclic amplification factor c_N that has a constant value of 2.0. This is the general approach taken by the European bearing specification EN 1337, although that specification uses different numerical values. The specification proposals are given in Appendix G.

2.4 QA/QC Issues

A secondary goal of this research program was to evaluate the QC and QA issues related to steel reinforced elastomeric bridge bearings. This issue was raised in the original request for proposals, because of concerns regarding current test requirements for elastomeric bearings, recent revisions to the M251 material specifications for elastomeric bearings, and the recent recommendations of NCHRP Report 449 (Yura et al., 2001). This was a secondary goal, in that no experimental research was proposed to investigate the issues, but the research team addressed it during the research. In particular:

- Surveys of state bridge engineers and practicing engineers were performed to determine concerns regarding the quality of elastomeric bearings and the cost and effectiveness of QA testing. Some of these survey issues are discussed in Appendix B.
- The researchers held discussions with the four major manufacturers to obtain their input on manufacturing and QC of elastomeric bearings.
- The researchers had extensive meetings with experts such as Professor Alan Gent on elastomers and common testing requirements. These meetings were held in conjunction with Advisory Group meetings at intervals throughout the research.
- The researchers closely monitored the bearings tested in their research program to evaluate the quality and performance of the bearing, and where possible they attempted to correlate this performance to the tested properties from the QA test results.

This evaluation brought to light a number of issues, which are briefly discussed here.

2.4.1 Quality of Current Elastomeric Bearings

Researchers tested a large number of elastomeric bearings in this study, however, they also have tested a large number of elastomeric bearings in prior research as reported in NCHRP Reports 298 and 325. A comparison of test results from present and prior studies shows that the quality of elastomeric bearings

today is, on average, higher than it was 20 years ago. This can be seen by comparing the average compressive stress at which initial debonding of elastomeric bearings was observed. That stress was larger in this study than in earlier ones. In addition, the progression of damage was significantly smaller than in earlier studies. This finding shows that the current QA/QC measures are proving effective.

2.4.2 Test Requirements

Requirements for testing materials and finished bearings have changed significantly in the last year.

Prior to 2006, material tests were specified largely in tables 18.2.3.1.1 (Neoprene) and 18.2.3.1.2 (Natural Rubber) of Chapter 18 of the AASHTO Bridge Construction Specifications. Tests were to be conducted on separate samples of material that did not have to be taken from the finished bearing. Most manufacturers made special samples for the purpose and cured them according to the same time and temperature history as the bearing.

Material test requirements have been moved to the AASHTO M251 Materials Specification. This change is certainly rational. However, two parallel testing regimes have been established, some tests have been eliminated, and some new tests have been introduced. Some problems are evident in the new arrangements. Details of the new testing arrangements are shown in Table 2.3.

A major change also was introduced by permitting two different test regimes. The first is applicable to all bearings while the second is optional, and may, at the engineer's discretion, be used for bearings designed by Method A and specified in terms of hardness alone.

In the first, universally applicable regime, the bearings are subject to a small number of material tests (the column headed "all bearings" in Table 2.3) that must, according to Section 4.2 of M251, be conducted on samples taken from the finished bearing. Some finished bearings from each lot also are to be subjected to further tests, defined in Section 8.8 of M251-06. In the second regime (applicable only to Method A bearings) and specified in Appendix X1 of M251-06, the elastomer is to be subjected to a larger battery of tests (column headed "Method A only" in Table 2.3), but the tests in Section 8.8 on finished bearings need not be conducted. The wording of Appendix X1 does not make clear whether the material tests specified in Table X1 are to be conducted on material taken from finished bearings, or whether special coupons may be molded for the purpose.

Table 2.3. Material tests.

ASTM ref.	Subject	Pre-2006 (Ch 18 Constr.)	M251-06 All brgs.	M251-06 Meth.A
2240	Hardness	yes		yes
412	Minimum G		yes	yes
412	Strength	yes	yes	yes
412	Elongation	yes	yes	yes
573	Heat resistance/aging	yes		yes
395	Compression set	yes		yes
1149	Ozone resistance	yes		
746	Low temp brittleness	yes	yes	yes
4014	Low Temp shear stiffness	yes		
	(crystallization)			

These changes constitute a significantly different test system for elastomers and bearings than existed before. Review of M251-06 suggests that the new arrangements need some further massaging, because the changes have introduced some potential problems. The most important issues are summarized here.

1. Section 8.8.4. Shear modulus test. Three methods of determining the shear modulus are specified: ASTM D4014, M251 Annex 1 (an inclined compression test) and M251 Annex 2 (the same test rig as the shear bond test in 8.8.3, similar to half of a D4014 quad shear test rig). The following comments apply:
   - Specifying three different permissible tests to determine one quantity (the shear modulus, G) is ill-advised. This is particularly true because the acceptable range for the measured G is only ±15%. Especially with natural rubber, which is subject to some variation because it is a natural product, such a tolerance might be hard to maintain even with a single test procedure. (It is worth remembering that the shear stress-strain curve is nonlinear, so the section of the curve used affects the outcome. This adds further uncertainty and is another reason for using a single method.) With three different procedures, each using a different shaped specimen and a different testing approach, the situation has a high potential for contractual disputes. Reliance on a single method would be preferable. Fortunately, for bearings designed by Method B only one method (ASTM D4014) is permitted. No reasons are given.
   - The geometric requirements given in M251 A 2.3.1 are inconsistent. The rubber is to be cut from a finished bearing, yet if the internal layer thickness is greater than 1.25 in., no specimen can be cut from it that will meet all the geometric requirements. Such thick layers are not likely, but they are perfectly possible.
   - The test purports to measure shear modulus and is to be applied to material used in bearing designed by Method A. Yet the LRFD Design Specification now permits bearings to be designed using Method A based on hardness alone. If shear modulus is not needed for design and is not specified, the reasons for conducting a test for it remain unclear.
2. It is believed that the tests indicated in Table 2.3 were eliminated in the interests of economy. However, Section 4.2 of

M251 now states that, "The properties of the cured elastomeric compound material listed in Table 1 shall be determined using samples taken from actual bearings." Preparing samples from a finished bearing imposes considerable extra costs, both for preparation time of the sample and in destruction and loss of a bearing. Although the changes only are just coming into force and no cost data are yet available, it is likely that the net effect will be to increase overall costs.

3. The M251-06 Specification distinguishes bearings specified by hardness and designed under Method A from all other bearings. The former may be tested under what appears to be a less stringent regime. This choice raises questions, because manufacturers typically have one procedure and one set of quality standards for making bearings. Furthermore, they often are unaware of the method used for design. Therefore there is no reason to believe that they will build in higher or lower quality for bearings designed by Method A. By contrast, bearing size and especially thickness does influence quality, because of the difficulties in maintaining accurate shim placement and layer thickness when many layers are used, and because of the difficulties in achieving an even cure through the thickness if h_{rt} is large. (The outer layers heat up sooner, and the rubber risks over-curing and reverting before the center has fully cured.) Researchers believe that, if different testing regimes are to be used, they should be differentiated on the basis of bearing size and not design method. This is particularly true because the stresses used in Method A are often, but not necessarily, lower than those in Method B.
4. The material test criteria specified in M251-06 Table 1 (for use with all bearings) and those in M251-06 Table X1 (for Method A bearings only) are inconsistent. For example, in Table 1, the elongation at break for all elastomers must be greater than 400%, regardless of hardness or shear modulus. Yet in Table X1, the elongations are specified as 450%, 400%, and 300% for hardnesses of 50±5, 60±5, 70±5 Shore A points. Inconsistency often leads to difficulties, including contractual disputes. It should be recognized that significant sums of money may depend on the outcome of a test, because in many cases the lot of bearings is to be rejected if the test fails. Therefore the tests should be as clear and unambiguous as possible. Clarity in intent also is likely to lead to more competitive pricing. If a manufacturer is unsure about the testing regime, it is likely that money will be added to the bid to cover uncertainties associated with testing. This is a standard and understandable risk-management procedure.
5. The AASHTO Design Specifications, Section 14.7.5.2 states the range of shear modulus permissible for use in design. The lower bound now stated in M251-06 for an as-tested value is the same (80 psi), but no upper bound is placed on the as-tested value (14.7.5.2 gives 175 psi for design). The two specifications thus differ in that respect. Note also that the design values are stated in ksi (as are all stresses in the Design Specifications) but those in M251 are in MPa and psi.
6. Section 8.3 of M251-06 requires that the manufacturer ". . . shall certify that each bearing in the lot satisfies the requirements of the design specification. . . ." This seems to place an unreasonable burden on the manufacturer. If the manufacturer did not design the bearings, how would he even know what load cases were used for design, let alone how to conduct the necessary stress analysis?

Prior to 2006, the AASHTO Construction Specifications required a long-term compression test (15 hours) on bearings designed by Method B. The difficulty and expense of conducting this test appeared to be a disincentive to using Method B. The present arrangements, whereby samples have to be taken from finished bearings to construct material coupons for testing method B bearings, might continue to act as a disincentive. For that reason and those discussed in paragraph 3 above, it is recommended that the criteria for more rigorous testing be associated with bearing size and not design method. It is proposed here that the criterion be $h_{rt} \geq$ 8 inches, or plan area ≥ 1000 in^2.

It is worth mentioning that the shear modulus of the elastomer and the required shear stiffness of the bearing should not be specified. The existence of end effects at the ends of the elastomer layers and some "bending" flexibility in the whole bearing, especially if it is thick, mean the shear stiffness of the bearing is not equal to GA/h_{rt}, where h_{rt} is the total rubber thickness. If the shear stiffness of the bearing is computed on this simple basis and if the shear modulus also is specified, the bearing manufacturer will be placed in the impossible position of being asked to satisfy two incompatible requirements. Further difficulties may be introduced if the tapered wedge test (Yura et al., 2001) is used and the effect of axial load on the lateral stiffness of the bearing is not correctly accounted for. For similar reasons, hardness and shear modulus should not be specified for a single material.

2.4.3 Number of Tests Required

The number of tests required is a concern. The frequency of testing depends on the number of bearings defined to constitute a lot, and that frequency therefore depends on the interpretation of the words "lot" and "elastomer batch." This is discussed in M251-06 Section 8.2. What happens if there are more than 100 identical bearings? Some states purchase bearings en masse, store them, and then provide them to the contractor as needed. Do the bearings need to be absolutely identical to constitute a lot or is some discrepancy permitted? The

definition of a batch also is important, and the definition differs between manufacturers that mix their own rubber and those that buy it premixed. Manufacturers that mix their own batch generally mean one mixer load, so the amount depends on the size of the mixer, whereas those that buy premixed material tend to mean a single purchase. Such a purchase may be very large and, depending on the rubber supplier, it might include many separate mixer loads.

The frequency of testing affects the cost, and manufacturers have expressed dissatisfaction over the specification's lack of clarity on this issue. Because the cost of testing must be included in the bid price, the latter will depend on the interpretation of the wording in the specification. The lack of clarity is perceived as causing a non-level playing field, and revision of these definitions is needed.

2.4.4 Material Test Requirements

A wide range of material and QA test requirements have historically been employed. These include:

- ASTM D2240 Shore A durometer hardness,
- ASTM D412 Tensile strength and elongation at break,
- ASTM D573 Heat resistance,
- ASTM D395 Compression set,
- ASTM D1149 Ozone resistance,
- ASTM D1149 Low temperature crystallization, and
- ASTM D1043 Instantaneous thermal stiffening.

Some discussion of these tests is warranted.

The hardness test has been in the AASHTO Specifications for many years. It is somewhat imprecise, in that two individuals may measure the same rubber sample and report different hardness values. For a finished bearing, it also gives different results when the bearing is loaded or not, and it can be affected by the proximity of a steel shim (for example if it is conducted on a high shape factor bearing with thin layers). Its main virtue is that it can be performed very quickly and easily and, not surprisingly, it has a long history of use. However, shear modulus G is a more precise and reliable measure. Hardness can be correlated approximately with Young's modulus, but the correlation contains some scatter. For this reason the AASHTO LRFD Design Specifications specify a range of G values that correspond to a particular hardness. Furthermore, the hardness test can be conducted easily on a finished bearing, whereas the shear modulus test requires a special coupon that must either be specially fabricated (and so may have different properties from the bearing itself, due to different curing time) or it must be cut from the bearing, a procedure both difficult and expensive and destroys the bearing.

The hardness measurement causes problems when an engineer specifies both hardness and shear modulus, because the relation between hardness and shear stiffness is not precise. From the point of view of accurate measurement of material properties, the hardness test should be eliminated, and the industry should rely totally on shear stiffness. However, in 2006 the AASHTO LRFD Design Specifications changed to permit bearings designed by Method A to use material specified by hardness alone. It is understood that this change was made in the interests of economy (that is, eliminating the need for the shear modulus test), and justified by the fact that some spare bearing capacity exists as a result of design by Method A so that some variation in material properties would not be critical. Whether the perceived economic benefits of this decision warrant the reduction in quality control is open to question; some of the main manufacturers have reported to the researchers that the cost of preparing and testing shear modulus samples is trivial. The test takes less than five minutes of a technician's time.

Questions sometimes have been raised about the precise correlation between a particular test and the final elastomer properties. Such precise correlations in general have not been established. For example, Lindley pointed out that an elastomer compound could be changed to improve any one characteristic, but only at the expense of another (Lindley 1982). Therefore imposition of minimum requirements for a number of different characteristics is the best way to ensure an elastomer of overall high quality. The temptation to reject a particular test, because a precise link with some characteristic of the finished bearing cannot be seen, should be resisted unless the matter has been studied carefully.

Researchers could detect no correlation between bearing performance and the elastomer's tensile strength and/or elongation at break. This finding is consistent with many specifications (for example, EN 1337, BS5400) that treat the total strain capacity as independent of rubber properties, but inconsistent with others (for example, BE1/76) that relate the total strain capacity to its elongation at break. All the bearings supplied for testing satisfied the AASHTO tensile strength and elongation requirements, and none of them performed badly. Some of the materials had strength or elongation significantly higher than the minimum required by the specification, but that excess material capacity did not correlate with particularly good bearing performance.

The argument in favor of testing for heat resistance and compression is again indirect. No bearings were received that failed these tests, so it was not possible in this study to determine their effectiveness. However, that may well be an indicator that the tests are effective in keeping unsuitable material from the market-place.

All of these material tests are relatively quick and easy to perform if the manufacturer's laboratory owns the required equipment, which is the case for the major suppliers. Cost savings that would be achieved by abandoning them appear to be trivial, especially compared to the costs of replacing

even a single bearing in a bridge. Current QA/QC procedures are resulting in good quality elastomeric bearings, and relaxation of the test requirements appears to carry considerable risk without a corresponding price benefit.

2.4.5 Very Large or Unusual Bearings

Discussions with design engineers, manufacturers, and state bridge engineers indicate that very large and unusual elastomeric bearings have become more common over time. Furthermore, any changes in the specifications that allow bearings to be designed for higher loads or more extreme movements are likely to increase that tendency further. Questions exist over ways to ensure good quality and good performance from such bearings.

First, the specification provisions are based on design models that have been verified almost exclusively by tests on small- to moderate-sized bearings, and questions remain whether they also apply to larger bearings. (Seismic isolation bearings are often larger—three or four feet in diameter—but they typically have shape factors that are much higher than those used for bridge expansion bearings. The compression strains are much smaller, and the shear deformations are much larger, than those typically used in bridges, so seismic isolation bearings do not provide a basis for complete verification of the design models.) Comparisons of test results on small- and moderate-sized bearings have not suggested the existence of a size effect, but without reliable tests on large bearings, it cannot be stated with certainty that one does not exist.

Second, the size of the bearing may create special problems in manufacturing that increase the need for testing. Elastomeric bearings are made by building up layers of elastomer and steel in the mold. Heat and pressure then are applied to vulcanize the elastomer. However, the heat is applied from the outside and must penetrate inwards by conduction. This takes time, and the outer regions of the bearing inevitably receive more heat and for a longer time than the inner regions. This is particularly true of thick bearings for two reasons. First, the steel shims are good thermal conductors and help to conduct the heat laterally, but this is not particularly helpful because the molding press generally applies the heat from the top and bottom only. Lateral heat flow is relatively unimportant. Second, vertical heat flow is critical because it occurs perpendicular to the steel and rubber layers, and heat conduction is poor in that direction. Consequently, a thick bearing is inherently more difficult to vulcanize. If at any location the rubber is not heated long enough, it will not be fully cured, and if it is heated to too high a temperature or for too long a time, it may revert. Either process will prevent achieving the desired material properties. Some manufacturers use embedded thermocouples to check the temperature distribution throughout such large bearings. This improves control of the process, but it does not eliminate the difficulties in curing large bearings.

Last, it may be difficult to test these large and unusual bearings because the required load is larger than the capacity of the available test machinery. This creates a practical problem, as the large bearings are the ones most in need of testing for verification, yet testing them is the most difficult. Some possible alternatives are discussed in Section 3.3 of this report.

CHAPTER 3

Interpretation, Appraisal, and Applications

3.1 Proposed Design Rules

Research showed that truck passage over a bridge causes shear strains in the bearing due to axial load effects that are much larger than the shear strains due to rotations. This fact causes difficulties in basing the design procedures directly on test results, because appropriate rotation data are available from the tests conducted for this study, but comparable compression fatigue data are not. The only ones available are those from NCHRP Report 298 (Roeder et al., 1987). The tests conducted in that study were on bearings without cover, which necessitated a method of measuring debonding different from the one used here, and renders very difficult the process of comparing the results of the two studies. Furthermore, most of the NCHRP 298 bearings were square with $S = 5$, whereas those used here were 22 in. × 9 in., with $S = 6.2$.

Attempts to construct a design model were made with Nonlinear and Linear Model for stress-strain relationships. In both cases equivalence of shear strains was assumed. The Nonlinear Model predicted behavior for a common bearing size that was in disagreement with field experience so that model was discarded, and the design methodology for Method B was based on the Linear Model. Suitable provisions for Method A then were derived from the proposed Method B architecture by developing a maximum probable rotation value and computing axial stress allowed by Method B to accompany it. That axial stress forms the basis for the Method A design procedure in which explicit account of rotations is not required. The proposed design provisions for both methods are presented in Appendix G. The development of these procedures is discussed in detail in Appendix F.

One of the difficulties designers have experienced with the existing Method B AASHTO LRFD design rules is that large rotations combined with light axial loads often make design impossible because the no uplift provisions force the bearing to be very thick and causes problems with instability. The proposed provisions address this difficulty by allowing lift-off in bearings that have no external plates.

The proposed Method B design provisions are based on the total shear strain approach, whereby shear strains from each type of loading are computed separately and then added. This concept has underlain the AASHTO design provisions for many years, but its use has not been transparent. The change to an explicit use of that approach is proposed now because it simplifies the specifications and is easier for designers to understand because of its transparency. It also is used by specifications elsewhere (for example, AASHTO Seismic Isolation Specifications, EN 1337), although the numerical values proposed here differ slightly from those used in other specifications. The difference with isolation bearings reflects that they are typically larger and thicker than conventional bridge bearings and are subject to different loading (that is, a very small number of large shear loadings during a lifetime). Differences with European specifications are based on the significant effect of cyclic loading seen during the tests for this project. Such extensive test data were not available during development of EN 1337. The proposed specification provisions are slightly more conservative than those of EN 1337.

The total allowable strain is higher than the one implicit in the 2004 AASHTO LRFD Specifications, but that fact is partially offset by the presence of a constant amplification factor that is applied to cyclic strains arising from traffic loading. The Method B design provisions in Appendix G, based on the Linear Model, provide design rules for bearings that:

- Are consistent with the debonding observed in the tests,
- Are readily satisfied by bearings in common use today, thus passing a necessary and objective criterion of reasonability,
- Penalize cyclic loads, in accordance with the findings of the testing program, which showed that cyclic loading led to much more debonding than did monotonic loading of the same amplitude,
- Remove the previous restrictions on lift-off for bearings without external plates, and from which the girder can readily separate over part of the surface,

- Introduce a new check for hydrostatic tension stress to guard against internal rupture of the elastomer in bearings that have external plates and are subjected to light axial load and large rotations, and
- Eliminate the absolute compressive stress limit (presently 1.6 ksi or 1.75 ksi) to encourage the use of bearings with higher shape factors for high load applications. Such bearings performed extremely well in testing program. A stress limit related to *GS* remains.

A cyclic amplification factor of 2.0 is proposed. This is higher and more conservative, than the European value of 1.0 or 1.5 (which value is to be chosen by the bridge's owner). However, the cyclic test program conducted for this research showed that cyclic loading is significantly more damaging than static loading. Thus the European minimum value of 1.0 appears to be unrealistically low. The European Specification (EN 1337) uses the same total strain capacity of 5.0 proposed here, so the existence of a higher cyclic amplification factor in the present proposals makes them inherently more conservative than those of EN 1337. Despite that, the proposed rules are still simpler, more versatile, and more liberal than those in the 2004 AASHTO LRFD Specifications. Their greater simplicity, combined with the potential for higher allowable stresses when rotation is low and is explicitly taken into account, may result in designers preferring them to Method A for the majority of steel-reinforced elastomeric bearings.

The total shear strain caused by compression, rotation, and shear displacements is calculated. For each component, strain is divided into a static and a cyclic component. Strains arising from truck loading, of which several million cycles must be expected during the life of the bridge, are treated as cyclic. All others, including shear from thermal effects, are regarded as static. The total shear strain must satisfy:

$$\left(\gamma_{a,st} + \gamma_{r,st} + \gamma_{s,st}\right) + 2.0\left(\gamma_{a,cy} + \gamma_{r,cy} + \gamma_{s,cy}\right) \le 5.0 \qquad (3\text{-}1)$$

where

$$\gamma_a = D_a \frac{\sigma_s}{GS} = \text{shear strain caused by axial load,}$$

$$\gamma_r = D_r \left(\frac{L}{h_{ri}}\right)^2 \theta_i = \text{shear strain caused by rotation, and}$$

$$\gamma_s = \frac{\Delta_s}{h_{rt}} = \text{shear strain caused by shear displacement.}$$

Subscripts "*st*" and "*cy*" indicate static and cyclic loading respectively.

This single provision replaces the four equations in the existing Article 14.7.5.3.2 ("Compressive Stress") and the six equations in the existing 14.7.5.3.5. ("Combined Compression and Rotation"). The provisions that presently limit the live load and total load separately are addressed by the presence in Equation (3-1) of the amplification factor of 2.0 on cyclic load effects. The existing restrictions on lift-off (present AASHTO Equation 14.7.5.3.5-1) have been removed for bearings without external bonded plates, because the tests showed no evidence of fatigue failure on the tension side of such bearings subjected to combined axial load and rotation. The potential for such fatigue was the basis for the provisions presently in force, which were based partly on research conducted on very small laboratory specimens (Caldwell et al., 1940). That study showed reversal of strain during cycling was particularly damaging, and, because at the time lift-off was taken to imply strain reversal, design provisions were developed to restrict lift-off. The removal of this restriction allows lift-off of the girder or sole plate from the bearing, which solves most of the existing problems with design for simultaneous light axial load and large rotation.

In the 2004 AASHTO LRFD Specifications, the total axial stress is restricted to 1.60 ksi or 1.75 ksi (in the presence or absence of shear displacements), regardless of shape factor. Study of the mechanics of bearings shows that load-carrying ability is more logically related to the product *GS* (shear modulus of the rubber times the shape factor) than to absolute stress, because *GS* largely controls the shear strain due to compression. The previous 1.75 ksi limit was imposed because, at the time, only a limited number of tests had been conducted on higher shape factor bearings.

However, that situation has now changed. Several bearings with higher shape factors were tested in this program, and many isolation bearings now have been built and tested, almost all of which have shape factors higher than 6, which lies near the top of the range commonly used for conventional bridge bearings. (Many isolation bearings have shape factors of 20 or more.) Isolation bearings also are typically stressed more highly than conventional bearings, and bearings tested in this program with shape factors of 9 and 12 were loaded repeatedly to a stress of 12 ksi (the test machine capacity), and showed no debonding at all (see tests SHF1-C2 and SHF2-C2 in Appendix A). The compressive capacity of such bearings is well demonstrated. The proposed limit of 3.0 on the static component of γ_a implies a permanent axial stress no higher than approximately 2.0*GS*, which is still conservative. For example, in the axial load tests, debonding initiated at average axial stresses between 4.7 *GS* and 7.8 *GS*, and specimens SHF1-C2 and SHF2-C2 did not debond at all under cycles of axial load to 12*GS*.

That limiting stress of 2.0*GS* is not expected to be used often. The size of many bearings is controlled by the desire to make them as wide as the girder flange in order to promote lateral stability during erection of the girders. The resulting compressive stresses are then relatively low. However, the need occasionally arises for a bearing with a very large capacity, and use of higher allowable compressive stresses permits an elastomeric bearing to be considered for those cases.

Restriction against uplift is necessary if the bearing has external plates bonded to it, because large rotations combined with light axial load could lead to hydrostatic tension and brittle internal rupture of the elastomer. Previously, this provision was unnecessary, because the no uplift provisions prevented such behavior. Gent and Lindley (1959b) studied the problem and found that rupture occurred at a hydrostatic tension stress of approximately 0.9*E*, or about 2.7*G*. The problem is expected to arise only rarely, but it must be addressed nonetheless. It is achieved by requiring

$$\frac{\sigma_{hyd}}{3G} \le 0.75 \tag{3-2}$$

where σ_{hyd} is the peak hydrostatic tension, computed by

$$\frac{\sigma_{hyd}}{3G} = S^3 \theta_L f(\alpha) \tag{3-3}$$

$$f(\alpha) = \frac{4}{3}\left\{\left(\alpha^2 + \frac{1}{3}\right)^{1.5} - \alpha\left(1-\alpha^2\right)\right\} \tag{3-4}$$

and

$$\alpha = \frac{\varepsilon_a}{S\theta_L} \tag{3-5}$$

where the axial strain, ε_a, is given by

$$\varepsilon_a = \frac{\sigma_a}{3B_a G S^2} \tag{3-6}$$

and is to be taken as positive for compression in Equation (3-6). Constant B_a is given approximately by

$$B_a = (2.31 - 1.86\lambda) + (-0.90 + 0.96\lambda)\left(1 - \min\left\{\frac{L}{W}, \frac{W}{L}\right\}\right)^2 \tag{3-7}$$

where L/W is the aspect ratio of the bearing in plan. For values of α greater than 0.333, the hydrostatic stress is compressive, and no limit is required. The values of ε_a and θ_L used in Equation (3-5) consist of the static components plus 2.0 times the cyclic components.

Although Equations (3-2) to (3-7) appear somewhat complicated, they are not difficult to evaluate, especially if programmed into a spreadsheet. The apparent complexity arises because the location of the maximum hydrostatic tension stress varies with the relative magnitudes of rotation and axial load. The equations were obtained for an infinite strip bearing by the linear theory and validated by FEA. Agreement was very good. They are conservative for other shapes.

The previous restriction on shear displacement (limited to half the rubber thickness) is retained without change, as are the provisions for compressive deflection, stability, steel reinforcement, and seismic conditions.

The foregoing concepts define Method B. Method A was formulated with the goal to be consistent with Method B to the greatest extent possible. That was done by developing a design rotation that represents the maximum value likely to occur in practice and using Method B to determine the corresponding allowable axial stress. Two restrictions on the use of Method A were found to be necessary. First, it should not be used if external bonded plates are present. This was done to avoid having to address the problems associated with hydrostatic tension. Most bearings are fabricated without external plates so the restriction is not expected to be serious.

Second, Method A may not be used if $S^2/n > 16$. This restriction is necessary to avoid excessive shear strains at the bearing's edge when the rotation is large. Bearings with few, thin layers do not accommodate rotations well and experience relatively large shear strains due to the rotation. They also have large values of S^2/n. The restriction is part of the price of ignoring rotations during design. The allowable axial stress is related to the limiting value of S^2/n: the higher the stress used, the lower must be the largest S^2/n permissible. Appendix F describes the process of selecting a suitable combination of allowable stress and maximum S^2/n. Care was taken to ensure that bearings suitable for a typical freeway overpass could still be designed using Method A, which is the common practice today.

One difficulty arose. Method A covers several bearing types other than steel-reinforced elastomeric bearings, and they are designed without any amplification factors to represent the effects of cyclic loading. Because this research program did not address those bearing types, no information was generated on their response to cyclic load, and there was no basis for altering the provisions for their design. It was decided to leave Method A designs in terms of nonamplified stresses, and to alter the allowable stresses developed from Method B accordingly.

In that regard, Methods A and B are not fully compatible. However, in other ways, they are more compatible than the case today. Under the 2004 Specifications, it is possible to design a bearing for a set of loads under Method A, and to find that, under Method B, same bearing with the same loads fails to meet all the design criteria. Under the proposed specifications, such occurrences will be much less common. (Review of the development of Method A, verified by trial and error, showed that this can only happen if the rotations are larger than the design rotations used in the development of Method A, and this is most improbable.)

Apart from the addition of these two restrictions, Method A follows the same structure as in the existing specifications. The allowable stresses in it are raised by 25%, in parallel with the increases in Method B.

3.2 Design Examples

A spreadsheet was prepared for designing bearings, based on the proposed design provisions in Appendix G. For any set of loadings, the spreadsheet computes the total shear strain and the hydrostatic tension stress. It also makes the checks required by the existing AASHTO LRFD Specifications, so that the proposed and existing designs can be compared.

The spreadsheet was used to prepare the design examples presented in this section. In the examples, the AASHTO notation of θ_i is used in place of θ_L for the rotation per layer, and reference is made to the number of each source equation from Appendix G. Numerical values were taken from the spreadsheet. Because of rounding, they may in some cases differ slightly from those obtained by following the calculations with a hand calculator. Numerical values are given to four digit accuracy to help minimize this problem. Such accuracy is not warranted in practice by the reliability of the material properties or the design equations.

Six examples are intended to illustrate different features of the design process and are summarized in Table 3.1. Relevant features in each are highlighted in the table. Most are self-explanatory. The "Rotation Sum" feature concerns the manner in which rotations are added. If, for example, initial girder camber causes a positive rotation, not all of which is removed by the application of full dead load, then the effect of adding live load might be to reduce the relative rotation of the top and bottom surfaces of the bearing. How then should the rotations be added in applying the proposed design equations?

Equations in the following examples numbered with G (such as G-10) refer to equations in Appendix G, the proposed specifications. Appendix G is located on the web at http://trb.org/news/blurb_detail.asp?id=8556.

Example 1

Common bearing, lift-off permitted, AASHTO Type V girders.

Design Criteria

A prestressed concrete girder bridge is supported on elastomeric bearings. The AASHTO Type V girders span 120 ft. and have 28 in. wide bottom flanges. Under full dead load, the load is 105 kips and the girder end is horizontal. The live load causes an axial load of 48 kips and a rotation of 0.0025 radians. Shear displacement due to thermal effects is ± 0.75 inches, all to be taken at one end of the girder because the other end of the bridge is fixed against longitudinal movement. Concrete shear keys prevent transverse movement at the girder ends. Design by Method A, if possible.

Solution

For shear displacements,

$$h_{rt} \geq 2\Delta_s = 2 * 0.75 = 1.5 \text{ inches} \qquad \text{(G-10)}$$

Try $W = 25$ in. (to fit the flange) and two internal layers of 0.75 in. each. Select an elastomer with $G = 0.110$ ksi (approx. 50 durometer). Trial and error (with a spreadsheet) shows that a bearing with gross plan dimensions of 25 in. × 10 in. will work. Calculations are as follows:

$$L_{eff} = 0.5 * (10.0 + 9.5) = 9.75 \text{ inches}$$

$$W_{eff} = 0.5 * (25.0 + 24.5) = 24.75 \text{ inches}$$

$$S = \frac{W_{eff} L_{eff}}{2h_{ri}\left(W_{eff} + L_{eff}\right)} = \frac{24.75 * 9.75}{2 * 0.75\left(24.75 + 9.75\right)} = 4.663$$

$$A = W_{eff} L_{eff} = 241.3 \text{ in}^2$$

For acceptance under Method A,

There are no external bonded plates OK

$$\frac{S^2}{n} = \frac{4.663^2}{2} = 10.872 < 16 \qquad \text{OK}$$

The total axial stress is

$$\sigma_a = \frac{105 + 48}{241.3} = 0.6340 \text{ ksi} < 1.25 \text{ ksi} \qquad \text{OK}$$

The total axial stress/GS is

$$\frac{\sigma_a}{GS} = \frac{0.6340}{0.110 * 4.663} = 1.236 < 1.25 \qquad \text{OK}$$

The bearing is thus satisfactory under Method A. It also proves to be satisfactory under both the existing and the

Table 3.1. Bearing design examples.

No.	Bridge type	Bearing type	Rotn. Sum	Hydrostatic	Skew
1	AASHTO psc	"Method A"	Simple	No	No
2	PSC girder	Standard	Complex	No	No
3	Steel girder	Standard	Simple	Yes	No
4	Steel girder	Standard	Simple	No	Yes
5	PSC box	Large	Simple	No	No
6	Special	High S	Simple	No	No

proposed Method B approaches. It does not satisfy the existing Method A because the axial stress/GS exceeds the limit of 1.0.

Example 2

Common bearing, lift-off permitted.

Design Criteria

A prestressed concrete girder bridge is supported on elastomeric bearings. The girders span 125 ft. and have 25 in. wide bottom flanges. Under construction conditions, the load is 50 kips and the rotation is 0.008 radians, due to camber. Under full dead load, the load is 120 kips and the girder end is horizontal. The live load causes a load of 70 kips and a rotation of 0.002 radians. Shear displacement due to thermal effects is ± 0.75 in., all to be taken at one end of the girder, because the other end of the bridge is fixed against longitudinal movement. Concrete shear keys prevent transverse movement at the girder ends. Thermal camber causes a rotation of 0.0015 radians.

Solution

For shear displacements,

$$h_{ri} \geq 2\Delta_s = 2 * 0.75 = 1.5 \text{ inches} \qquad \text{(G-10)}$$

Try $W = 23$ in. (to fit the flange) and three internal layers of 0.5 in. each. Select an elastomer with $G = 0.110$ ksi (approx. 50 durometer). Assume $K = 450$ ksi (default value).

Trial and error shows that the minimum possible gross length is 7.013 in. Use 8 in. to avoid the absolute minimum. Edge cover is 0.25 in. The shims are therefore 22.5 in. × 7.5 in. Calculations are as follows. The subscripts *para* and *perp* indicate conditions relevant to rotation about axes parallel and perpendicular to the support face. Thus, in a bridge without skew, bending of the girder causes a rotation θ_{para}, while torsion of the girder would cause an end rotation θ_{perp}. Here the long side of the bearing is placed parallel to the support face.

$$L_{eff} = 0.5 * (8.0 + 7.5) = 7.75 \text{ inches}$$

$$W_{eff} = 0.5 * (23.0 + 22.5) = 22.75 \text{ inches}$$

$$S = \frac{W_{eff} L_{eff}}{2h_{ri}\left(W_{eff} + L_{eff}\right)} = \frac{22.75 * 7.75}{2 * 0.5\left(22.75 + 7.75\right)} = 5.781$$

$$A = W_{eff} L_{eff} = 176.3 \text{ in}^2$$

$$\lambda = S\sqrt{\frac{3G}{K}} = 5.781\sqrt{\frac{3 * 0.11}{450}} = 0.1565$$

Coefficients needed for shear strains are

$$D_{a1} = 1.060 + 0.210\lambda + 0.413\lambda^2 = 1.1030$$

$$D_{a2} = 1.506 - 0.071\lambda + 0.406\lambda^2 = 1.5048$$

$$D_{a3} = -0.315 + 0.195\lambda - 0.047\lambda^2 = -0.2856$$

$$D_{a,para} = \max\left\{D_{a1}, \left(D_{a2} + D_{a3}\frac{L}{W}\right)\right\}$$

$$= \max\left\{1.1030, \left(1.5048 - 0.2856\frac{7.75}{22.75}\right)\right\} = 1.4075$$

$$D_{a,perp} = \max\left\{1.1030, \left(1.5048 - 0.2856\frac{22.75}{7.75}\right)\right\} = 1.1030 \text{(G-4)}$$

$$D_{r,para} = \min\left\{\frac{1.552 - 0.627\lambda}{2.233 + 0.156\lambda + L/W}, 0.5\right\}$$

$$= \min\left\{\frac{1.552 - 0.627 * 0.1565}{2.233 + 0.156 * 0.1565 + 0.3407}, 0.5\right\} = 0.5 \text{ (G-7)}$$

$$D_{r,perp} = \min\left\{\frac{1.552 - 0.627\lambda}{2.233 + 0.156\lambda + L/W}, 0.5\right\}$$

$$= \min\left\{\frac{1.552 - 0.627 * 0.1565}{2.233 + 0.156 * 0.1565 + 2.9355}, 0.5\right\}$$

$$= 0.2800 \qquad \text{(G-7)}$$

Under service conditions:

Axial load = 120 kips DL + 70 kips LL,

Shear deformation = 0.75 in.,

Rotation (rad.) = 0.005 misalignment + 0.0015 thermal + 0.002 LL, and

$$\sigma_a = \frac{120 + 2.0 * 70}{176.3} = 1.475 \text{ ksi}$$

Because the rotation occurs about the weak axis, the shear strains on the long side are critical. Shear strain there due to (amplified) axial load is

$$\gamma_a = D_{a,para}\frac{\sigma_a}{GS} = 1.4075\frac{1.475}{0.110 * 5.781} = 3.264 \qquad \text{(G-3)}$$

The components of the total amplified rotation are illustrated in Figure 3.1. Under full DL, the girder is horizontal. If thermal camber is ignored, the rotation under amplified (DL + LL) is (0.0 + 2 * 0.002) = 0.004 rad. downwards. However, the thermal camber is always upwards so, if it is included, the amplified sum of the DL + thermal + 2 * LL gives a smaller total of only 0.0015 rad. downwards, and is not the critical load case. Alternatively, in the interests of simplicity, a very conservative estimate always can be obtained by taking the sum of the absolute values of the components or, in this case, 0.0 (DL) + 0.0015(thermal) + 2 * 0.002(LL) = 0.0055 rad.

Figure 3.1. Girder end rotation components.

To any of these totals must be added the allowance for misalignment of 0.005 rad., which should always be taken in the sense that is most disadvantageous.

The misalignment allowance is small (approximately ⅛ in. elevation difference between the two ends of the 23 in. long bearing). Despite that, it still constitutes about half of the total design rotation, and demonstrates the importance of the accuracy of the initial setting. Here the conservative estimate of 0.0055 rad. is used for purposes of illustration. Including the misalignment allowance, the total rotation is

$$\theta_{tot} = 0.005 + 0.0015 + 2.0(0.002) = 0.0105 \text{ rad.}$$

Shear strain due to rotation about the weak axis is

$$\gamma_r = D_{r,para}\left(\frac{L}{h_{ri}}\right)^2 \theta_i = 0.5000\left(\frac{7.75}{0.5}\right)^2\left(\frac{0.0105}{3}\right) = 0.420 \quad \text{(G-6)}$$

Shear strain due to shear displacement is

$$\gamma_s = \frac{\Delta_s}{h_{rt}} = \frac{0.75 \text{ inches}}{1.5 \text{ inches}} = 0.5 \quad \text{(G-10)}$$

The total shear strain check is given by

$$\gamma_{tot} = \gamma_a + \gamma_r + \gamma_s = 3.264 + 0.420 + 0.500 = 4.185 \le 5.0 \quad \text{(G-1)}$$

The shear strain due to the static component of the axial load is

$$\gamma_a = D_{a,para}\frac{\sigma_a}{GS} = 1.4075\frac{(120/176.3)}{0.110 * 5.781} = 1.507 < 3.0 \quad \text{(G-2)}$$

The bearing has no external plates, so a check on hydrostatic tension is not necessary. Stability criteria are satisfied.

Under initial conditions:

Load = 50 kips
Total rotation = 0.005 + 0.008 = 0.013 rad.
Shear displacement = 0.0
These loadings are static, so no amplification factor is needed.

$$\sigma_a = \frac{50}{176.3} = 0.284 \text{ ksi}$$

Shear strain due to axial load is

$$\gamma_a = D_{a,para}\frac{\sigma_a}{GS} = 1.4075\frac{0.284}{0.110 * 5.781} = 0.628 \quad \text{(G-3)}$$

Shear strain due to rotation is

$$\gamma_r = D_{r,para}\left(\frac{L}{h_{ri}}\right)^2 \theta_i = 0.5000\left(\frac{7.75}{0.5}\right)^2\left(\frac{0.013}{3}\right) = 0.521 \quad \text{(G-6)}$$

Total shear strain for rotation about the weak axis is

$$\gamma_{tot} = \gamma_a + \gamma_r + \gamma_s = 0.628 + 0.521 + 0.000 = 1.148 < 5.0 \quad \text{(G-1)}$$

For rotation about the strong axis, the service level shear strain due to axial load is

$$\gamma_a = D_{a,perp}\frac{\sigma_a}{GS} = 1.1030 * \frac{1.475}{0.110 * 5.781} = 2.558 \quad \text{(G-3)}$$

The total amplified rotation is due to misalignment alone

$$\theta_{tot} = 0.005 \text{ rad.}$$

Shear strain due to rotation is

$$\gamma_r = D_{r,perp}\left(\frac{L}{h_{ri}}\right)^2 \theta_i = 0.2800\left(\frac{22.75}{0.5}\right)^2\left(\frac{0.005}{3}\right) = 0.966 \quad \text{(G-6)}$$

Shear strain due to shear displacement is zero, so the total shear strain is

$$\gamma_{tot} = \gamma_a + \gamma_r + \gamma_s = 2.558 + 0.966 + 0.000 = 3.524 \le 5.0 \quad \text{(G-1)}$$

Under initial conditions, the strains are

$$\gamma_a = D_{a,perp}\frac{\sigma_a}{GS} = 1.1030\frac{0.284}{0.110 * 5.781} = 0.492 \quad \text{(G-3)}$$

The total amplified rotation is

$$\theta_{tot} = 0.005 \text{ rad.}$$

Shear strain due to rotation is

$$\gamma_r = D_{r,perp}\left(\frac{L}{h_{ri}}\right)^2 \theta_i = 0.2800\left(\frac{22.75}{0.5}\right)^2\left(\frac{0.005}{3}\right) = 0.966 \quad \text{(G-6)}$$

Shear strain due to shear displacement is zero, so the total shear strain is

$$\gamma_{tot} = \gamma_a + \gamma_r + \gamma_s = 0.492 + 0.966 + 0.000 = 1.458 \le 5.0 \quad \text{(G-1)}$$

According to the existing LRFD Method B specifications, this bearing would just fail the compressive stress limit of 1.66GS. It also would just fail the combined stress requirement. However, it does satisfy all the performance checks with the proposed specifications.

The bearing may also be evaluated under the proposed Method A. Results are as follows:

No bonded external play exist OK

$$\frac{S^2}{n} = \frac{5.781^2}{3} = 11.139 < 16 \quad \text{OK}$$

The total (nonamplified) compressive stress is

$$\sigma_a = \frac{120 + 70}{176.3} = 1.078 \text{ ksi} < 1.25 \text{ ksi} \quad \text{OK}$$

The total (nonamplified) compressive stress/GS is

$$\frac{\sigma_a}{GS} = \frac{1.078 \text{ ksi}}{0.110 * 5.781} = 1.695 > 1.25 \quad \text{OK}$$

The bearing therefore does not satisfy the proposed Method A requirements. By adding an extra shim, and making four layers at ⅜ in. each rather than 3 layers at ½ in., the design satisfies Method A. Under Method B, the bearing is quite highly stressed in compression and the rotations are quite small, so it is not surprising that, with three layers of rubber, it does not quite satisfy Method A criteria.

Example 3

Steel bridge, common bearing size, large camber, but lift-off prevented. Hydrostatic tension is possible.

Design Criteria

A steel plate girder bridge is supported on elastomeric bearings. The girders span 150 ft. and have 22 in. wide flanges. Under construction conditions, the load is 32 kips and the rotation is 0.04 radians (camber). (This camber is extreme but was selected to create conditions in which hydrostatic tension might pose problems. Such large cambers are likely only with very slender steel girders.) Under full dead load, the end of the girder is exactly horizontal and the total load is 115 kips. The live load causes a load of 70 kips and a rotation of 0.002 radians. Shear displacement due to thermal effects is ± 1.0 in., all to be taken at one end. The bearing is to have external plates bonded to the elastomer, and is to be bolted to the girder directly after erection. Use a 50 durometer elastomer with $G = 0.110$ ksi.

Solution

Try a bearing 20 in. wide, with a total rubber thickness of 2 in. Note that, under initial conditions, hydrostatic tension may cause a problem. Check it first. Trial and error (with a spreadsheet) shows that a bearing 20 in. × 8 in., with four ½ in. thick rubber layers, will work. Calculations are shown below.

The bearing properties (for rotation about the weak axis) are:

$$L_{eff} = 0.5 * (8.0 + 7.5) = 7.75 \text{ inches}$$

$$W_{eff} = 0.5 * (20.0 + 19.5) = 19.75 \text{ inches}$$

$$S = \frac{W_{eff} L_{eff}}{2h_{ri}(W_{eff} + L_{eff})} = \frac{19.75 * 7.75}{2 * 0.5(19.75 + 7.75)} = 5.566$$

$$A = W_{eff} L_{eff} = 153.1 \; in^2$$

$$\lambda = S\sqrt{\frac{3G}{K}} = 5.566\sqrt{\frac{3 * 0.11}{450}} = 0.1507$$

Coefficients needed for shear strains are

$$D_{a1} = 1.060 + 0.210\lambda + 0.413\lambda^2 = 1.1010$$

$$D_{a2} = 1.506 - 0.071\lambda + 0.406\lambda^2 = 1.5045$$

$$D_{a3} = -0.315 + 0.195\lambda - 0.047\lambda^2 = -0.2867$$

$$D_{a,para} = \max\left\{D_{a1}, \left(D_{a2} + D_{a3}\frac{L}{W}\right)\right\}$$

$$= \max\left\{1.1010, \left(1.5045 - 0.2867\frac{7.75}{19.75}\right)\right\} = 1.3920$$

$$D_{a,perp} = \max\left\{1.1010, \left(1.5045 - 0.2867\frac{19.75}{7.75}\right)\right\} = 1.1010 \text{ (G-4)}$$

$$D_{r,para} = \min\left\{\frac{1.552 - 0.627\lambda}{2.233 + 0.156\lambda + L/W}, 0.5\right\}$$

$$= \min\left\{\frac{1.552 - 0.627 * 0.1507}{2.233 + 0.156 * 0.1507 + 0.3924}, 0.5\right\}$$

$$= 0.5 \quad \text{(weak axis)} \quad \text{(G-6)}$$

$$D_{r,perp} = \min\left\{\frac{1.552 - 0.627\lambda}{2.233 + 0.156\lambda + L/W}, 0.5\right\}$$

$$= \min\left\{\frac{1.552 - 0.627 * 0.1507}{2.233 + 0.156 * 0.1507 + 2.5484}, 0.5\right\}$$

$$= 0.3033 \quad \text{(strong axis)} \quad \text{(G-6)}$$

The axial stiffness coefficient, B_a, is given by Eq. G-33 as

$$B_a \approx (2.31 - 1.86\lambda) + (-0.90 + 0.96\lambda)\left(1 - \min\left\{\frac{L}{W}, \frac{W}{L}\right\}\right)^2$$

$$= (2.31 - 1.86 * 0.1507) + (-0.90 + 0.96 * 0.1507)(1 - 0.3924)^2$$

$$= 1.7508 \quad \text{(G-16)}$$

Under initial conditions, the axial stress is

$$\sigma_a = \frac{P}{A_{eff}} = \frac{32}{153.1} = 0.209 \text{ ksi}$$

The axial strain [Eq. (G-16)] is then

$$\varepsilon_a = \frac{\sigma_a}{3G\left(A_a + B_a S^2\right)} = \frac{0.209}{0.330\left(1.0 + 1.7508 * 5.566^2\right)}$$

$$= 0.01147 \qquad \text{(G-15)}$$

The rotation is 0.04 (camber) + 0.005 (misalignment), so the dimensionless variable α is

$$\alpha = \frac{\varepsilon_a}{S\theta_i} = \frac{0.01147}{5.566 * 0.045 / 4} = 0.1832 \qquad \text{(G-15)}$$

$$f(\alpha) = \frac{4}{3}\left\{\left(\alpha^2 + \frac{1}{3}\right)^{1.5} - \alpha\left(1 - \alpha^2\right)\right\} = 0.0603 \qquad \text{(G-13)}$$

The hydrostatic tension can be obtained from Eq. (G-30) as

$$\frac{\sigma_{hyd}}{G} = 3S^3\theta_i f(\alpha) = 3 * 5.566^3 * \left(\frac{0.045}{4}\right) * 0.0603$$

$$= 0.3508 < 2.25 \qquad \text{(G-12)}$$

Hydrostatic tension exists, but its magnitude is acceptable. If hydrostatic tension had posed a problem it might have been solved by specifying a construction procedure that requires the bearing not to be bolted to the girder until after the slab has been poured and the rotation due to camber had been eliminated. However, such a provision is undesirable because it could be forgotten on site. Making the bearing thicker would be a better alternative.

Under initial load, for rotation about the weak axis, the shear strains due to compression are

$$\gamma_a = D_{a,para}\frac{\sigma_a}{GS} = 1.3920 * \frac{0.209}{0.110 * 5.566} = 0.475 \qquad \text{(G-3)}$$

Shear strain due to rotation is

$$\gamma_r = D_{r,para}\left(\frac{L}{h_{ri}}\right)^2 \theta_i = 0.5000\left(\frac{7.75}{0.5}\right)^2\left(\frac{0.045}{4}\right) = 1.351 \qquad \text{(G-6)}$$

Total shear strain is

$$\gamma_{tot} = \gamma_a + \gamma_r + \gamma_s = 0.475 + 1.351 + 0.000 = 1.827 \qquad \text{(G-1)}$$

Under full service load, the calculations are similar to those of Example 1 and are not presented here.

It is instructive to check the bearing against the existing LRFD design specifications under initial conditions, given the large rotation and light axial load. Eq. 14.7.5.3.5-1 of the LRFD Specifications requires

$$\sigma_s > 1.0GS\left(\frac{\theta}{n}\right)\left(\frac{B}{h_{ri}}\right)^2 = 1.0 * 0.110 * 5.566\left(\frac{0.045}{4}\right)\left(\frac{8}{0.5}\right)^2$$

$$= 1.763 \text{ ksi}$$

(Note that B and σ_s in the existing specifications are the same as the quantities L and σ_a in this report. Also, gross, rather than effective, bearing dimensions are used for all calculations in the existing Specifications).

However

$$\sigma_s = \frac{32 \text{ kips}}{20 * 8 \text{ inch}} = 0.200 \text{ ksi}$$

Thus, the bearing fails by a significant margin to satisfy the uplift provisions of the existing Specifications because of the combination of high rotation and low axial load. The fact that the initial conditions prove acceptable under the proposed Method B provisions is an important change.

A girder with such a large camber also poses potential problems during construction. The bottom flange will elongate, and the bearing will move longitudinally, as the girder is stressed by the addition of the dead weight of the deck and other components. An approximate value for the magnitude of the movement can be obtained by considering the two major sources of it. In the interests of simplicity, the girder is assumed here to be symmetric. The girder is assumed to be 5 ft. deep (span/depth = 30).

End rotation of the girder gives a movement at each end of

$$\Delta = \frac{d}{2}\theta = \frac{60}{2}0.04 = 1.2 \text{ in.}$$

The girder also flattens out from its cambered shape. The neutral axis by definition does not change length, but its horizontal projected length does, because its initial curved shape changes to a straight line by the time the camber has been completely eliminated. The change in length is given by

$$\Delta = \int_0^L \frac{1}{2}\left(\frac{dy}{dx}\right)^2 dx$$

If the cambered shape is a parabola, this gives

$$\Delta = 2.667\frac{a_0^2}{L}$$

If it is sinusoidal

$$\Delta = \frac{\pi^2}{4}\frac{a_0^2}{L} \approx 2.467\frac{a_0^2}{L}$$

where a_0 = the initial camber height. The exact cambered shape is seen to have little effect on the magnitude of the longitudinal movement. Using the parabolic shape, and noting that

$$\theta_{camber} = 4\frac{a_0}{L}$$

$$\Delta = 2.667\frac{a_0^2}{L} = 2.667\left(\frac{\theta}{4}\right)^2 L = 2.667\left(\frac{0.04}{4}\right)^2 1800 = 0.48 \text{ in.}$$

The movement must occur at the nonfixed end of the bridge, where

$$\Delta_{total} = 2 * 1.2 + 0.48 = 2.88 \text{ in.}$$

This is significantly larger than the ±1.0 inches of thermal expansion, so provision should be made for resetting the girder on the bearings during construction. This problem is more likely to occur in steel bridges because they are typically more flexible than concrete ones.

Example 4

Common bearing, but lift-off allowed. The bridge also has 55 degrees skew. No thermal effects. The complexities in this example pertain to the skew.

Design Criteria

A steel plate girder bridge is supported on elastomeric bearings. The girders span 150 ft. and have 22 in. wide flanges. Under construction conditions, the load is 32 kips and the rotation is 0.04 radians (bending camber), and there is no torsional rotation. Under full dead load, the girder is exactly horizontal in bending, has a torsional rotation of 0.01 radians, and the total load is 115 kips. The live load causes a load of 70 kips and rotations of 0.002 radians (bending of girder) and 0.003 radians (torsion of girder). Shear displacement due to thermal effects is ± 1.0 in., all to be taken at one end, in the longitudinal direction. Use an elastomer with $G = 0.110$ ksi.

The bearings are to be oriented with their long edges parallel to the support. Guides at the support prevent movement perpendicular to the girder axes, but allow longitudinal displacement.

Solution

Try a rectangular bearing that will fit under the girder flange, with a total rubber thickness of 2 in. Trial and error (with a spreadsheet) shows that a bearing 18 in. × 9 in. will carry the loads and will fit in the space available. Calculations for the service loading are shown below. The orientation and labeling of the axes are shown in Figure 3.2.

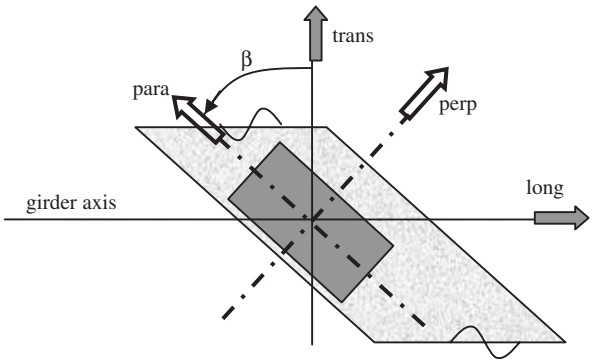

Figure 3.2. Orientation of axes for skew bridge.

The bearing properties (for rotation about the weak axis) are:

$$L_{eff} = 0.5 * (9.0 + 8.5) = 8.75 \text{ inches}$$

$$W_{eff} = 0.5 * (18.0 + 17.5) = 17.75 \text{ inches}$$

$$S = \frac{W_{eff} L_{eff}}{2h_{ri}\left(W_{eff} + L_{eff}\right)} = \frac{17.75 * 8.75}{2 * 0.5(17.75 + 8.75)} = 5.861$$

$$A = W_{eff} L_{eff} = 155.3 \text{ in}^2$$

$$\lambda = S\sqrt{\frac{3G}{K}} = 5.861\sqrt{\frac{3 * 0.11}{450}} = 0.1587$$

Coefficients needed for shear strains are

$$D_{a1} = 1.060 + 0.210\lambda + 0.413\lambda^2 = 1.1037$$

$$D_{a2} = 1.506 - 0.071\lambda + 0.406\lambda^2 = 1.5050$$

$$D_{a3} = -0.315 + 0.195\lambda - 0.047\lambda^2 = -0.2852$$

$$D_{a,para} = \max\left\{D_{a1}, \left(D_{a2} + D_{a3}\frac{L}{W}\right)\right\}$$

$$= \max\left\{1.1037, \left(1.5050 - 0.2852\frac{8.75}{17.75}\right)\right\} = 1.3643$$

$$D_{a,perp} = \max\left\{1.1037, \left(1.5050 - 0.2852\frac{17.75}{8.75}\right)\right\} = 1.1037 \text{(G-4)}$$

$$D_r = \min\left\{\frac{1.552 - 0.627\lambda}{2.233 + 0.156\lambda + L/W}, 0.5\right\}$$

$$= \min\left\{\frac{1.552 - 0.627 * 0.1587}{2.233 + 0.156 * 0.1587 + 0.4930}, 0.5\right\} = 0.5$$

$$\left(\text{weak axis}\right) \text{ (G-7)}$$

$$D_r = \min\left\{\frac{1.552 - 0.627\lambda}{2.233 + 0.156\lambda + L/W}, 0.5\right\}$$

$$= \min\left\{\frac{1.552 - 0.627 * 0.1587}{2.233 + 0.156 * 0.1587 + 2.0286}, 0.5\right\} = 0.3389$$

$$\left(\text{strong axis}\right) \text{ (G-7)}$$

Under service conditions:

Load = 115 kips DL + 70 kips LL

The local rotation and shear demands on the bearing for the strong (perp) and weak (para) axis rotation directions must be computed from the global coordinate system, defined by the longitudinal and transverse directions. In each case, the rotations due to loading are computed first, then the allowance for misalignment is added. The bearings are oriented at a skew angle of $\beta = 55$ degrees. With the positive directions as shown in Figure 3.2, the rotations in the global coordinate system are:

Girder bending: $\theta_{trans} = 0.000(DL) - 0.002(LL)$ rad.

Girder torsion: $\theta_{long} = 0.010(DL) + 0.003(LL)$ rad.

The rotations in the local bearing axes (perp and para) are obtained by using the transformation matrix:

$$\begin{Bmatrix}\theta_{perp}\\ \theta_{para}\end{Bmatrix}=\begin{bmatrix}\cos\beta & \sin\beta\\ -\sin\beta & \cos\beta\end{bmatrix}\begin{Bmatrix}\theta_{long}\\ \theta_{trans}\end{Bmatrix}$$

$$=\begin{Bmatrix}0.005736(DL)+0.0000824(LL)\\ -0.008192(DL)-0.003605(LL)\end{Bmatrix}\text{rad.}$$

The total amplified rotations, including the misalignment allowance, are therefore

$$\begin{Bmatrix}\theta_{perp}\\ \theta_{para}\end{Bmatrix}=\begin{Bmatrix}0.005736+2*0.0000824+0.005\\ -0.008192-2*0.003605-0.005\end{Bmatrix}=\begin{Bmatrix}+0.01090\\ -0.02040\end{Bmatrix}\text{rad.}$$

The shear deformations are obtained using the same transformation matrix

$$\begin{Bmatrix}\Delta_{perp}\\ \Delta_{para}\end{Bmatrix}=\begin{bmatrix}\cos\beta & \sin\beta\\ -\sin\beta & \cos\beta\end{bmatrix}\begin{Bmatrix}\Delta_{long}\\ \Delta_{trans}\end{Bmatrix}=\begin{Bmatrix}0.5736\\ -0.8192\end{Bmatrix}\text{in.}$$

The amplified axial stress is

$$\sigma_a=\frac{115+2.0*70}{155.3}=1.642\text{ ksi}$$

For shear strains on the long side (rotation about the weak or para axis), the shear strain due to (amplified) axial load is

$$\gamma_a=D_{a,para}\frac{\sigma_a}{GS}=1.3643*\frac{1.642}{0.110*5.861}=3.475 \qquad \text{(G-3)}$$

Shear strain due to rotation about the weak (para) axis is

$$\gamma_r=D_{r,para}\left(\frac{L}{h_{ri}}\right)^2\theta_i=0.5000\left(\frac{8.75}{0.5}\right)^2\left(\frac{0.02040}{4}\right)$$

$$=0.781 \qquad \text{(G-6)}$$

Shear strain due to shear deformation is

$$\gamma_s=\frac{\Delta_s}{h_{rt}}=\frac{0.5736\text{ inches}}{2.0\text{ inches}}=0.287 \qquad \text{(G-10)}$$

The total shear strain check is given by

$$\gamma_{tot}=\gamma_a+\gamma_r+\gamma_s=3.475+0.781+0.287$$

$$=4.542\le 5.0 \qquad \text{(G-1)}$$

The shear strain due to the static component of the axial load also is acceptable

$$\gamma_a=D_{a,para}\frac{\sigma_a}{GS}=1.3643\frac{(115/155.3)}{0.110*5.861}=1.567<3.0 \qquad \text{(G-3)}$$

For rotation about the strong, or perp, axis, the service level shear strain due to axial load is

$$\gamma_a=D_{a,perp}=\frac{\sigma_a}{GS}=1.1037*\frac{1.642}{0.110*5.861}=2.811 \qquad \text{(G-3)}$$

Shear strain due to rotation is

$$\gamma_r=D_{r,perp}\left(\frac{L}{h_{ri}}\right)^2\theta_i=0.3389\left(\frac{17.75}{0.5}\right)^2\left(\frac{0.01090}{4}\right)$$

$$=1.164 \qquad \text{(G-6)}$$

The total shear strain is

$$\gamma_{tot}=\gamma_a+\gamma_r+\gamma_s=2.811+1.164+0.410$$

$$=4.385\le 5.0 \qquad \text{(G-1)}$$

According to the existing LRFD Method B specifications, this bearing would just fail the compressive stress limit of 1.66GS, and would fail by a substantial margin of the uplift provision (about the strong axis) and the combined stress limit. Failure to meet the latter two criteria is not surprising, because they are very conservative and were a large part of the reason for conducting the research.

The bearing also fails to satisfy the proposed Method A requirements. The total axial stress/GS is

$$\frac{\sigma_s}{GS}=\frac{(115+70)/(17.75*8.75)}{0.110*5.861}=1.848>1.25\text{ ksi}$$

The shear strains due to combined loading about the strong (perp) axis also prove to be excessive.

Example 5

Long-span box girder bridge, large bearing, lift-off permitted.

Design Criteria

A prestressed concrete box girder bridge is supported on elastomeric bearings. There is no skew. The girders span 300 ft. Under full dead load, the end rotation is 0.003 (cambered upwards) and the load is 1,200 kips. The live load causes a load of 120 kips and a rotation of 0.0018 radians (downwards). Shear displacement due to thermal effects is –2.75, +1.00 in. Allow for 0.0015 radians of thermal rotation in the final condition.

Solution

For shear displacements,

$$h_{rt}\ge 2\Delta_s=2*2.75=5.5\text{ inches} \qquad \text{(G-10)}$$

Axial forces appear to dominate the design. Try a high shape factor bearing (generally good for axial capacity but bad for rotation capacity.) Make the bearing approximately 2 to 1 aspect ratio, to minimize the rotational effects. Assume ¼ in. edge cover.

Use $G = 0.135$ ksi (approx. 55 durometer) to increase the load capacity.

Trial and error shows that a bearing of 30 in. × 15 in., with 11 layers at 0.5 in. each will suffice. Final calculations are as follows:

The bearing properties (for rotation about the weak axis) are:

$$L_{eff} = 0.5 * (15.0 + 14.5) = 14.75 \text{ inches}$$

$$W_{eff} = 0.5 * (30.0 + 29.5) = 29.75 \text{ inches}$$

$$S = \frac{W_{eff} L_{eff}}{2h_{ri}\left(W_{eff} + L_{eff}\right)} = \frac{29.75 * 14.75}{2 * 0.5\left(29.75 + 14.75\right)} = 9.861$$

$$A = W_{eff} L_{eff} = 438.8 \; in^2$$

$$\lambda = S\sqrt{\frac{3G}{K}} = 9.861\sqrt{\frac{3 * 0.135}{450}} = 0.2958$$

Coefficients needed for shear strains are

$$D_{a1} = 1.060 + 0.210\lambda + 0.413\lambda^2 = 1.1583$$

$$D_{a2} = 1.506 - 0.071\lambda + 0.406\lambda^2 = 1.5205$$

$$D_{a3} = -0.315 + 0.195\lambda - 0.047\lambda^2 = -0.2614$$

$$D_{a,para} = \max\left\{D_{a1}, \left(D_{a2} + D_{a3}\frac{L}{W}\right)\right\}$$
$$= \max\left\{1.1583, \left(1.5205 - 0.2614\frac{14.75}{29.75}\right)\right\} = 1.3909$$

$$D_{a,perp} = \max\left\{1.1583, \left(1.5205 - 0.2614\frac{29.75}{14.75}\right)\right\}$$
$$= 1.1583 \qquad \text{(G-4)}$$

$$D_{r,para} = \min\left\{\frac{1.552 - 0.627\lambda}{2.233 + 0.156\lambda + L/W}, 0.5\right\}$$
$$= \min\left\{\frac{1.552 - 0.627 * 0.2958}{2.233 + 0.156 * 0.2958 + 0.4958}, 0.5\right\}$$
$$= 0.4924 \qquad \text{(weak axis)} \quad \text{(G-7)}$$

$$D_{r,perp} = \min\left\{\frac{1.552 - 0.627\lambda}{2.233 + 0.156\lambda + L/W}, 0.5\right\}$$
$$= \min\left\{\frac{1.552 - 0.627 * 0.2958}{2.233 + 0.156 * 0.2958 + 2.0169}, 0.5\right\}$$
$$= 0.3181 \qquad \text{(strong axis)} \quad \text{(G-7)}$$

The axial stiffness coefficient, B_a, is given by Eq. G-33 as

$$B_a \approx \left(2.31 - 1.86\lambda\right) + \left(-0.90 + 0.96\lambda\right)\left(1 - \min\left\{\frac{L}{W}, \frac{W}{L}\right\}\right)^2$$
$$= \left(2.31 - 1.86\lambda\right) + \left(-0.90 + 0.96 * 0.2958\right)\left(1 - 0.4958\right)^2$$
$$= 1.6032 \qquad \text{(G-16)}$$

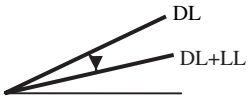

Figure 3.3. DL and LL rotations for bearing design.

Under service conditions (amplified loads):

$$\sigma_a = \frac{1200 + 2.0 * 120}{438.8} = 3.282 \text{ ksi}$$

For rotation about the critical parallel axis, shear strain due to axial load is shown in Figure 3.3.

$$\gamma_a = D_{a,para}\frac{\sigma_a}{GS} = 1.3909 * \frac{3.282}{0.135 * 9.861} = 3.429 \qquad \text{(G-3)}$$

The rotation consists of 0.003 rad. (DL) and –0.0018 rad. (LL). These two oppose each other, as shown in Figure 3.3, so the peak rotation theoretically occurs under dead load alone. Therefore the rotations should be treated as a static load of the DL + LL [0.0030 + (–0.0018) = 0.0012 rad.] plus a live load of –(–0.0018) = +0.0018 rad. 1.0 times the static rotation plus 2.0 times the cyclic then gives 1.0 * 0.0012 + 2.0 * 0.0018 = 0.0048 rad., to which must be added the misalignment allowance. The total amplified rotation is then 0.0048 + 0.005 = 0.0098 rad.

Shear strain due to rotation is

$$\gamma_r = D_{r,para}\left(\frac{L}{h_{ri}}\right)^2 \theta_i = 0.4924\left(\frac{14.75}{0.5}\right)^2\left(\frac{0.0098}{11}\right) = 0.382 \qquad \text{(G-6)}$$

Shear strain due to shear displacement is

$$\gamma_s = \frac{\Delta_s}{h_{rt}} = \frac{2.75 \text{ inches}}{5.5 \text{ inches}} = 0.5 \qquad \text{(G-10)}$$

The total shear strain is

$$\gamma_{tot} = \gamma_a + \gamma_r + \gamma_s = 3.429 + 0.382 + 0.500 = 4.311 < 5.0 \qquad \text{(G-1)}$$

The static axial stress is

$$\sigma_a = \frac{1200}{438.8} = 2.735 \text{ ksi}$$

and the corresponding shear strain is

$$\gamma_a = D_{a,para}\frac{\sigma_a}{GS} = 1.3909 * \frac{2.735}{0.135 * 9.861} = 2.857 < 3.0 \qquad \text{(G-3)}$$

Similar calculations for rotation about the strong axis, with only the construction misalignment rotation of 0.005, give

$$\gamma_a = D_{a,perp}\frac{\sigma_a}{GS} = 1.1583 * \frac{3.282}{0.135 * 9.861} = 2.855 \qquad \text{(G-3)}$$

$$\gamma_r = D_{r,perp}\left(\frac{L}{h_{ri}}\right)^2 \theta_i = 0.3181\left(\frac{29.75}{0.5}\right)^2\left(\frac{0.005}{11}\right) = 0.512 \quad \text{(G-6)}$$

$$\gamma_{tot} = \gamma_a + \gamma_r + \gamma_s = 2.855 + 0.512 + 0.000 = 3.367 < 5.0 \quad \text{(G-1)}$$

The shim thickness, based on $F_y = 36$ ksi, must satisfy

$$h_s \geq \frac{3h_{\max}\sigma_a}{F_y} = \frac{3 * 0.5 * 3.008}{36} = 0.1253 \text{ inches}$$

AASHTO Eq. (14.7.5.3.7-1)

This thickness requires 10 gage sheet steel, which is slightly thicker than the 11 gage commonly used for convenience in manufacturing. It illustrates the need for thicker shims when the axial stress on the bearing is high. The bearing has no external plates, so hydrostatic tension does not need to be checked. Stability criteria are satisfied. Initial conditions also are satisfactory. Because the bearing thickness is less than 8 in. and its plan area is less than 1000 in^2, special testing is not required.

Note that, according to the existing LRFD Specifications, this bearing would fail the compressive stress limits and the combined stress limits under final conditions. However, it has a shape factor (approx 10) that is higher than in most bridge bearings. It also would fail to satisfy the proposed Method A requirements, because the nonamplified axial stress is 3.01 ksi, which significantly exceeds the limit of 1.25 ksi. While it is quite large, it is still well within the fabrication capabilities of most manufacturers. For example, vibration isolation bearings are often twice as thick as this.

Example 6

Heavily loaded special purpose bearing, lift-off permitted.

Design Criteria

An elastomeric bearing is used to support a steel beam that is intended to yield cyclically under seismic loading in a large bridge. Special installation procedures ensure that there is no misalignment whatsoever. The dead load is the self-weight of the beam, which is negligible. The seismic load consists of 12 cycles of load to 2200 kips, accompanied by a rotation of 0.00167 rad. and a shear displacement of 0.25 in. The space available is 20 in. × 24 in.

Solution

Because the number of cycles of load is much smaller than under traffic load, treat the seismic load as static. The axial load appears to control the design, so use a high shape factor and a relatively hard elastomer with $G = 175$ psi, (approx 60 durometer). Assume ¼ in. edge cover.

Trial and error show that a bearing of 24 in. × 20 in., with 2 layers at 0.25 in. each will suffice. Final calculations are as follows:

The bearing properties (for rotation about the weak axis) are:

$$L_{eff} = 0.5 * (20.0 + 19.5) = 19.75 \text{ inches}$$

$$W_{eff} = 0.5 * (24.0 + 23.5) = 23.75 \text{ inches}$$

$$S = \frac{W_{eff}L_{eff}}{2h_{ri}(W_{eff} + L_{eff})} = \frac{23.75 * 19.75}{2 * 0.25(23.75 + 19.75)} = 21.566$$

$$A = W_{eff}L_{eff} = 469.1 \text{ in}^2$$

$$\lambda = S\sqrt{\frac{3G}{K}} = 21.566\sqrt{\frac{3 * 0.175}{450}} = 0.7366$$

Coefficients needed for shear strains are

$$D_{a1} = 1.060 + 0.210\lambda + 0.413\lambda^2 = 1.4338$$

$$D_{a2} = 1.506 - 0.071\lambda + 0.406\lambda^2 = 1.6740$$

$$D_{a3} = -0.315 + 0.195\lambda - 0.047\lambda^2 = -0.1969$$

$$D_{a,para} = \max\left\{D_{a1}, \left(D_{a2} + D_{a3}\frac{L}{W}\right)\right\} = \max\left\{1.4338, \left(1.6740 - 0.1969\frac{19.75}{23.75}\right)\right\} = 1.5103$$

$$D_{a,perp} = \max\left\{1.4338, \left(1.6740 - 0.1969\frac{23.75}{19.75}\right)\right\} = 1.4338 \quad \text{(G-4)}$$

$$D_{r,para} = \min\left\{\frac{1.552 - 0.627\lambda}{2.233 + 0.156\lambda + L/W}, 0.5\right\} = \min\left\{\frac{1.552 - 0.627 * 0.7366}{2.233 + 0.156 * 0.7366 + 0.8316}, 0.5\right\} = 0.3429$$

(weak axis) (G-7)

$$D_{r,perp} = \min\left\{\frac{1.552 - 0.627\lambda}{2.233 + 0.156\lambda + L/W}, 0.5\right\} = \min\left\{\frac{1.552 - 0.627 * 0.7366}{2.233 + 0.156 * 0.7366 + 1.2025}, 0.5\right\} = 0.3070$$

(strong axis) (G-7)

Under service conditions (amplified loads):

$$\sigma_a = \frac{2200}{469.1} = 4.690 \text{ ksi}$$

Shear strain due to axial load is

$$\gamma_a = D_{a,para}\frac{\sigma_a}{GS} = 1.5103 * \frac{4.690}{0.175 * 21.566} = 1.877 \quad \text{(G-3)}$$

Shear strain due to rotation is

$$\gamma_r = D_{r,para}\left(\frac{L}{h_{ri}}\right)^2 \theta_i = 0.3429\left(\frac{19.75}{0.25}\right)^2\left(\frac{0.00167}{2}\right) = 1.783 \quad \text{(G-6)}$$

Shear strain due to shear displacement is

$$\gamma_s = \frac{\Delta_s}{h_{rt}} = \frac{0.25 \text{ inches}}{0.5 \text{ inches}} = 0.500 \quad \text{(G-10)}$$

The total shear strain is

$$\gamma_{tot} = \gamma_a + \gamma_r + \gamma_s = 1.877 + 1.783 + 0.500 = 4.160 < 5.0 \quad \text{(G-1)}$$

The bearing has no external plates, so hydrostatic tension does not need to be checked. Stability criteria are satisfied. Initial conditions also are satisfactory. Because the bearing thickness is less than 8 in. and its plan area is less than 1000 in^2, special testing is not required.

Note that, according to the existing Method B LRFD Specifications, this bearing would not be permitted, largely because the applied axial stress exceeds the limit of 1.60 ksi, in the presence of shear deformations. However, during the testing phase of the research, some bearings with shape factor 9 were loaded to 12 ksi (that is, to a stress of 12 *GS*) with no signs of damage. The bearing in this example is required to carry only 1.876 *GS*.

Note also that the initial assumption that the axial force dominated proved incorrect. The shear strain due to total (amplified) axial load is 1.877, whereas the shear strain due to rotation is 1.783, so the magnitudes of the axial and rotation effects are similar.

If the total shear strain of 4.160 were to be regarded as unacceptably high, the simplest way to reduce it would be to use more rubber layers and lower the rotation component of the shear strain. However, there is no need to design for lower stresses because the shear strains are already low enough to prevent any debonding under such a small number of cycles. In addition, the loading is caused by the extreme seismic event, so some debonding damage may be tolerable.

3.3 QC/QA Procedures

Chapter 2 summarized some issues related to QA/QC testing and evaluation procedures. Evaluation of QA/QC procedures was not the primary goal of this research, so less effort was spent on it than was given to testing and FEA. Nevertheless, several recommendations are appropriate and are described here.

- It is clear that today's elastomeric bearings are of higher quality than those made in the past. Two of the reasons are the concentration of manufacturing into four major companies and the effectiveness of the QA/QC requirements imposed by the specifications. Each of the four major companies is large enough to support an effective QA/QC operation, and each takes pride in producing quality bearings. This perhaps is made possible by the relatively stringent specifications, which tend to inhibit low-cost, low-quality fabricators from entering the market. The presence of such operators would create intense price competition, to the likely detriment of quality with little if any real reduction in bridge costs. This observation should be taken into account when considering any QA/QC tests for modification or elimination. The cost advantages that might be gained through elimination of some of these tests are small, whereas the potential losses associated with lower quality standards are high. The cost of replacing a bearing in a bridge, including any possible litigation costs, is several orders of magnitude higher than the cost of a material test in a manufacturer's laboratory. As a result, it is suggested that major changes should be undertaken only after very careful consideration of the costs and benefits.
- The test procedures previously associated with the current Method B were fairly complex and expensive, and they appear to have deterred some engineers from using the design method. Yet the compressive stresses allowed by Method B may be only slightly higher than those permitted under Method A. (The increase depends on the amplitude of the rotation, which is not accounted for explicitly by Method A.) The long-duration load test was particularly troublesome, but has now been eliminated. Therefore, it is proposed that any additional testing be required for large bearings rather than those designed using Method B. Large bearings are tentatively defined as thicker than 8 in. or with a plan area larger than 1000 in^2. There remains the question of what additional testing to apply to such bearings. The regimes in M251-06 have some serious drawbacks, but the AASHTO T-2 Committee has chosen to eliminate the long term test. It is recommended that the choice of required additional testing be a matter for discussion between the T-2 Committee members, a representative group of manufacturers, and the researchers. Each group is a stakeholder in the issue and brings specialist knowledge to the table that is necessary to reach a good decision.
- Very large and unusual bearings pose problems. Their size may make testing them difficult, because the loads needed might exceed the capacity of most test machinery, especially if the test load is to be significantly higher than the service load. However, they are the bearings most in need of testing, because of the difficulties involved in curing large bodies of rubber and the consequences of a failure are more serious in a large bearing than in a small one. Three possible alternatives are envisaged:
  - First is to require that the manufacturer produce an extra full sized bearing for testing. It then should be cut up as needed, and destructive shear and compressive tests should be performed on the parts to evaluate the material properties throughout the bearing.

  - Second is to core the center of one of the large bearings. Portions of the bearing core could be tested in shear and compression to provide the information needed through the thickness of the bearing. The cored bearing could then be refilled with precured elastomer and put into service. If the core is taken in the center of the bearing and the effect of the coring on the strength of the reinforcement is considered during design, the refilled bearing may provide good service if the bearing proves satisfactory in all other ways.
  - Third is to test the bearing with a tapered plate. The taper angle should be selected to create a combination of rotation and compression on the most heavily stressed edge that leads to the same local shear strain as would be caused by the desired test load applied through parallel load plates. Calculations should be done using the linear theory strain coefficients, D_a and D_r.
- Current definitions of the number of test specimens required by the AASHTO M251-06 Specifications are less clear than they should be. For example, the definition of a "lot" of bearings may lead to excessive testing. There is little reason for duplicating tests on bearings of similar bearing sizes and geometries made from the same compound. It is suggested that a set of bearings made from one compound and whose dimensions differ by no more than 10% be grouped into a single lot for the purposes of establishing test requirements. Inconsistencies between various specifications and within specifications should also be resolved.
- The definition of the word "batch" also should be reviewed for consistency with practice. The process of mixing the ingredients for a rubber compound is called batching. Some manufacturers batch their own rubber while others buy it prebatched, from a separate supplier. Thus the word "batch" could mean the bearings made from a single delivery of premixed rubber, which might be enough for only some of the bearings for a whole bridge, or it could mean a group of bearings for the same job. The different interpretations may lead to different numbers of bearings being tested.

CHAPTER 4

Summary, Conclusions, and Recommendations

4.1 Summary

The rotational response of elastomeric bearings was studied using testing and analysis. The program concentrated on steel-reinforced elastomeric bearings. The test bearings were purchased from the four largest manufacturers in the country.

The test program included static and cyclic rotation tests on full bearings, and material tests and diagnostic tests on full bearings to evaluate their instantaneous state of damage. Many of the tests were conducted in a specially constructed test machine capable of applying to a bearing independently controlled, constant axial force, constant shear deformation, and cyclic rotation.

In the static test series, the parameters investigated were combinations of axial load and rotation. In the cyclic load tests, they included the effects of axial load, rotation angle and number of cycles, bearing geometry (aspect ratio and shape factor), materials, shim plate edge treatment, and manufacturer.

The behavior of the bearings was modeled in three ways. An approximate linear model, based on small deflection theory, was used to investigate basic behavioral phenomena and to derive design equations. FEAs also were conducted using large deformations and special constitutive laws for nonlinear, nearly incompressible materials. The goals were to evaluate the suitability of the simpler linear models, to investigate behaviors that could not be studied in the laboratory and to determine the relationship between local deformations, which could not be measured, and global displacements, which could. Finally, empirical models were developed to predict the fatigue behavior of the bearings under cyclic loading.

The results of the tests and analyses were combined and used to develop design procedures.

4.2 Conclusions

The following conclusions were drawn from this research.

4.2.1 Conclusions on Behavior Measured in Tests

1. Steel reinforced elastomeric bearings are extremely robust. In tests, bearings that had been subjected to loads approximately 10 times their design value and had suffered considerable visible damage were still able to carry the vertical load. While this ability is useful because it would prevent immediate collapse of the bridge, the vertical deflection and the damage to the bearing would seriously impair the bridge's serviceability.
2. The bearings tested in this study came from the four largest manufacturers in the country. All were of high quality. The test results showed that the quality of bearings today is higher than it was 20 years ago. No one manufacturer stood out as universally superior to the others.
3. No clear and unique definition of failure exists for an elastomeric bearing. The first form of damage is typically local tension debonding of the edge cover from the edge of the shims. More intense static loading, or continued cyclic loading, may lead to delamination, characterized by the propagation of a horizontal shear crack back into the elastomer layers. It typically runs in the rubber, close to the steel-rubber interface. At very high axial loads, the steel shims yield and fracture. The debonding and delamination mechanisms tend to be progressive and occur more readily under cyclic loading. Shim fracture occurs only in response to very high axial load, either static or cyclic.
4. The tension debonding of the edge cover from the vertical face of the steel shim has no adverse effect on the performance of the bearing. However, it presages the start of shear delamination from the horizontal surface of the shims, which will change the bearing's stiffness, and will eventually cause the bearing to tear apart. These behaviors will have a negative impact on the bridge superstructure.
5. The lack of a unique definition of failure makes development of design specifications difficult, because the demarcation

between acceptable and unacceptable behavior is not binary but rather requires judgment over the level of damage that is acceptable. Furthermore, the difficulties are aggravated by the facts that the quality of the manufacturing influences the loading required to cause a given level of damage, and damage accumulates as a fatigue process. Fatigue data typically show considerable scatter and the process is difficult to characterize reliably.

6. In this study, tension debonding of the rubber cover from the shim edge was used as the critical damage measure.
7. The fatigue resistance of the rubber did not show a clear correlation with any obvious material property such as tension strength or elongation at break.
8. Sharp edges on the shims promote debonding. If they are deburred with a special tool, or rounded with a belt sander, debonding is delayed. More precise rounding of the edges than that (for example, with machine tools) provides little additional benefit.
9. Adding shear deformation of 30% causes no noticeable change in the number of cycles required to reach a given level of debonding.

4.2.2 Conclusions on Analytical and Numerical Modeling

1. Bearings made from 60-durometer elastomer performed better under comparable loads than did nominally identical 50-durometer bearings, because the increased stiffness reduced the maximum shear strain. The observation that they performed even better than predicted by theory supports the view that shear strain rather than stress is an appropriate measure of fatigue demand.
2. Bearings with shape factors of 9 and 12 performed better than did bearings of shape factor 6 under loading that caused similar total shear strains in each. Theory suggests that, when the induced shear strains are the same, the performance should be the same. This finding supports the use of bearings with large shape factors.
3. The approximate linear theory originally developed by Gent and his coworkers provides a reasonable estimate of the rotational stiffness. The compressive stiffness was harder to match, because it displays significant nonlinearity and because determining the point of zero displacement is difficult.
4. FEA in general confirmed, at low loads and rotations, the validity of the small displacement analyses. In particular, they showed that superposition of load-cases was valid, that the stiffness and strain coefficients developed by Stanton and Lund using linear theory were accurate enough for use in design, and that the value of internal hydrostatic stress predicted by the simple linear theory was valid.
5. FEA also showed several behaviors that would otherwise have been very hard to observe. First was the existence of a small local region of high hydrostatic stress at the outer, vertical edge of the shim, which, in combination with the very large local strains there, appears to be responsible for the tension debonding observed in almost all the tests. Second was the lateral movement of the shims at mid-height, when pure rotation is applied to the bearing. If the bearing is thought of as a very short column, this effect is analogous to the lateral deflection at mid-height of the column when end moments are applied. This shim displacement alters the strain field in the critical region at the edge of the shims, and may affect the debonding behavior there.

4.2.3 Conclusions on Development of Design Procedures

1. Obtaining reliable laboratory measurements of local shear strains in the rubber is impossible. Therefore it was necessary to use computed strains in the models for predicting debonding.
2. Initial debonding under static load occurred at a total shear strain that was nearly the same in a range of tests with different load and rotation combinations. This finding was used to develop a total shear strain limit for monotonic load.
3. Analyses of trucks passing over typical bridges showed that the cyclic axial load effects of the loading create shear strains in the elastomer much larger than those caused by the rotation.
4. An empirical but rational fatigue model was developed to predict the level of cyclic debonding as a function of the constant axial load, the amplitude of the cyclic rotation, and the number of cycles. It is referred to here as the Nonlinear Model because it made use of a nonlinear axial load-displacement relationship. It was able to predict well the fatigue life of the bearings, even though the dataset included a wide variety of loadings and bearing geometries. However, it had to be abandoned because it predicted extensive debonding in a class of bearing that is widely used for freeway overpasses, whereas such damage is not seen in practice. A description of it is retained in Appendix F so that, if suitable cyclic axial test data become available, it could be developed for use in a specification.
5. An alternative and simpler design method was developed. It is referred to herein as the Linear Model. It was based on a linear relationship between axial force and deflections, and did not attempt to link the progress of damage continuously to the number of cycles of load. It fitted the test data by relating the total applied shear strain to the number of cycles at a specific level of damage (25% debonding).

When applied to bearings commonly used for typical freeway overpasses, it predicted that very little debonding should occur. This prediction is in agreement with field observations.

6. The Method B design procedure based on the Linear Model is simple to use. The major changes from the present specifications are: the permissible combinations of load and rotation are controlled by an explicit total strain approach; lift-off is allowed if no external bonded plates exist; and a check is required for rupture by hydrostatic tension if external plates do exist. The limit on absolute axial stress has been removed, but a limit in terms of *GS* remains.
7. Method A design procedure was developed from Method B by computing a maximum probable rotation on the bearing, and finding the corresponding axial stress that would be allowed under the Method B rules. In order to optimize the usefulness of Method B (by keeping the allowable stress as high as reasonably possible) some restrictions on its use proved necessary. Only seldom are these restrictions likely to provide active constraints.

4.3 Recommendations

4.3.1 Recommendations for Implementation

1. The design methodology proposed in Appendix G for both Method A and Method B is written in language and a format suitable for direct adoption in the AASHTO LRFD Specifications. Those design requirements provide better correlation with behavior observed in the tests than do the existing ones, they are more transparent to the user, and they are simpler to implement. They also address combinations of loading, including light axial load and large rotations that prove problematic under the existing specifications.
2. The criteria for additional, more stringent, testing presently required for Method B bearings should be reconsidered, and an alternative is proposed. Design by the existing Method B triggers the need for more rigorous testing. The cost of that testing acts as a disincentive to the use of Method B. That in turn inhibits the use of high shape factor bearings, which are encouraged under the proposed Method B and were shown in the test program to be very effective in inhibiting the initiation and propagation of damage due to debonding and delamination. More rigorous testing is most urgently needed for large bearings, particularly thick ones, because they are more difficult to fabricate. Consequently, it is proposed that bearing size, and not the design method used, be used as the criterion for more rigorous testing. This raises the practical problem that suitable testing facilities with enough capacity to load such a bearing may not be available. Several approaches are proposed for resolving that problem.
3. The edges of all steel shims in all bearings should be deburred or otherwise rounded prior to being molded in the bearing. Doing so reduces the stress concentration in the rubber at the critical location at the edge of the shim. The proposed strain limits in Appendix G are contingent on this being done.

4.3.2 Recommendations for Further Research

1. Average axial strains measured in the tests were found to differ from those calculated by both linear elastic methods and nonlinear elastic FE models. An approximate, semi-empirical, nonlinear model was developed, but an improved understanding of axial load effects and their nonlinearities is desirable.
2. The fatigue effects of axial loading should be investigated experimentally and analytically, so that they can be incorporated into the design method in a rational way.
3. Creep of the rubber should be investigated and included in the design method. The axial load tests showed significant continued displacement after the load was reached and held constant, resulting in increased strains for a given stress. For a design method based on shear strain limits, it is important to know the actual strains. The effect of load duration on strength should also be investigated.
4. The effects of aspect ratio should be further investigated. For the limited number of tests in this research, the bearings with smaller aspect ratios performed much better than expected on the basis of maximum shear strains calculated using theoretical models.

Bibliography

AASHTO. (1961). Standard Specification for Highway Bridges, 8th Edition. American Association of State Highway Officials, Washington, D.C.

AASHTO. (1989). Standard Specification for Highway Bridges, 14th Edition. American Association of State Highway and Transportation Officials, Washington, D.C.

AASHTO. (1991). Standard Specification for Highway Bridges, 15th Edition. American Association of State Highway and Transportation Officials, Washington, D.C.

AASHTO. (1994). Load and Resistance Factor Design Specification for Highway Bridges, 1st Edition. American Association of State Highway and Transportation Officials, Washington, D.C.

AASHTO. (1996). Standard Specification for Highway Bridges, 16th Edition. American Association of State Highway and Transportation Officials, Washington, D.C.

AASHTO. (1997). AASHTO M 251-Plain and Laminated Elastomeric Bridge Bearings. American Association of State Highway and Transportation Officials, Washington, D.C.

AASHTO. (1998). AASHTO LRFD Bridge Construction Specifications. American Association of State Highway and Transportation Officials, Washington, D.C.

AASHTO. (2005). AASHTO LRFD Bridge Design Specifications. American Association of State Highway and Transportation Officials, 444 N Capitol St. NW, Suite 249, Washington, DC.

ASTM D4014. (2003). Plain and steel-laminated elastomeric bearings for bridges. American Society for Testing Materials, Philadelphia, PA.

Bradley, G., Taylor., A., and Chang, P. (1997). Testing of rubber isolation bearings. Final Report to the National Institute of Standards and Technology, Gaithersburg, MD.

British Standards Institution. (1980). *Steel, Concrete and Composite Bridges,* BS5400 Parts 1, 2, 4, 5, 6, 7, 8, 10. London, England.

Cadwell, S. M., Merrill, R. A., Sloman C. M., and Yost, F. L. (1940). Dynamic fatigue life of rubber. Industrial and Engineering Chemistry, 12(1), pp. 19–23.

Conversy, F. (1967). Appareils d'Appui en Caoutchouc Frette. Annales des Ponts et Chaussees, VI, Nov–Dec.

Design of Neoprene Bearing Pads. (1959). E. I. DuPont de Nemours and Company, Wilmington, DE.

Design Requirements for Elastomeric Bridge Bearings. (1976). Technical Memorandum No. BE1/76, Highways Directorate, Department of the Environment, Great Britain.

EN1337-3. (2006). *Structural Bearings—Part 3: Elastomeric Bearings.* European Commission for Standardization, Milan, Italy.

English, B. A., Klingner, R. E, and Yura, J. A. (1994). *Elastomeric Bearings: Background Information and Field Study.* Research Report CTR 1304-1, Center for Transportation research, University of Texas at Austin, June.

Gent, A. N. (1964). Elastic stability of rubber compression springs. *Journal of Mechanical Engineering Science,* 6(4), pp. 318–326.

Gent, A. N., and Lindley, P. B. (1959a). *Internal Rupture Of Bonded Rubber Cylinders In Tension.* Royal Society of London, Series A, Vol. 249, pp. 195–205.

Gent, A. N., and Lindley, P. B. (1959b). The compression of bonded rubber blocks. Proc. Inst. Mech. Engrs. Vol. 173, pp. 111–222.

Gent, A. N., and Meinecke, E. A. (1970). Compression, bending and shear of bonded rubber blocks. *Polymer Engineering and Science,* 10(1), Jan., pp. 48–53.

Gent, A. N., and Lindley, P. B. (1959). Internal rupture of bonded rubber cylinders in tension. *Royal Society of London Proceedings, Series A.,* Vol. 249, pp. 195–205.

Gent, A. N., and Yeoh, O. H. (2003). Crack growth in twisted rubber disks. Part 3. Effects of crack depth and location," Rubber Chemistry and Technology, Vol. 76(5), 2003, pp. 1276–1289.

Gurtin, M. E. (1981). An introduction to continuum mechanics. *Mathematics and Science in Engineering,* Vol. 158, Academic Press.

Haryngx, J. A. (1948). *On Highly Compressible Helical Springs And Rods, and Their Application for Vibration Free Mounting.* Phillips Research Reports, Parts I-III, N. V. Phillips, Gloeilampenfabrieken, Eindhoven, Netherlands.

Helnwein, P., Huemer, T., and Eberhardsteiner, J. (1998). Numerische Untersuchung betreffend eine neue Probenform zur Untersuchung der Druckabhängigkeit des Reibungsbeiwertes von Gummi (Numerical Analysis Regarding a New Test Specimen for the Investigation of the Pressure Dependence of the Friction Coefficient of Rubber). Institute for Strength of Materials, Vienna University of Technology, technical report, 20 pages, in German.

Helnwein, P., Huemer, T., Liu, W. N., Payer, H.-J., Meschke, G., and Mang, H. A. (1998). Numerische Untersuchungen des Traktionsverhaltens von Profilstollen auf schneebedeckten Fahrbahnen (Numerical Analyses of the Traction Mechanisms of Tire Tread on Snow-Covered Surfaces). Institute for Strength of Materials, Final Report, Vienna University of Technology, technical report, 80 pages, in German.

Helnwein, P., Liu, C. H., Meschke, G., and Mang, H. A. (1993). A new 3d finite element model for cord-reinforced rubber composites—applications to analysis of automobile tires. *Finite Elements in Analyses and Design,* 14, 1–16.

Herrmann, L. R., and Hamidi, R. (1988). *Nonlinear Behavior Of Elastomeric Bridge Bearings: Volume I—Theory And Application.* Final

Report of State of California, Dept. of Transportation, Research Technical Agreement 13945-53B273.

Herrmann, L. R., Hamidi, R., Shafigh-Nobari, F., and Lim, C. (1988). Nonlinear behavior of elastomeric bearings, I: Theory. *ASCE, Journal of Engineering Mechanics,* Vol 114, No. 11, pp. 1811–30.

Herrmann, L. R., Hamidi, R., Shafigh-Nobari, F., and Ramaswamy, A. (1988). Nonlinear behavior of elastomeric bearings, II: FE analysis and verification. *ASCE, Journal of Engineering Mechanics,* Vol 114, No. 11, pp. 1831–53.

Holownia, B. (1980). The effect of various types of carbon black on elastic constants of elastomers. *Plastics and Rubber: Materials and Applications,* Aug. pp. 129–132.

Huang, E. R. (2003). *Disk Bearings.* MSCE thesis, University of Washington, Seattle. In preparation.

Kuester, Colin M. (2006). *Improved Rotational Limits for Elastomeric Bridge Bearings.* MSCE thesis, Dept. of Civil Eng., University of Washington, Seattle.

Lake, G. J., and Yeoh, O. H. (1980). Measurement of rubber cutting resistance in the absence of friction. *Rubber Chemistry and Technology,* Vol. 53(1), 1980, pp. 210–227.

Lake, G. J., and Yeoh, O. H. (1982). On the strength of vulcanized rubbers. Deformation, Yield and Fracture of Polymers, International Conference, 1982, pp. 14.1–14.7.

Lehman, D. E., Roeder, C. W., and Larson, R. (2003). *Cotton Duck Bearing Pads: Engineering Evaluation and Design Recommendations.* Final Report to Washington State Department of Transportation, October 2003.

Lindley, P. B, and Teo, S. C. (1978). Some numerical stiffnesses of soft elastic blocks bonded to rigid end plates. *Plastics and Rubber, Materials Applications,* Aug. pp. 113–116.

Lindley, P. B. (1979). Compression moduli for blocks of soft elastic material bonded to rigid end plates. *Journal of Strain Analysis,* Vol. 14., No. 1, pp. 11–16.

Lund, H. H. (2003). *Lateral Buckling of Prestressed Concrete Girders Supported on Elastomeric Bearings.* MSCE thesis, University of Washington, Seattle. In preparation.

Malvern, L. E. (1969). *Introduction to the Mechanics of a Continuous Medium.* Prentice-Hall, Englewood Cliffs, NJ.

Meschke, G., and Helnwein, P. (1994). Large-strain 3D-analysis of fibre-reinforced composites using rebar elements: Hyperelastic formulations for cords. *Computational Mechanics,* 13, 241–254.

MSC.Marc, Volume A: Theory and User Information. (2003). MSC. Software Corporation, Santa Ana, CA.

Ogden, R. W. (1984). *Non-Linear Elastic Deformations.* Dover Publications, Mineola, NY.

Rejcha, C. (1964). Design of elastomeric bearings. PCI Journal, 9(2), Oct, pp. 62–78.

Roeder, C. W., Stanton, J. F., and Taylor, A. (1990). Fatigue of steel-reinforced elastomeric bearings. *Journal of Structural Division,* ASCE, No. ST2, Vol. 116, New York, pp. 407–26.

Roeder, C. W., Stanton, J. F., and Feller, T. (1989). *NCHRP Report 325: Low Temperature Behavior and Acceptance Criteria for Elastomeric Bridge Bearings.* TRB, National Research Council, Washington, D.C.

Roeder, C. W., Stanton, J. F., and Taylor, A. W. (1987). *NCHRP Report 298: Performance of Elastomeric Bearings.* TRB, National Research Council, Washington, D.C.

Schrage, Ingo. (1979). *Über den Bewegungswiderstand von unverankerten Elastomer-Lagern* (Friction in Unsecured elastomeric Bearings). PhD dissertation. Rheinisch-Westfälische Technische Hochschule, Aachen, Germany.

Stanton, J. F., and Lund, H. (2006). Effects of bulk compressibility on the response of elastomeric bearings. Accepted for publication, *Journal of Structural Engineering,* ASCE, Reston VA.

Stanton, J. F., and Roeder, C. W. (1982). *NCHRP Report 248: Elastomeric Bearings Design, Construction, and Materials.* TRB, National Research Council, Washington, D.C.

Stanton, J. F., Roeder, C. W., and Campbell, T. I. (1999). *NCHRP Report 432: High-Load Multi-Rotational Bridge Bearings.* TRB, National Research Council, Washington, D.C.

Stanton, J. F., Scroggins, G., Taylor, A. W., and Roeder, C. W. (1990). Stability of laminated elastomeric bearings. Journal of Engineering Mechanics, Vol. 116, (6), pp. 1351–1371.

Timoshenko, S. P., and Gere, J. M. (1961). *Theory of Elastic Stability.* 2nd ed. McGraw Hill, New York.

White, Christopher J. (2006). *Response of Elastomeric Bearings to Rotation.* MSCE thesis. Dept. of Civil Eng., University of Washington, Seattle.

Yeoh, O. H. (1984). On hardness and young's modulus of rubber. *Plastics and Rubber Processing and Applications,* Vol. 4(2), 1984, pp. 141–144.

Yeoh, O. H. (1993). Some forms of the strain energy function for rubber. *Rubber Chemistry and Technology,* Vol. 66(5), 1993, pp. 754–771.

Yeoh, O. H. (2001). Analysis of deformation and fracture of 'pure shear' rubber test piece. *Plastics, Rubber and Composites,* Vol. 30(8), 2001, pp. 389–397.

Yeoh, O. H. (2003). Some benchmark problems for FEA from torsional behavior of rubber. *Rubber Chemistry and Technology,* Vol. 76(5), 2003, pp. 1212–1227.

Yeoh, O. H., and Fleming, P. D. (1997). New attempt to reconcile the statistical and phenomenological theories of rubber elasticity. *Journal of Polymer Science, Part B: Polymer Physics,* Vol. 35(12), 1997, pp. 1919–1931.

Yura, J., Kumar, A., Yakut, A., Topkaya, C., Becker, E., and Collingwood, J. (2001). *NCHRP Report 449: Elastomeric Bridge Bearings: Recommended Test Methods.* TRB, National Research Council, Washington, D.C.

NOTATION

a = dimensionless coefficient in fatigue model
A = area of the bearing = WL
A_a = dimensionless coefficient in axial stiffness
A_{az} = dimensionless coefficient in axial stiffness = A_a (App. E)
a_{ij} = dimensionless coefficient in FEA error analysis
A_{net} = plan area of bearing based on net dimensions
AR = aspect ratio = the smaller of L/W and W/L.
A_r = dimensionless coefficient in rotational stiffness
A_{ry} = dimensionless coefficient in rotational stiffness = A_r (App. E)
b = dimensionless coefficient in fatigue model
B_a = dimensionless coefficient in axial stiffness
B_{az} = dimensionless coefficient in axial stiffness (App. E)
B_r = dimensionless coefficient in rotational stiffness for compressible layers
B_{r0} = dimensionless coefficient in rotational stiffness for incompressible layers
B_{ry} = dimensionless coefficient in rotational stiffness = B_r
$\mathbf{C}$ = Right Cauchy-Green strain tensor
C_{10}, C_{20}, C_{30} = Material parameters for Yeoh's model
C_a = dimensionless coefficient in shear strain due to axial load
C_{azzx} = dimensionless coefficient in shear strain due to axial load = C_a (App. E)
c_n = dimensionless coefficient in fatigue model
C_r = dimensionless coefficient in shear strain due to rotational
C_{ryzx} = dimensionless coefficient in shear strain due to rotational = C_r (App. E)
c_S = limiting permissible of S^2/n for Method A design
c_σ = dimensionless stress coefficient (lift-off equations)
D = debonding level
D = diameter of the bearing (App. G)
D_a = dimensionless shear strain coefficient for axial load
D_r = dimensionless shear strain coefficient for rotation
e = Euler's constant (basis of Napieran logarithm)
$\mathbf{E}$ = Green-Lagrange strain tensor
E = Young's modulus
E_{az} = apparent Young's modulus for axial loading
E_{ry} = apparent Young's modulus for rotational loading
F_r = dimensionless coefficient for rotation (uplift equations)
G = shear modulus
g_0, g_1 = dimensionless coefficients in fatigue model

H_a = dimensionless coefficient for axial load (uplift equations)
H_r = dimensionless coefficient for rotation (uplift equations)
h_{ri} = thickness of *ith* interior layer of elastomer
h_{rt} = total thickness of all interior layers of elastomer
I = moment of inertia (second moment of area)
K = bulk modulus
K_a = total axial stiffness
K_r = total rotational stiffness
L = length of bearing based on gross dimensions (= plan dimension of the bearing perpendicular to the axis of rotation under consideration)
l = span of a girder
L_{net} = net length of bearing (average of gross and shim dimensions)
M = moment on bearing
m = exponent in fatigue model
N = number of cycles
n = number of interior layers of elastomer
N_{cr} = characteristic number of cycles
p = force per unit length
P = total axial force
P_{sd} = minimum vertical force due to permanent loads
$\mathbf{S}$ = 2nd Piola-Kirchhoff stress tensor
S = shape factor
S_i = shape factor of instantaneous compressed region (lift-off equations)
t = thickness of elastomeric layer
W = gross width of elastomeric layer (= plan dimension of the bearing parallel to the axis of rotation under consideration)
W_{net} = net width of elastomeric layer (average of gross and shim dimensions)
x,y,z = coordinates in Cartesian system
Δ_a = axial deflection
Δ_s = maximum total shear displacement of the bearing at the service limit state.
I_1, (I_1^*) = first invariant of $\mathbf{C}$ (specialized for uniaxial tension)
α = dimensionless load combination parameter = $\varepsilon_a/S\theta_L$
δ_{bottom} = vertical displacement of bottom shim
δ_{top} = vertical displacement of top shim
ε_a = average axial strain for bearing under axial load
ε_{ai} = axial strain at the middle of the instantaneous compressed region (lift-off equations)
ε_{az} = average axial strain = ε_a
ε_{zz} = local vertical normal strain in rubber layer
γ_a = shear strain in *z-x* plane due to axial loading
$\gamma_{a,cy}$ = cyclic portion of shear strain in *z-x* plane due to axial loading
$\gamma_{a,max}$ = absolute maximum shear strain in *z-x* plane due to axial loading
$\gamma_{a,st}$ = static portion of shear strain in *z-x* plane due to axial loading
γ_{cap} = shear strain capacity
γ_t = shear strain in *z-x* plane due to rotation loading

$\gamma_{r,cy}$ = cyclic portion of shear strain in *z-x* plane due to rotation loading
$\gamma_{r,max}$ = absolute maximum shear strain in *z-x* plane due to rotation loading
$\gamma_{r,st}$ = static portion of shear strain in *z-x* plane due to rotation loading
γ_{r0} = shear strain constant in fatigue model
γ_s = shear strain in *z-x* plane due to shear displacement
$\gamma_{s,cy}$ = cyclic portion of shear strain in *z-x* plane due to shear displacement
$\gamma_{s,st}$ = static portion of shear strain in *z-x* plane due to shear displacement
$\gamma_{tot,max}$ = maximum total shear strain in *z-x* plane
γ_{zx} = local shear strain in *z-x* plane
η = relative length of the instantaneous compressed region (lift-off equations)
λ = compressibility index = $S\sqrt{3G/K}$
$\lambda_1, \lambda_2, \lambda_3$ = principal stretches (App. E)
θ = end rotation of a girder (rotation demand on bearing)
θ_c = characteristic rotation for which the vertical displacement on the "tension" side becomes net upwards
θ_i = rotation of the *ith* layer of elastomer
θ_L = rotation per layer
θ_x, θ_y = rotation of whole bearing about *x* or *y* axis
ρ = dimensionless rotation ratio (lift-off equations)
σ_a = average axial stress
σ_{a0} = fictitious average axial stress for entire bearing surface (lift-off equations)
σ_{hyd} = hydrostatic stress (mean direct stress)
$\sigma_{rupture}$ = (hydrostatic) rupture strength of rubber
σ_{zz} = local vertical normal stress in rubber layer
τ_{zx} = local shear stress in *z-x* plane
ξ = dimensionless position parameter = $2x/L$

APPENDIXES

Appendixes to the contractor's final report for NCHRP Project 12-68, "Improved Rotational Limits of Elastomeric Bearings," are available on the TRB Web site at http://trb.org/news/blurb_detail.asp?id=8556. The appendixes are the following:

Appendix A Test Data
Appendix B Survey of Current Practice
Appendix C Test Apparatus and Procedures
Appendix D Test Results Overview
Appendix E Finite Element Analysis
Appendix F Development of Design Procedures
Appendix G Proposed Design Specifications

Abbreviations and acronyms used without definitions in TRB publications:

AAAE	American Association of Airport Executives
AASHO	American Association of State Highway Officials
AASHTO	American Association of State Highway and Transportation Officials
ACI–NA	Airports Council International–North America
ACRP	Airport Cooperative Research Program
ADA	Americans with Disabilities Act
APTA	American Public Transportation Association
ASCE	American Society of Civil Engineers
ASME	American Society of Mechanical Engineers
ASTM	American Society for Testing and Materials
ATA	Air Transport Association
ATA	American Trucking Associations
CTAA	Community Transportation Association of America
CTBSSP	Commercial Truck and Bus Safety Synthesis Program
DHS	Department of Homeland Security
DOE	Department of Energy
EPA	Environmental Protection Agency
FAA	Federal Aviation Administration
FHWA	Federal Highway Administration
FMCSA	Federal Motor Carrier Safety Administration
FRA	Federal Railroad Administration
FTA	Federal Transit Administration
IEEE	Institute of Electrical and Electronics Engineers
ISTEA	Intermodal Surface Transportation Efficiency Act of 1991
ITE	Institute of Transportation Engineers
NASA	National Aeronautics and Space Administration
NASAO	National Association of State Aviation Officials
NCFRP	National Cooperative Freight Research Program
NCHRP	National Cooperative Highway Research Program
NHTSA	National Highway Traffic Safety Administration
NTSB	National Transportation Safety Board
SAE	Society of Automotive Engineers
SAFETEA-LU	Safe, Accountable, Flexible, Efficient Transportation Equity Act: A Legacy for Users (2005)
TCRP	Transit Cooperative Research Program
TEA-21	Transportation Equity Act for the 21st Century (1998)
TRB	Transportation Research Board
TSA	Transportation Security Administration
U.S.DOT	United States Department of Transportation